Three Phase Integrated Load and Harmonic Flows

A thesis presented for the degree of
Doctor of Philosophy in Electrical and Electronic Engineering
in the University of Canterbury, Christchurch, New Zealand.

C.D.Callaghan B.E., M.E.
August 1989

ABSTRACT

This thesis investigates two algorithms for the steady state analysis of HVDC convertor plant.

The first is an already well established frequency domain technique, known as IHA (Iterative Harmonic Analysis), and the investigation centres on the nature of the algorithm under divergent conditions. In particular, a mathematical analysis of the algorithm is used to prove that divergence of the algorithm is not necessarily indicative of a physical harmonic instability.

The second algorithm is developed to exploit the IHA technique within the context of the three phase a.c.-d.c. loadflow as an alternative convertor model which incorporates (rather than ignores) the effects of harmonics. The resulting three phase integrated load and harmonic flow algorithm is a significant improvement on the existing single phase load & harmonic flow algorithms.

Finally, the integrated algorithm is applied to two test systems drawn from the New Zealand primary network, and is shown to be a significant improvement over the IHA algorithm alone, resolving the inconsistencies which exist between the fundamental frequency and harmonic models of the convertor.

CONTENTS

LIST OF FIGURES

LIST OF TABLES

LIST OF PRINCIPAL SYMBOLS

The following list of symbols is intended for guidance only, since all symbols are defined in the text. The flavour of some of the following symbols may vary slightly from chapter to chapter. Those symbols labelled as being 'generic' are used to refer to either the time domain waveform or the phasor representation, and may or may not include distortion. All functions of time may drop the (t) provided ambiguities are avoided.

a_a, a_b, a_c — off-nominal transformer tap ratios.

$\mathbf{a}$ — a constant vector.

big() — a function which returns the largest element in its vector argument.

b_3 — third harmonic Fourier coefficient.

[C] — a connection matrix.

C_1, C_2, C_3 — zero crossings of the fundamental commutating voltages.

[D] — d.c. iteration Jacobian.

E — internal generator emf.

f() — non-linear function in the harmonic space.

$\frac{\partial \mathbf{f}}{\partial \mathbf{V}}$ — Jacobian of the non-linear function f().

$\frac{\partial f_i}{\partial V_j}$ — element of $\frac{\partial \mathbf{f}}{\partial \mathbf{V}}$.

g() — a general vector-valued function.

h — harmonic order.

$i_a(t), i_b(t), i_c(t)$ — three phase current waveforms.

$i_a^3(t), i_b^3(t), i_c^3(t)$ — third harmonic current waveforms.

$i_{CA}^3(t), i_{CB}^3(t), i_{BA}^3(t)$ — third harmonic branch currents in delta winding.

$i_d(t)$ — d.c. current waveform.

$\mathbf{I}^{(k)}$ — k^{th} iteration harmonic current vector.

I_d — d.c. current (generic).

I_h — an harmonic current (generic).

$\hat{I}_d^h$ — h^{th} harmonic d.c. current component magnitudes.

$\mathrm{I_N}$ — an harmonic Norton current source vector.

[J] — Jacobian of the IHA iterating function.

l_a, l_b, l_c — commutating inductances.

l_{ac}, l_{ba}, l_{cb} — commutating *loop* inductances.

N_C — number of convertors.

N_T — number of terminal busbars.

N_V — number of independent harmonic voltages.

N_θ — number of independent firing instants.

P_d — d.c. side power.

P_h — h^{th} harmonic power.

pu — per unit.

t — time.

T_s — sampling interval.

$v_a(t), v_b(t), v_c(t)$ — three phase voltage waveforms.

$v_{ac}(t), v_{ba}(t), v_{cb}(t)$ — three commutating voltage waveforms.

$v_a^3(t), v_b^3(t), v_c^3(t)$ — third harmonic phase voltage waveforms.

$v_{ac}^3(t), v_{ba}^3(t), v_{cb}^3(t)$ — third harmonic commutating voltage waveforms.

$v_d(t)$ — the d.c. voltage waveform.

$v^+(t), v^-(t)$ — common-cathode and common-anode voltage waveforms.

$\mathrm{V}^{(k)}$ — k^{th} iteration harmonic voltage vector.

V_a, V_b, V_c — three phase voltages (generic).

$\hat{V}_a^h, \hat{V}_b^h, \hat{V}_c^h$ — h^{th} harmonic phase voltage magnitudes.

$\hat{V}_{ac}^h, \hat{V}_{ba}^h, \hat{V}_{cb}^h$ — h^{th} harmonic ccommutating voltage magnitudes.

V_{ac}, V_{ba}, V_{cb} — three commutating voltages (generic).

V_d — the d.c. voltage (generic).

V_h — an harmonic voltage (generic).

V_T, V_T' — terminal busbar voltages (generic).

V^+, V^- — common-cathode and common-anode voltages (generic).

$\mathrm{V_0}$ — a constant harmonic voltage vector.

$\mathrm{x}^{(k)}$ — a general k^{th} iteration vector.

x_a, x_b, x_c — commutating reactances.

x_{ac}, x_{ba}, x_{cb} — commutating *loop* reactances.

X_C — commutating reactance.

X_{SYS} — system reactance.

$[\mathrm{Y}]$ — harmonic space admittance matrix.

$[Y]_h$ — h^{th} harmonic admittance matrix.

ZC_i — i^{th} zero crossing of the commutating voltages.

Z_h — an harmonic impedance (generic).

α — firing angle (generic).

α_i — i^{th} firing angle.

$\alpha_{\min}$ — minimum firing angle.

Δ — signifies a mismatch quantity.

θ — general angle (generic).

θ_i — i^{th} firing instant.

$\boldsymbol{\theta}$ — a vector of firing instants.

$\boldsymbol{\Theta}$ — a vector-valued function returning the latest firing instants.

μ — commutation overlap angle (generic).

μ_i — i^{th} commutation overlap angle.

ξ_i — convergence measure for phase i.

τ — dummy variable of integration or continuation method parameter.

$\phi_a^h, \phi_b^h, \phi_c^h$ — phases of h^{th} harmonic phase voltages.

$\phi_{ac}^h, \phi_{ba}^h, \phi_{cb}^h$ — phases of h^{th} harmonic commutating voltages.

ϕ_h — h^{th} harmonic impedance phase.

ω — fundamental frequency (rad.s^{-1}).

LIST OF ABBREVIATIONS

BIRM — Binary Inclusion Relaxation Method.

CPU — Central Processing Unit.

EMTDC — Electromagnetic Transients for DC.

EMTP — Electromagnetic Transients Program.

FFT — Fast Fourier Transform.

GCF — Greatest Common Factor.

HA — Harmonic Analysis Iteration.

HVDC — High Voltage Direct Current.

IHA — Iterative Harmonic Analysis.

LHS — Left Hand Side.

MRFFT — Mixed Radix Fast Fourier Transform.

NLR — Non Linear Resistor.

OLTC — On Load Tap Changer.

PC — Personal Computer.

PQH — P Iteration, Q Iteration, Harmonic Iteration.

RHS — Right Hand Side.

SCR — (p2.) Silicon Controlled Rectifier.

— (p43 and folowing) Short Circuit Ratio.

TCS — Transient Convertor Simulation.

ACKNOWLEDGEMENTS

Completion of this thesis marks the end of a major portion of my life, and it would be unfair to let it pass without some acknowledgement of those people who have played a significant part in it.

Firstly, to my supervisor, Professor Jos Arrillaga, without whose gentle supervision this project would never have left the ground.

Secondly, to my colleagues whose friendship, support and advice helped lighten the long term effort. In particular I would like to single out Drs. Julian Eggleston, Neville Watson, Enrique Acha & Ranil de Silva, and postgraduates Gordon Cameron, Aurelio Medina, Sankar and Jerczy Ciechanowicz.

Thirdly, to my employers, TransPower (NZ) Ltd., by whose generous study leave and financial support I am able to complete this thesis.

Thanks also to my parents, who have never wavered in their support and confidence in my abilities over (especially) the past three years. They will, nonetheless, be relieved when it is all over.

I would like to make special mention of Dr. Richard Fright, who was a source of both friendship and inspiration not only to me, but to all who were associated with him.

Finally, to my many friends in the Cathedral of the Blessed Sacrament Choir and Orchestra, the Canterbury Opera Trust and the St. Teresa's liturgy group, to those who entered my life as strangers, stayed as flatmates and left as friends, and to all of the above, I offer my sincerest thanks.

CHAPTER 1

INTRODUCTION

1.1 HARMONIC SOURCES IN POWER SYSTEMS

To the casual observer the power system is often seen to be a bastion of certainty - an ideal source of single frequency power, neither deviating in magnitude, phase or frequency. The truth is rather different, however, and this has necessitated the development of power system analysis as it exists today.

Although, for many years, the purity of the power system waveform was held to be unquestionable, the current message is that power systems, as with almost all other systems, suffer from pollution - pollution in the form of harmonics.

In principle, any non-linear device is a potential source of waveform distortion, and the modern power system is full of examples. In spite of the linearity of transformer and generator models developed for, say, loadflow purposes, both of these fundamental power system elements are examples of non-linear devices, due to the non-linearity of the transformer magnetising characteristic, and the coupling between frequencies within the stator-rotor interactions in the generator.

However, the real culprits behind the wholesale harmonic pollution of the power system are the power electronic switches, whose presence permeates almost every aspect of the electricity industry : from generation, through transmission and distribution to consumption.

In New Zealand they are of particular importance given that nearly half of the South Island hydro resources are given over to supplying rectifier loads, while the North Island receives a significant proportion of its supply from the South Island via an HVDC interconnection. With planning underway to double the capacity of this link (and therefore the attendant harmonic generation) the associated harmonic phenomena can only increase.

1.2 HARMONIC ANALYSIS OF POWER SYSTEMS

Effective action to reduce the generation of harmonics, or to reduce in some way their detrimental effects may only be taken if the presence of harmonics can be predicted, and moreover quantitatively assessed during design stages. This is, however, only possible if suitable analysis tools are available.

Harmonic analysis can, in principle, be carried out in a number of ways. The two most significant classes of analysis tools are physical simulation and digital computation.

Physical simulation, as the name implies, simulates the network under study, and provided a suitably steady state can be reached, the harmonics present may be assessed. This method, however, while having to its advantage the inherent directness of simulating the physical network, suffers from a lack of one-to-one correspondence between the actual and simulated components. For example, the magnetisation characteristics of a scaled down transformer will almost never match those of the actual device, and so some accuracy will be lost in the simulation. The transmission line is another example of a power system component which cannot be simply represented in the laboratory without resorting to a large number of π-sections in order to model the harmonic response of the line. In addition, the mutual coupling between the lines is difficult to model, yet can be extremely significant at higher frequencies.

Digital computation as a simulation tool is becoming more and more attractive, with the explosion in computer technology bringing about large reductions in costs, to the point where the cost of hardware is typically incidental to the cost of the software. Applications which, a decade ago, would have occupied a specialised mainframe computer for a considerable period now run comfortably on a standard PC. Coupled with the inherent flexibility of computer simulation, the computer becomes an ideal simulation tool, limited only by the imagination and ingenuity of the programmer/user.

However, since not all analysis methods are necessarily suitable, three approaches to the harmonic analysis of large power convertors are here presented, with a view to selecting the one most suitable for the purpose of evaluating the steady state harmonic operation of large and medium sized convertor installations.

1.2.1 EMTDC

EMTDC (Woodford *et al.*, 1983) is a convertor analysis application based on the time-honoured Electromagnetic Transient Program (EMTP) (Dommel, 1969). As such, it incorporates component models based on the EMTP model. In particular, capacitors and inductors are represented as resistors in parallel with a dependent current source. The current source and resistor values are dependent on the original component value and the step size of the solution method (which is by trapezoidal integration), as shown in figure 1.1

The resistor/source combinations are assembled into a large matrix which is then inverted, prior to solution. If there are any suitable dividing points between different sections of the network, then the network can be subdivided into *subsystems* which may be solved separately, thus reducing the size of the matrices involved in the solution procedure.

If, for reasons of numerical accuracy or stability, the step size is changed, then the whole matrix must be reassembled and re-inverted.

In simulating the action of convertor, singularities such as switching instants should (ideally) fall exactly on one of the solution points. To accomplish this, however, the simulation step size may need to be changed, requiring the attendant network reformation. Alternatively, at the expense of introducing a small error into the solution points, the singularity may be assumed to occur at the nearest solution point.

Rather than modelling switchings explicitly, the convertor valves or SCRs are modelled as pure resistors which are given arbitrarily small values during conduction, and

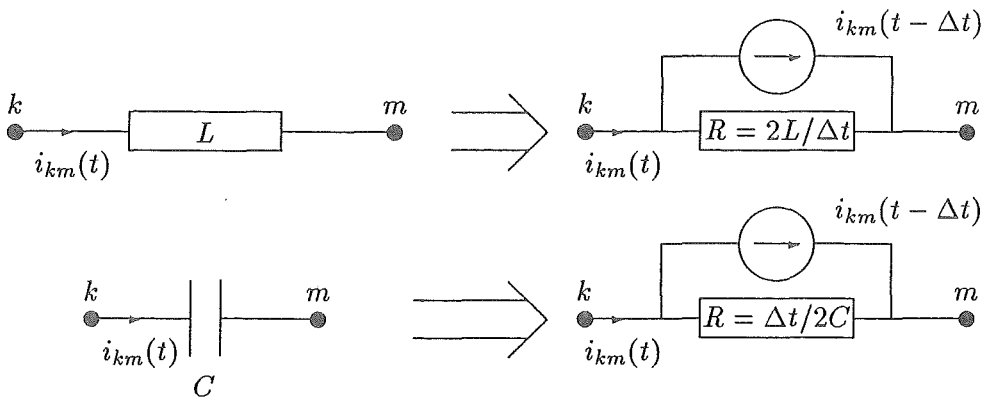

Figure 1.1: Capacitor and Inductor models in EMTP/EMTDC

correspondingly large values during non-conduction.

Equipment external to the convertor (generators, lines & transformers) are represented using the normal EMTP models. This allows lines to be modelled with account taken for their distributed nature, including frequency dependence.

The step-by-step integration of the solution allows easy incorporation of converter controller strategies, although problems of numerical oscillation, due to the approximations inherent in retaining a constant step size, have been reported (Campos-Barros and Rangel, 1985), and the integration scheme is susceptible to numerical noise, as discussed by Marti and Lin (1989).

One of the principal disadvantages from the users point of view is that setting up a particular system requires the writing of FORTRAN subroutines to 'drive' the simulation (e.g. to provide fault application/removal or convertor control strategies). On the other hand, creative use of the package is aided by the fact that subroutines to model convertor components and controllers are provided, and these are easily called from the 'driving' routine provided by the user.

Harmonic analysis using EMTDC requires sampling at the Nyquist rate, but higher rates are necessary if any form of transient behviour precedes the steady state. 100 samples per cycle of the highest required frequency has been found to be a useful rate.

In summary, EMTDC is a commercially available convertor simulation package which has gained relatively wide acceptance in the technical community. Harmonic analysis may be performed by running the solution into the steady state and extracting the harmonics using a Fourier transform. Provided that the errors due to the constant step size are acceptable, this is a reasonable method.

1.2.2 TCS

TCS, or Transient Convertor Simulation, developed at the University of Manchester (Al-Khashali, 1976) and subsequently at the University of Canterbury (Heffernan, 1980), has a similar solution technique to that of EMTDC, in that both employ step-by-step integration methods. However, in TCS the system is represented by actual values of

resistance, capacitance and inductance, and as such the solution is independent of step size. Network state-space equations are assembled and solved using inductor flux and capacitor charge as the state variables and the resulting matrices need only be inverted once. The convertor switching operations are performed by reassembling the convertor terminal nodes to represent the current switching state, and using diakoptic techniques to appropriately modify the inverted matrices to reflect this.

The EMTDC restriction of constant step size, therefore, does not apply, and so the solution points may be adjusted to fall *on* the exact instants of valve turn-on or turn-off. The step size is selected dynamically to suit the immediate conditions : a larger step size during steady conduction; a smaller one during faults, fast transients and commutations.

One of the earlier restrictions of TCS was that, since only resitive, inductive and capacitive components can be modelled, lines were modelled as a multiplicity of cascaded π sections which, for any degree of accuracy, required a large number of primitive components. This made the solution of such a network computationally expensive. However, recent work has enabled the a.c. system response to be modelled by a set of equivalent filter branches which optimally represent the frequency response of the system seen from the convertor busbar (Watson *et al.*, 1985). This allows the formation of a frequency dependent, mutually coupled representation of the a.c. system with a realistic number of primitive components. This procedure, still relatively new, may be applied to the d.c. system representation in a similar way (Watson, 1987).

For the purposes of harmonic assessment, the solution must have reached a suitably steady state, and a Fourier transform used to extract the harmonic content. Because of dynamic step size selection and the ability to accurately model the a.c. system response, harmonic assessment by TCS might be expected to be more accurate than EMTDC. However, also because of dynamic step size selection, the output solution points are unequally spaced, and since most numerical Fourier transform algorithms require evenly spaced data, interpolation must be used to obtain a set of suitable points. The time required to reach a steady state may be upward of 10 cycles,which is computationally expensive, considering only 1 cycle's worth of information is retained.

In summary, TCS is an accurate time domain simulation with the ability to model frequency dependent mutually coupled networks. However, as a harmonic assessment tool, it suffers from the drawback that several cycles of transient behaviour must be simulated before the steady state is reached.

1.2.3 IHA

IHA (Iterative Harmonic Analysis) is a general technique for solving for the harmonic generation of a non-linear device. It is essentially a frequency domain technique, although, for practical devices with switching non-linearities, regular excursions are made into the time domain.

The starting point for IHA is a loadflow solution, which gives the fundamental conditions at the device terminals, and this is used, in the first instance, to calculate an estimate of the device current waveform over one cycle under quasi steady state conditions. This current is then injected into the supply network to determine the harmonic voltages at the supply terminals. The updated voltages are used to re-estimate the

harmonic currents, which, in turn, may be used to re-evaluate the terminal voltage distortion. Thus, an iterative structure becomes apparent, as shown in figure 1.2.

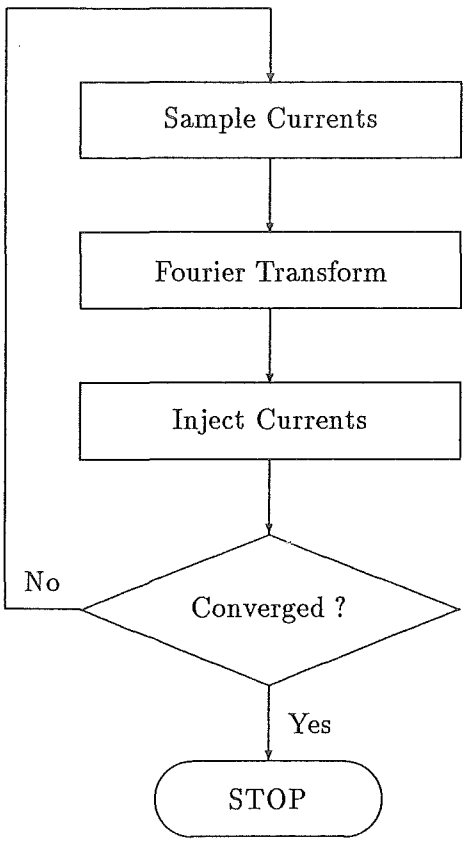

Figure 1.2: Structure of IHA algorithm

The number of iterations required depends on a number of factors, but the most important of these are the nature of the non-linearity and the harmonic impedance of the supply network. It is intuitively apparent that if either the device is particularly sensitive to the presence of distortion, or the harmonic impedances are particularly high, then the solution will take longer to converge.

The advantages of IHA for harmonic assessment lie in the fact that it is a frequency domain technique, and that it is designed for harmonic analysis, rather than merely being applied to it. The data requirements of the algorithm are fairly simple, being the initial loadflow point and the harmonic admittance matrix for the supply network. The latter provide a frequency dependent and mutually coupled network representation, and are reasonably simple to calculate, given a suitable program (Densem, 1983). Since the solution is in the frequency domain, there are no transients to decay before a steady state solution can be reached.

1.3 THE PRESENT WORK

This chapter has briefly described the causes and effects of harmonics in the power system. Three harmonic analysis techniques for HVDC convertor plant have been described and compared in, at least, a primitive sense. Of these three techniques (EMTDC, TCS, IHA), IHA appears to be best suited to the harmonic analysis, since this is its primary purpose, and since it doesn't suffer from the drawback of the time domain methods.

The next chapter discusses the application of IHA specifically to the HVDC convertor, and sets down the quasi-steady state equations which describe the convertor operation.

Chapter 3 is devoted to an examination of the facts surrounding divergence of IHA, and its physical interpretation. Particular attention is given to developing a 'theory' which (in principle) unifies all cases of divergence.

Chapter 4 develops a new three phase integrated load and harmonic flow algorithm based on existing three phase analysis tools, and employing the IHA algorithm as a fundamental part of it. A set of simple test cases are examined to assess the nature of the integrated algorithm.

Chapter 5 applies the integrated algorithm to a pair of systems pertinent to the New Zealand situation, both of which serve to justify the development and use of the new technique. In particular, harmonic interactions between remote harmonic sources are examined in the New Zealand context, thus opening a new field of potential research.

Finally, chapter 6 draws the conclusions together and offers suggestions for further research directions.

CHAPTER 2

APPLICATION OF IHA TO THE CONVERTOR

2.1 INTRODUCTION

The application of IHA to the convertor is by no means new, but may be traced back (in admittedly cruder form) to the late 1960s. Reeve *et al.* (1971) were among the first to describe the method, and it was quickly recognised by others.

Research into the topic at Canterbury began with the work of Harker (1980) who first formulated the problem here, and was subsequently extended by Eggleston (1985), who investigated a number of applications.

However, before detailing the mathematical model of the convertor, the general steady state operation of the standard 6-pulse convertor will be reviewed.

2.2 CONVERTOR OPERATION

The Graetz bridge is the universal building block of most convertor schemes, and consists of 6 valves (or thyristors) connected as shown in figure 2.1

The numbering on the valves is the firing order, and is based on the order in which the valves become forward biased. The emphasised valves (1 & 2) are assumed to be conducting at the instant shown, and, as such, the d.c. current is supplied from phase 'a', and returns via phase 'c', while the d.c. voltage, V_d, is the instantaneous difference between V_a and V_c.

The next valve to conduct (valve 3) may be fired at any instant during the interval it is forward biased, or, in other words, while V_b exceeds V_a. When this happens, V^+ begins to follow V_b, and since it is greater than V_a, then current in phase 'a' reduces to zero. As depicted in figure 2.1, with no supply impedance, this process, known as commutation, would occur instantaneously, and therefore the current in phase 'a' would be a rectangular pulse, lasting from the firing of valve 1 to the firing of valve 3. The commutation process takes place 6 times per fundamental frequency cycle, and it is analysis of this process in the presence of arbitrary distortion which is fundamental to the application of IHA to the convertor.

2.2.1 Commutation Process

In practice, the bridge is supplied from a network of finite impedance, and, as such, the change over from one valve to another takes a finite length of time. Although, in principle, the whole system impedance takes part in the commutation process, if the voltage at the terminal busbar of the convertor can be assumed to be reasonably sinusoidal (as

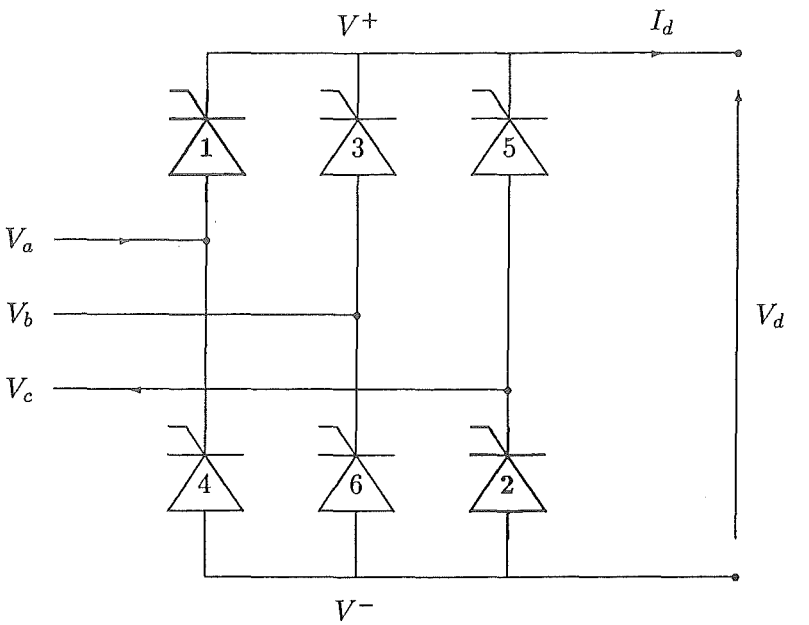

Figure 2.1: The basic Graetz bridge.

it would be with adequate filtering), then the principal role in the commutation process is played by the reactance of the convertor transformer.

If the situation of figure 2.1 is taken and redrawn at the instant of firing of valve 3, with transformer leakage inductances represented, then the configuration of figure 2.2 results.

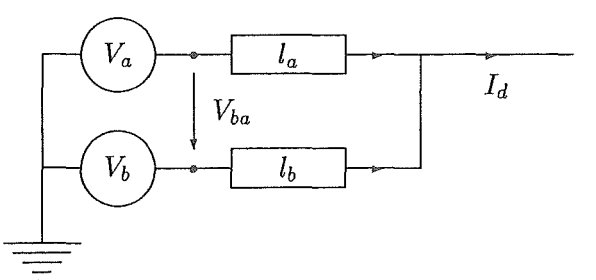

Figure 2.2: Equivalent circuit of the commutation process.

Applying Kirchoff's Voltage Law around the loop gives

$$v_a - l_a \frac{di_a}{dt} = v_b - l_b \frac{di_b}{dt} \tag{2.1}$$

or

$$v_{ba} = l_b \frac{di_b}{dt} - l_a \frac{di_a}{dt} \tag{2.2}$$

Applying Kirchoff's Current Law at the common cathode V^+ :

$$i_a + i_b = I_d \tag{2.3}$$

and if I_d is assumed to be reasonably flat, as would be the case with sufficient smoothing reactance in the d.c. circuit, then :

$$\frac{di_a}{dt} + \frac{di_b}{dt} = 0 \tag{2.4}$$

or

$$\frac{di_b}{dt} = -\frac{di_a}{dt} \tag{2.5}$$

and therefore

$$v_{ba}(t) = (l_a + l_b)\frac{di_b}{dt} \tag{2.6}$$

Solution of this equation is given by

$$i_b(t) = \frac{1}{l_{ab}} \int_0^t v_{ba}(\tau)\, d\tau + i_b(0) \tag{2.7}$$

and

$$i_a(t) = I_d - i_b(t) \tag{2.8}$$

where l_{ab} is the sum of the leakage inductances of the 2 phases, and $\tau = 0$ at the firing instant of valve 3.

The above equation is, of course, only valid during the commutation, since, when i_a is completely extinguished, valve 1 ceases to conduct, and can only be restarted by the application of a firing pulse while forward biased. Note also that at $\tau = 0$ the full load current is flowing in valve 1 (i.e. in phase 'a') and therefore $i_b(0) = 0$.

For a purely sinusoidal supply $v_{ba}(\tau) = \hat{V}_{ba} \sin(\omega\tau + \alpha)$, where α is the firing delay measured from the zero crossing of v_{ab}, the solution becomes :

$$\begin{aligned} i_b(t) &= \frac{\hat{V}_{ba}}{l_{ab}} \int_0^t \sin(\omega\tau + \alpha)\, d\tau \\ &= \frac{\hat{V}_{ba}}{\omega l_{ab}} [-\cos(\omega\tau + \alpha)]_0^t \\ &= \frac{\hat{V}_{ba}}{x_{ab}} [\cos(\alpha) - \cos(\omega t + \alpha)] \end{aligned} \tag{2.9}$$

where x_{ab} is the sum of the transformer *reactances* of the 2 phases.

The commutation concludes when $i_b(t) = I_d$, or, in other words, when

$$\cos(\omega t + \alpha) = \cos(\alpha) - \frac{I_d x_{ab}}{\hat{V}_{ba}} \tag{2.10}$$

Note that for $x_{ab} = 0$, i.e. no commutating reactance, $\cos(\omega t + \alpha) = \cos(\alpha)$, and therefore the commutation is instantaneous. As either I_d or x_{ab} increase, the commutation period lengthens, while for increasing commutating voltage ($\hat{V}_{ba}$) the commutation period shortens.

The potential at the common cathode point (V^+) during the commutation is given by :

$$\begin{aligned} v^+(t) &= v_a(t) - l_a\frac{di_a}{dt} \\ &= v_b(t) - l_b\frac{di_b}{dt} \end{aligned} \tag{2.11}$$

but since $\frac{di_a}{dt} = -\frac{di_b}{dt}$,

$$v^+ = \frac{1}{2}[v_a(t) + v_b(t) + (l_a - l_b)\frac{di_b}{dt}] \tag{2.12}$$

which has the physical interpretation that v^+ follows the average of the 2 phase voltages, provided that the commutating inductances are equal. Since i_b is the incoming phase, $\frac{di_b}{dt} > 0$ during the commutation, and therefore v^+ is reduced for $l_b > l_a$, and increased for $l_b < l_a$.

In each complete cycle there are 6 commutations, and therefore 6 periods of steady conduction. These are given in figure 2.3, which depicts one complete cycle of rectification, with points labelled as they will be referred to in the mathematical description of the convertor. Briefly, they are :

ZC_i - the point in time at which valve i becomes forward biased.

α_i - the delay between ZC_i and the firing instant of valve i.

θ_i - the instant in time at which valve i is fired.
i.e. $\theta_i = \mathrm{ZC}_i + \alpha_i$

μ_i - the time taken for valve i to commutate on.

2.3 MATHEMATICAL MODEL OF THE CONVERTOR.

The mathematical model of the convertor is determined by certain practical requirements. Provision must be made for accurate transformer models, and for the presence of distortion on both sides of the convertor. Since the purpose of the convertor model is to provide an updated estimate of its current waveform, a (quasi) steady state model is required, which takes as input the voltage distortion at the terminal busbar, and the current flowing on the d.c. side, and produces, as output, the a.c. current waveforms and the d.c. voltage waveform for the given input conditions.

2.3.1 Current Waveforms.

The a.c. current waveforms are calculated making no assumptions about the presence (or otherwise) of distortion at the terminal busbar or in the d.c. current. The 12 sections of the current waveforms (6 commutations and 6 periods of steady conduction) are calculated sequentially from the firing of valve 1.

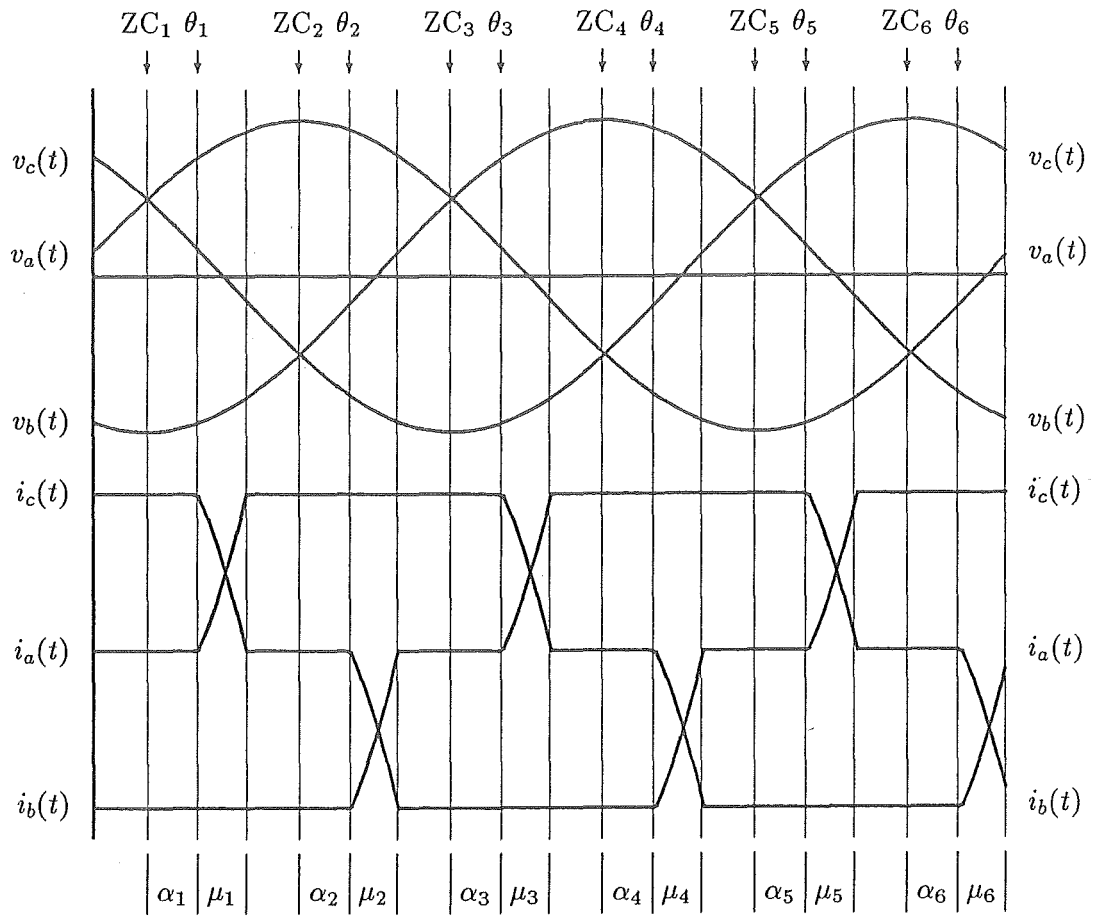

Figure 2.3: One cycle of rectification.

2.3.1.1 Commutating Current.

In order to calculate the commutating current in the presence of distortion, the distorted commutating voltage must be referred to the secondary of the convertor transformer. In so doing, the transformer is essentially 'split' into an ideal transformer (representing winding arrangements and off-nominal taps only) in series with its leakage impedance, with the referred commutating voltages in between. This may be more easily visualised with reference to figure 2.4.

Mathematically the process of referring the harmonic voltages across the transformer, for the two of the most common winding arrangements, is accomplished as follows.

The primary voltages are given by :

$$
\begin{aligned}
v_a(t) &= \sum_h \hat{V}_a \sin(h\omega t + \phi_a^h) \\
v_b(t) &= \sum_h \hat{V}_b \sin(h\omega t + \phi_b^h)
\end{aligned}
$$

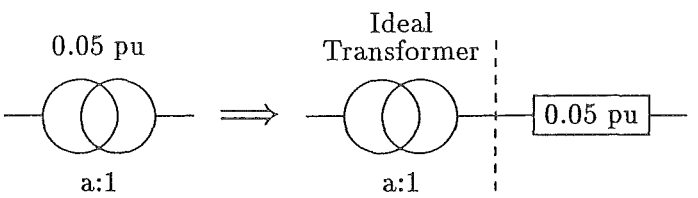

Figure 2.4: Separation of the transformer into (ideal) winding configuration plus leakage

$$v_c(t) = \sum_h \hat{V}_c \sin(h\omega t + \phi_c^h) \tag{2.13}$$

where $\hat{V}_a^h, \hat{V}_c^h, \hat{V}_c^h, \phi_a^h, \phi_b^h, \phi_c^h$ are the peak magnitudes and phases of the h^{th} harmonic on phases 'a', 'b' and 'c' respectively. $\sum_h$ indicates summation over all relevant harmonics, h.

For the case of a star-star transformer, the winding configuration is given in figure 2.5.

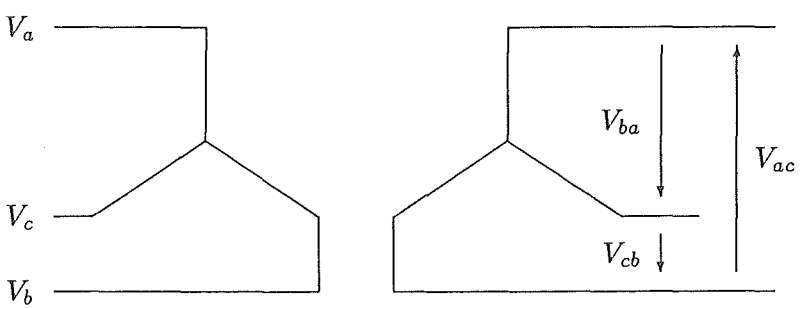

Figure 2.5: Star-Star transformer winding configuration.

The time functions of the voltages referred to the secondary are therefore :

$$\begin{aligned}
v_{ac}(t) &= \frac{1}{a_a}\sum_h \hat{V}_a^h \sin(h\omega t + \phi_a^h) - \frac{1}{a_c}\sum_h \hat{V}_c^h \sin(h\omega t + \phi_c^h) \\
v_{ba}(t) &= \frac{1}{a_b}\sum_h \hat{V}_b^h \sin(h\omega t + \phi_b^h) - \frac{1}{a_a}\sum_h \hat{V}_a^h \sin(h\omega t + \phi_a^h) \\
v_{cb}(t) &= \frac{1}{a_c}\sum_h \hat{V}_c^h \sin(h\omega t + \phi_c^h) - \frac{1}{a_b}\sum_h \hat{V}_b^h \sin(h\omega t + \phi_b^h)
\end{aligned} \tag{2.14}$$

The relations for the star-delta configuration (figure 2.6) are somewhat more direct :

$$v_{ac}(t) = \frac{-1}{a_c}\sum_h \hat{V}_c^h \sin(h\omega t + \phi_c^h)$$

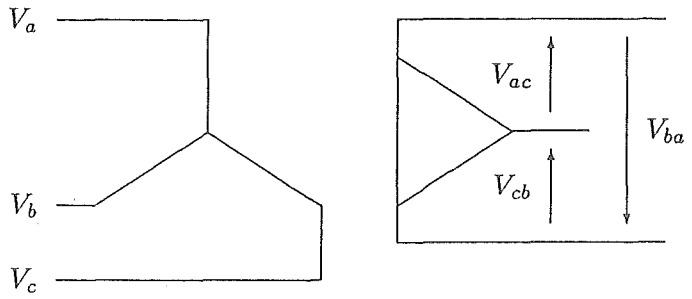

Figure 2.6: Star-Delta transformer winding configuration.

$$\begin{aligned} v_{ba}(t) &= \frac{-1}{a_a}\sum_h \hat{V}_a^h \sin(h\omega t + \phi_a^h) \\ v_{cb}(t) &= \frac{-1}{a_b}\sum_h \hat{V}_b^h \sin(h\omega t + \phi_b^h) \end{aligned} \tag{2.15}$$

The commutating on of a valve, and the attendant commutating off of another, is modelled using a similar technique to that demonstrated earlier in the chapter, where the commutation current of phase 'b' was shown to be

$$i_b(t) = \frac{1}{l_{ab}}\int_0^t v_{ba}(\tau)\, d\tau + i_b(0) \tag{2.16}$$

In the presence of harmonics the purely sinusoidal $v_{ba}(\tau)$ is replaced by its harmonic series $\sum_h \hat{V}_{ba}^h \sin(h\omega\tau + \phi_{ba}^h)$, where $\hat{V}_{ba}^h$ and ϕ_{ba}^h are derived from equation 2.14 or 2.15 as appropriate.

Therefore, the commutating current in phase 'b' is given by :

$$\begin{aligned} i_b(t) &= \frac{1}{l_{ab}}\int_{\frac{\theta_3}{\omega}}^t \sum_h \hat{V}_{ba}^h \sin(h\omega\tau + \phi_{ba}^h)\, d\tau \\ &= \frac{1}{\omega l_{ab}}\int_{\theta_3}^{\omega t} \sum_h \hat{V}_{ba}^h \sin(h\omega\tau + \phi_{ba}^h)\, d(\omega\tau) \\ &= \frac{1}{x_{ab}}\left[-\sum_h \frac{\hat{V}_{ba}^h}{h}\cos(h\omega\tau + \phi_{ba}^h)\right]_{\phi_3}^{\omega t} \\ &= \frac{1}{x_{ab}}\left[\sum_h \frac{\hat{V}_{ba}^h}{h}\left[\cos(h\theta_3 + \phi_{ba}^h) - \cos(h\omega t + \phi_{ba}^h)\right]\right] \end{aligned} \tag{2.17}$$

which has a similar form to that given for the case where harmonics are ignored. Similar equations hold for phases 'a' & 'c' with a cyclic change of suffices :

$$i_a(t) = \frac{1}{x_{ac}}\left[\sum_h \frac{\hat{V}_{ac}^h}{h}\left[\cos(h\theta_1 + \phi_{ac}^h) - \cos(h\omega t + \phi_{ac}^h)\right]\right] \tag{2.18}$$

$$i_c(t) = \frac{1}{x_{bc}}\left[\sum_h \frac{\hat{V}_{cb}^h}{h}\left[\cos(h\theta_5 + \phi_{cb}^h) - \cos(h\omega t + \phi_{cb}^h)\right]\right] \tag{2.19}$$

Alternatively, if some resistance is to be explicitly included in the commutating impedance, then the equation derived by Yacamini and de Oliveira (1986) may be used. This equation is given by :

$$i_n(t) = \sum_{h=1}^{50}(X_h e^{-t/T_{nm}} + S_h \sin(h\omega t + \phi_h)) + Y(1 - e^{-t/T_{nm}}) + C_{nm} \qquad (2.20)$$

where

$$\begin{aligned} X_h &= \frac{B_h}{L_{nm}} \frac{H_h - 1/T_{nm}}{h^2\omega^2 + 1/T_{nm}^2} \\ S_h &= \frac{B_h}{h\omega L_{nm}} \sqrt{\frac{H_h^2 + h^2\omega^2}{h^2\omega^2 + 1/T_{nm}^2}} \\ Y &= \frac{R_m I_d}{R_{nm}} \end{aligned}$$

n is the incoming phase number, m is that of the outgoing phase and

$$\begin{aligned} R_{nm} &= R_n + R_m \\ L_{nm} &= L_n + L_m \\ T_{nm} &= L_{nm}/R_{nm} \\ A_h &= \hat{V}_{hn}\cos(h\theta_n + \phi_{hn}) - \hat{V}_{hm}\cos(h\theta_n + \phi_{hm}) \\ B_h &= \hat{V}_{hn}\sin(h\theta_n + \phi_{hn}) - \hat{V}_{hm}\sin(h\theta_n + \phi_{hm}) \\ H_h &= h\omega A_h/B_h \\ \phi_h &= \tan^{-1}(\frac{1}{h\omega T_{nm}}) - \tan^{-1}(\frac{H_h}{h\omega}) \end{aligned}$$

where $\hat{V}_{hn}$ & ϕ_{hn} are the magnitude and phase of the h^{th} harmonic of the phase to neutral voltage of the incoming phase, and $\hat{V}_{hm}$ & ϕ_{hm} are similarly defined for the outgoing phase. C_{nm} is an integration constant such that $i_n(0) = 0$.

Whichever equation is used, the instantaneous current in the phase that is commutating off is given by :

$$i_{\text{off}}(t) = i_d(t) - i_{\text{on}}(t) \qquad (2.21)$$

where $i_{\text{off}}(t)$ and $i_{\text{on}}(t)$ are the currents in the commutating off and commutating on phases respectively, and $i_d(t)$ is the instantaneous d.c. current, given by :

$$i_d(t) = I_d + \sum_h \hat{I}_d^h \sin(h\omega t + \phi_d^h) \qquad (2.22)$$

where I_d is the d.c. component of the d.c. current, and $\hat{I}_d^h$ & ϕ_d^h are the h^{th} harmonic components of ripple in the d.c. current.

A commutation is assumed to be concluded when the instantaneous value of the commutating on current exceeds that of the d.c. current.

2.3.1.2 Steady Conduction

During periods of steady conduction (and at least one phase is conducting steadily at all times) the current flowing in that phase is that current flowing on the d.c. side of the convertor, as given in equation 2.22, with a positive sign if that phase is connected to the common cathode point, and a negative sign if connected to the common anode.

During periods of non-conduction, the current in the non-conducting phase is set to zero.

2.3.1.3 Assembling the Current Waveforms

The current waveforms are sampled at regular intervals, beginning at $\omega t = \theta_1$ - the firing instant of valve 1. The reason for this is that the conducting state of all valves and all phase currents are well defined at this instant. Inherent in this logic is the assumption that no commutation will last more than 60°.

The process of sampling the currents is described by table 2.1, which gives the instantaneous values of each of the phase currents, with the limits between which the values are valid.

Limits		Phase A current	Phase B current	Phase C current
θ_1	$\theta_1 + \mu_1$	$i_a(t)$	$-i_d(t)$	$i_d(t) - i_a(t)$
$\theta_1 + \mu_1$	θ_2	$i_d(t)$	$-i_d(t)$	0
θ_2	$\theta_2 + \mu_2$	$i_d(t)$	$-i_d(t) - i_c(t)$	$i_c(t)$
$\theta_2 + \mu_2$	θ_3	$i_d(t)$	0	$-i_d(t)$
θ_3	$\theta_3 + \mu_3$	$i_d(t) - i_b(t)$	$i_b(t)$	$-i_d(t)$
$\theta_3 + \mu_3$	θ_4	0	$i_d(t)$	$-i_d(t)$
θ_4	$\theta_4 + \mu_4$	$i_a(t)$	$i_d(t)$	$-i_d(t) - i_a(t)$
$\theta_4 + \mu_4$	θ_5	$-i_d(t)$	$i_d(t)$	0
θ_5	$\theta_5 + \mu_5$	$-i_d(t)$	$i_d(t) - i_c(t)$	$i_c(t)$
$\theta_5 + \mu_5$	θ_6	$-i_d(t)$	0	$i_d(t)$
θ_6	$\theta_6 + \mu_6$	$-i_d(t) - i_b(t)$	$i_b(t)$	$i_d(t)$
$\theta_6 + \mu_6$	$\theta_1 + 2\pi$	0	$-i_d(t)$	$i_d(t)$

Table 2.1: A.C. current waveform sampling process.

2.3.2 The D.C. Voltage

At the same time as the current waveforms are sampled, the d.c. voltage waveform may also be sampled, since it may be divided up into the same 12 periods of conduction and commutation.

During periods of steady conduction, only one valve on each side of the bridge conducts, and therefore the d.c. voltage is merely the appropriate phase to phase voltage. Inherent in this is the assumption that there is no forward voltage drop across the

commutating impedance, which is justified because the current flowing during steady conduction is essentially flat, and therefore the only voltage drop is across the resistive component of the impedance.

During commutations, there are 3 valves conducting, and calculation of the d.c. voltage is more complex. The approach used here is similar to that used in the single frequency case, described earlier.

Figure 2.7 depicts the situation with valve 1 commutating to valve 3.

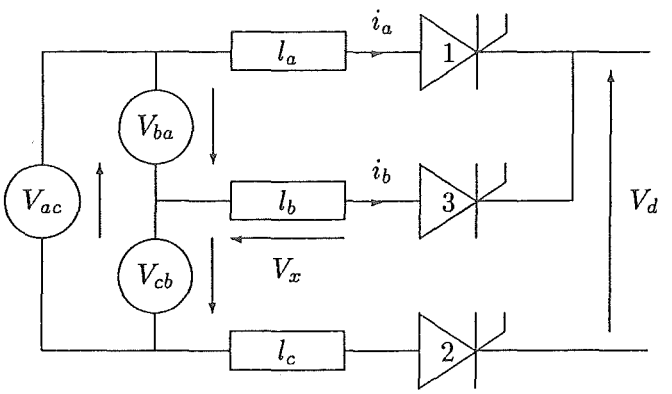

Figure 2.7: Calculation of D.C. voltage during commutation.

From figure 2.7 it can be seen that :

$$v_d(t) = -v_{cb}(t) - v_x(t) \tag{2.23}$$

where $v_x(t) = l_b \frac{di_b}{dt}$. Applying Kirchoff's Voltage law around the commutating loop,

$$v_{ba}(t) = l_{ab} \frac{di_b}{dt} \tag{2.24}$$

so that

$$v_x(t) = \frac{-l_b}{l_{ab}} v_{ba}(t) \tag{2.25}$$

and therefore

$$v_d(t) = \frac{-l_b}{l_{ab}} v_{ba}(t) - v_{cb}(t) \tag{2.26}$$

where $v_{ba}(t)$ and $v_{cb}(t)$ are represented by the harmonic time series described earlier. The 12 sections of the d.c. voltage waveform, therefore, are given in the table 2.2.

2.4 SOLUTION TECHNIQUE.

The steady state harmonic generation of the convertor is solved using the IHA technique described briefly in chapter 1. The solution is logically separated into three distinct

Limits		$v_d(t)$	Conducting Valves
θ_1	$\theta_1+\mu_1$	$\frac{-l_a}{l_{ac}}V_{ac}-V_{ba}$	1,5,6
$\theta_1+\mu_1$	θ_2	$-V_{ba}$	1,6
θ_2	$\theta_2+\mu_2$	$\frac{l_c}{l_{bc}}V_{cb}+V_{ac}$	1,2,6
$\theta_2+\mu_2$	θ_3	V_{ac}	1,2
θ_3	$\theta_3+\mu_3$	$\frac{-l_b}{l_{ab}}V_{ba}-V_{cb}$	1,2,3
$\theta_3+\mu_3$	θ_4	$-V_{cb}$	2,3
θ_4	$\theta_4+\mu_4$	$\frac{l_a}{l_{ac}}V_{ac}+V_{ba}$	2,3,4
$\theta_4+\mu_4$	θ_5	V_{ba}	3,4
θ_5	$\theta_5+\mu_5$	$\frac{-l_c}{l_{bc}}V_{cb}-V_{ac}$	3,4,5
$\theta_5+\mu_5$	θ_6	$-V_{ac}$	4,5
θ_6	$\theta_6+\mu_6$	$\frac{l_b}{l_{ab}}V_{ba}+V_{cb}$	4,5,6
$\theta_6+\mu_6$	$\theta_1+2\pi$	V_{cb}	5,6

Table 2.2: D.C. voltage sampling process.

parts : solution of the a.c. network, solution of the convertor operation and solution of the d.c. network.

Solution of the convertor operation (under arbitrary harmonic conditions) has been described in section 2.3, and needs little further elaboration, while the details of solving the a.c. and d.c. networks are given in sections 2.4.3 & 2.4.4.

Figure 2.8 is the flowchart of the IHA algorithm applied the the convertor, the steps of which are described more fully in the following sections.

2.4.1 Read Initial Conditions

The initial operating state of the convertor as determined by a loadflow is read in. It consists of the terminal busbar fundamental voltage magnitudes and phases ($\hat{V}_a$, $\hat{V}_b$, $\hat{V}_c$, ϕ_a, ϕ_b, ϕ_c), the commutating reactances (x_a,x_b,x_c), the set of firing angles (α_i), the d.c. current level (I_d), the transformer taps (a_i) and the transformer connection information. Also required are the a.c. and d.c. system harmonic admittance matrices.

2.4.2 Calculate A.C. Harmonic Currents

The a.c. current waveforms are sampled using the 12 section current model equations described in section 2.3, table 2.1. The three phases are sampled simultaneously with the d.c. voltage waveform, which is calculated using the 12 section d.c. voltage model described in section 2.3, table 2.2. The time domain waveforms are then transformed into the frequency domain using the Fast Fourier Transform (FFT) algorithm, yielding a cos series referenced to θ_1, the firing instant of the first valve. This series is referred back to the system angle reference by time-shifting the series by $-\theta_1$, which is equivalent to rotating each frequency h by $-h\theta_1$. In addition, the phasors are then rotated by a further $\frac{\pi}{2}$ radians to convert the cos series into a sin series.

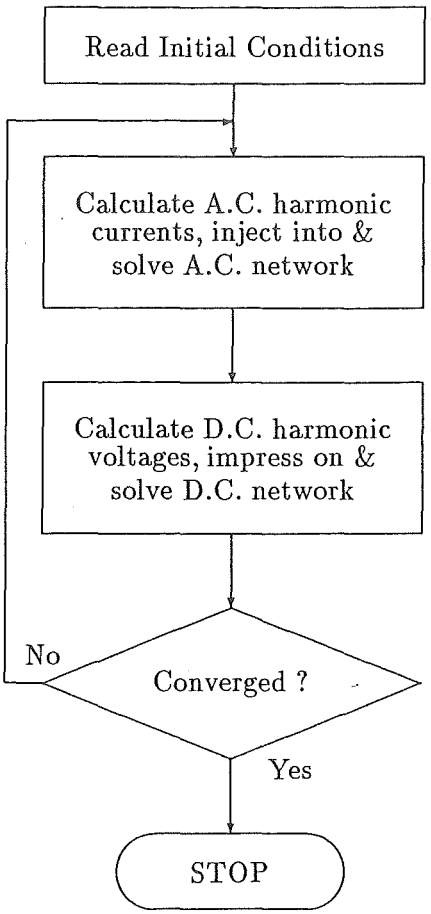

Figure 2.8: Flowchart of the IHA process applied to the convertor.

2.4.3 Solution of the A.C. Network

The harmonic currents are injected into the a.c. system harmonic admittance matrices, one frequency at a time.

The size of the admittance matrices depends on 2 parameters : N_T - the number of terminal busbars, and N_C - the number of convertors. A terminal busbar is one to which at least one convertor is connected (via a transformer), so that $N_C \geq N_T$ always. For example, the sample system in figure 2.9 has 3 convertors, but they are connected to only 2 busbars - therefore $N_T = 2$ & $N_C = 3$.

The admittance matrices for the a.c. system up to the terminal busbars are formed externally, and are of order $3N_T \times 3N_C$ - in figure 2.9 they are 6×6.

A 6×6 admittance matrix is formed for each convertor transformer (based on its leakage impedance and winding arrangement) and added to the system admittance matrices to give a composite matrix of size $3(N_T + N_C) \times 3(N_T + N_C)$. The structure of this matrix for the example of figure 2.9 is as follows :

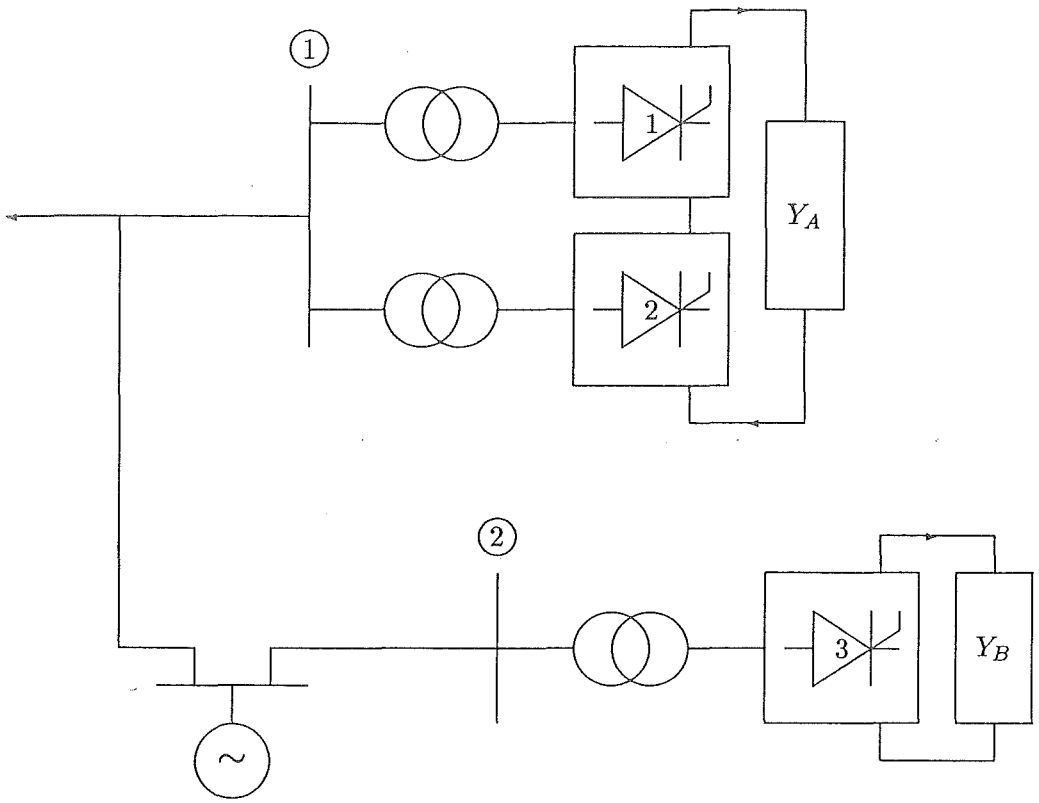

Figure 2.9: Example of convertor interconnection.

$$\begin{pmatrix} 0 \\ 0 \\ I_1 \\ I_2 \\ I_3 \end{pmatrix} = \begin{bmatrix} Y_{11}+Y_{PP1}+Y_{PP2} & Y_{12} & Y_{PS1} & Y_{PS2} & \\ Y_{21} & Y_{22}+Y_{PP3} & & & Y_{PS3} \\ Y_{SP1} & & Y_{SS1} & & \\ Y_{SP2} & & & Y_{SS2} & \\ & Y_{SP3} & & & Y_{SS3} \end{bmatrix} \begin{pmatrix} V_{P1} \\ V_{P2} \\ V_{S1} \\ V_{S2} \\ V_{S3} \end{pmatrix} \tag{2.27}$$

where $Y_{PPi}, Y_{PSi}, Y_{SPi}$ and Y_{SSi} are the primary-self, primary-secondary, secondary-primary and secondary-self three phase admittance matrices for convertor transformer i, and the terms $Y_{11}, Y_{12}/Y_{21}$ and Y_{22} are the self, mutual and self three phase nodal admittance matrices for terminal busbars 1 and 2 respectively. This is repeated for each frequency of interest.

The left hand side (LHS) excitation vector contains zero in the first two places, since the external harmonic injections take place at the convertor busbars only, while the right hand side (RHS) result vector contains the harmonic voltages at both the primary and secondary of the convertor transformer.

Equation 2.27 is solved by factorizing the admittance matrix and performing for-

ward & backward substitution to solve for the primary voltages V_{Pi}. The secondary harmonic voltages (V_{Si}) are also found, but, being of little practical use, are discarded.

2.4.4 Solution of the D.C. Network

The d.c. voltage harmonics are impressed on the d.c. system impedance at each frequency, to give the harmonic currents flowing in the d.c. network. The d.c. system harmonic admittance matrix is formed externally, and therefore must contain the interconnection information for the d.c. network at harmonic frequencies. The matrix is of order N_C, and for the example of figure 2.9 has the following structure :

$$\left[Y_{dc}^h\right] = \begin{bmatrix} Y_A^h & Y_A^h & 0 \\ Y_A^h & Y_A^h & 0 \\ 0 & 0 & Y_B^h \end{bmatrix} \tag{2.28}$$

and the currents are found by simple matrix multiplication :

$$\begin{pmatrix} I_{d1}^h \\ I_{d2}^h \\ I_{d3}^h \end{pmatrix} = \begin{bmatrix} Y_A^h & Y_A^h & 0 \\ Y_A^h & Y_A^h & 0 \\ 0 & 0 & Y_B^h \end{bmatrix} \begin{pmatrix} V_{d1}^h \\ V_{d2}^h \\ V_{d3}^h \end{pmatrix} \tag{2.29}$$

at each frequency h.

Since each set of V_{di}^h is a sin series referenced to the system angle reference, the harmonic currents found by solving equation 2.29 are also a sin series with the same angle reference. This must be accounted for when the d.c. current harmonics are used to calculate the instantaneous d.c. current values in the a.c. current and d.c. voltage sampling procedure.

2.5 CONVERGENCE

Convergence is said to have been obtained when the harmonics of successive iterations are sufficiently close that further iterations would yield no significant change. In other words, the harmonic voltages and currents form a self-sustaining set. Determining whether or not this condition has been reached can be accomplished in a number of ways.

Directly comparing the harmonic voltages of successive iterations is the most obvious, with the advantage that every harmonic is individually inspected for convergence. However, it is difficult to assign a realistic tolerance to such a test : characteristic harmonics are generally present at a higher level than non-characteristic harmonics, which rules out the possibility of using some absolute tolerance level, such as, say 0.000001 pu, since different harmonics will converge to different levels. If a relative or percentage measure of the difference between successive iterations is used, it eliminates that problem, but replaces it with another. Very small amounts of uncharacteristic harmonics are generated even in the most balanced case, and the relative change in these between successive iterations can be greater than 100%, giving the impression that convergence has not been obtained even if the overall solution is not significantly affected.

Another way of determining convergence is to compare some suitable attribute of the two sets of harmonic voltages. One such attribute which has been used successfully in the past is the set of zero crossings, ZC_i. These can be calculated from either the commutating voltages or the phase voltages using a suitable numerical method, and taking, as initial conditions, the zero crossings from the previous iteration. When the shift in zero crossings between iterations reduces to below some tolerance, e.g. 0.0001 radians ($\simeq 0.006°$), then the harmonics are assumed to have converged. One advantage of this method which garnered much favour in earlier days was the efficient use of memory, since it is only necessary to retain 6 values per convertor ($ZC_1 - ZC_6$) from the previous iteration, compared with up to 300 (3 phases, 50 harmonics per phase, real and imaginary values for each harmonic) values in the case of direct comparison. The major setback of this method is the susceptibility of the numerical method (typically a *regula falsi* method) used for recalculating the zero crossings to fail in the presence of distortion. This was originally assumed to be due to the presence of multiple zero crossings, indicating excessive distortion. However it can also be caused by 'flattening' of the commutating voltage during commutations, resulting in a near zero slope on the voltage waveform which confuses the numerical method.

The method adopted throughout most of this thesis is a combination of the direct comparison and attribute comparison techniques, since it requires the previous iteration harmonic voltages to be retained, but only uses three attributes (one per phase) to ascertain convergence or otherwise. The attribute for each phase i at iteration k is defined as :

$$\xi_i = \sum_h \|V_i^{h,k} - V_i^{h,k-1}\| \frac{\|V_i^{h,k}\| + \|V_i^{h,k-1}\|}{2} \tag{2.30}$$

which corresponds to summing the magnitudes of the phasor differences between successive iterations, weighted by the average of the two phasor magnitudes, so that more weight is assigned to the larger harmonics, less to the smaller ones. Convergence is assumed when all the convergence attributes have reduced to less than 0.001 of their original values, where the original values are those calculated on the first iteration, and therefore measure the impact of the introduction of the harmonics. This method has the advantage that it is relatively insensitive to 'noise level' harmonics (since they are small in magnitude) and a tolerance level is assigned which adapts to the particular case. For example, using an absolute tolerance level on a system with low harmonic distortion would result in very few iterations before apparent convergence, with the result that full harmonic interaction may not have taken place. Conversely, in a system with high harmonic distortion, the convergence criterion might never be satisfied, even though the harmonic interaction had been adequately solved.

2.6 SIMPLE TEST SYSTEM

The following simple example (figure 2.10) is cited to demonstrate the validity of the IHA technique applied to the static convertor. The solution may be obtained by 2 methods : IHA and direct solution.

The direct solution is based on the fact the E is a purely sinusoidal voltage source. The commutating reactance is taken as the series combination of X_{SYS} and X_C, and

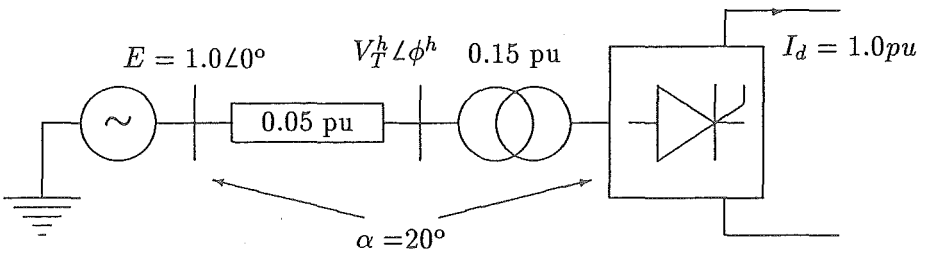

Figure 2.10: A simple test system.

is used (with α and E) to calculate the current waveform in each phase. These are transformed into the frequency domain using an FFT, and are then used to calculate the harmonic voltages at the terminal busbar. As the presence of distortion in the current waveform does not affect E (it is a perfect voltage source) the solution need proceed no further.

The fundamental conditions from the direct method (the terminal busbar fundamental voltage and the effective delay angle measured with respect to it) are used to fuel the IHA technique. The characteristic harmonics are compared in table 2.3.

	Current				Voltage			
	Direct Method		IHA		Direct Method		IHA	
h	Mag.	Phase.	Mag.	Phase.	Mag.	Phase.	Mag.	Phase.
1	0.7762	−30.47°	0.7762	−30.33°	0.9809	−1.95°	0.9809	−1.95°
5	0.1391	27.44°	0.1391	28.16°	0.0348	−62.6°	0.0348	−61.8°
7	0.0886	−33.93°	0.0885	−32.92°	0.0310	−124.0°	0.0310	−123.0°
11	0.0386	21.74°	0.0384	23.24°	0.0212	−68.3°	0.0211	−66.8°
13	0.0244	−42.35°	0.0241	−40.63°	0.0158	−132.35°	0.0157	−130.6°
17	0.0072	−6.79°	0.0069	−6.34°	0.0061	−96.8°	0.0059	−96.3°
19	0.0038	−113.3°	0.0038	−116.9°	0.0036	156.7°	0.0036	153.1°
23	0.0058	−123.2°	0.0062	−121.9°	0.0066	146.8°	0.0071	148.0°
25	0.0064	168.0°	0.0068	170.3°	0.0079	77.95°	0.0085	80.3°

Table 2.3: Comparison of Direct and IHA solutions for a simple case.

The effective firing angle used in the IHA solution is simply the firing angle with respect to the perfect source E, modified by the phase shift between E and the terminal busbar, i.e.

$$\alpha_{\text{mod}} = 20.0° - 1.95°$$

and the IHA process converged in 8 iterations. The resultant waveforms for the 3

phase voltages and currents are given in figure 2.11.

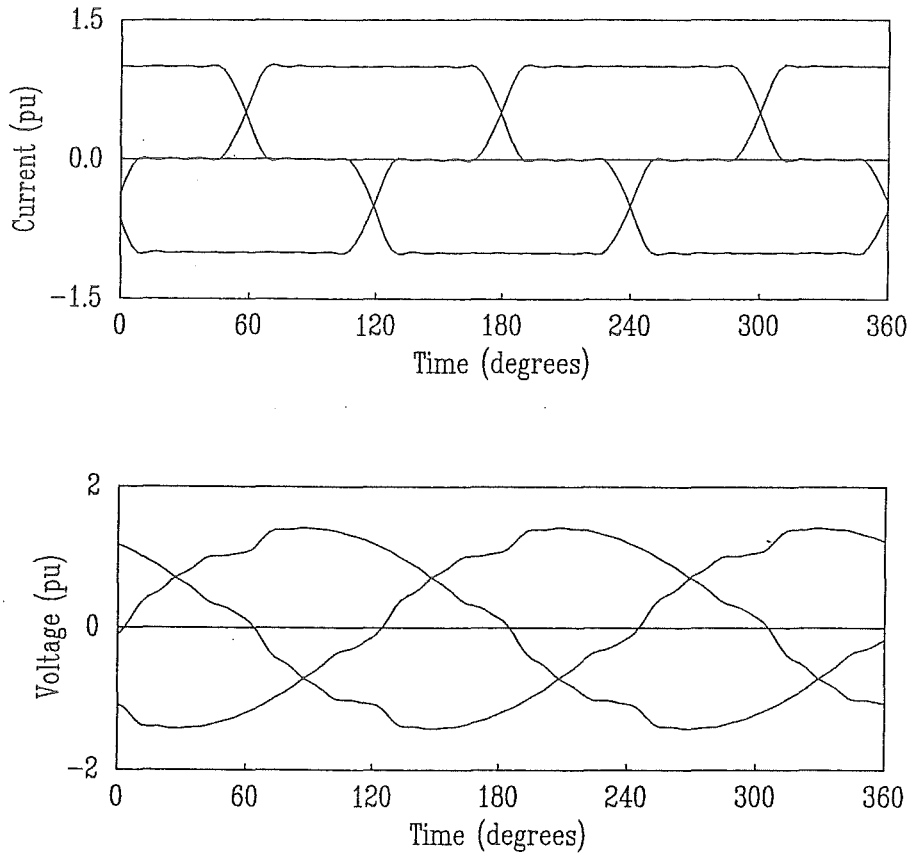

Figure 2.11: Reconstructed waveforms from the IHA results of the simple test system.

The similarity between the results of IHA and the direct method prove that IHA is eminently suited to this type of analysis, and a convergent solution is very accurate indeed. This imparts a considerable degree of confidence in the iterative approach, which is necessary, since most practical situations preclude verification with the direct method. For example, the presence of only one simple shunt component between the source voltage E and the convertor would prevent the direct method from being used.

2.7 CONCLUSIONS

This chapter has been concerned with developing the mathematical theory of steady-state Graetz bridge operation such that it may be used within the iterative structure of the general IHA algorithm described in chapter 1.

Equations governing the calculation of a.c. current waveforms and d.c. voltage waveforms have been derived in terms of the distorted commutating voltages, the commutating impedances, and the d.c. current including arbitrary ripple components. Since no assumptions have been made either about the magnitude of the harmonics present, or the degree of balance of the supply voltages or commutating impedances, or even the frequency response of the supply system, the mathematical representation is completely general.

Inclusion of the convertor transformer has been achieved by incorporating it into the admittance matrix of the supply network, and the general structure of the admittance matrices on both the a.c. and d.c. sides of the bridge have been derived to complete the description of the application of IHA to the convertor.

The criteria by which convergence may be measured have been discussed, and a method based on a combination of direct comparison and attribute comparison has been selected on the basis that it could adapt itself to suit a particular situation.

Finally a simple test system has been solved by both IHA and a direct solution (to which it was readily adaptable) and the comparison of results was sufficiently good to inspire confidence in the converged IHA solution.

Since IHA has been shown to be accurate (by the example at the end of this chapter and elsewhere) the next step is to examine it under divergent/non-convergent conditions to determine whether convergence can still be achieved, whether non-convergent conditions can be predicted, and what (if any) is the physical interpretation of a divergent solution.

CHAPTER 3

INSTABILITY IN ITERATIVE HARMONIC ANALYSIS

3.1 INTRODUCTION

Since its introduction in simple form in the early seventies, IHA has been shown to be an accurate means of assessing the harmonics of non-linear devices, including static power convertors (Reeve *et al.*, 1971; Yacamini and de Oliveira, 1980) and transformers in saturation (Dommel *et al.*, 1986). More recent work has favourably compared the IHA algorithm to an equivalent time domain simulation and to an analytically solvable system with excellent results, verifying not only the formulation of the IHA approach, but also of the time domain study (TCS) (Arrillaga *et al.*, 1987). However, if the algorithm should fail to converge, as it is known to do, then an explanation is required; especially so if the operating conditions are reasonable.

Most mathematical algorithms can be shown to be unstable in certain situations, and these situations determine the suitability of the algorithm to the application. Time domain simulations involving step-by-step integration of the system differential equations can become unstable when the integration algorithm used is not compatible with the form of the solution. Use of finite precision arithmetic is also a problem, since any error in the calculation of the next solution point will (generally) be carried forward into the calculation of subsequent points. Similar considerations are likely to apply to IHA type algorithms, as is the observation that a genuinely unstable situation would be reflected to some degree in the performance of the algorithm.

The term 'harmonic instability' is defined by both Ainsworth (1981) and Arrillaga (1983) as being magnification of non-characteristic frequencies by a convertor system containing, initially, no unbalance or asymmetry, and there have been a number of examples of harmonic instabilities reported in the context of HVDC transmission in recent years. Holmborn and Martensson (1966) reported on a third harmonic instability which often developed in the Cross-Channel link under certain a.c. system conditions, rendering the link inoperable. This problem was alleviated by the inclusion of a third harmonic filter — a solution which was adopted at the design stage of the Sardinian HVDC terminal (Natale *et al.*, 1966). A similar problem, although this time related to the second harmonic, was found to exist in the Kingsnorth scheme (Last *et al.*, 1966). Within New Zealand, excessive ninth harmonic was observed at the Benmore terminal of the New Zealand HVDC interconnection, and a ninth harmonic filter was necessary to solve this problem (Robinson, 1966). Kauferle *et al.* (1970) characterised harmonic instabilities by the excessive levels of harmonic distortion associated with them, often rendering the link inoperable.

For the purposes of precision, the term harmonic instability will henceforth be used

only to refer to a case where the physical system is harmonically unstable, and cases in which IHA fails to converge will be termed 'algorithmically unstable'.

3.1.1 Review of IHA Research

Prior to 1970, the topic of convertor harmonics was approached by considering aspects of harmonic generation separately. Commutating impedance unbalance was analysed separately from terminal voltage unbalance, and the effects of controllers considered separately again. In fact Rissik (1939) described in the late thirties many of the harmonic phenomena still under investigation today.

Reeve and Baron's algorithm (Reeve *et al.*, 1971) was virtually the earliest application of IHA to the convertor, and, although somewhat cruder than current formulations, apparently still suffered from problems of convergence. This was seen by the authors as indicating either an harmonic instability, or at least a potantial harmonic instability.

Yacamini and de Oliveira described their formulation of the algorithm in 1980 (Yacamini and de Oliveira, 1980), and were clear in their statement that if the IHA algorithm failed to converge, then the physical system would suffer from a harmonic instability. They also claimed that their algorithm did not suffer from "...problems of numerical instability...", although in this, it is more likely that they were referring to the type of numerical problems experienced in time domain simulation.

Bruce Harker developed a simplified version of IHA at Canterbury (Harker, 1980), and investigated a third harmonic resonant condition which demonstrated the phase angle controller as being inferior to the symmetrical firing controller in terms of uncharacteristic harmonic generation, and showed the phase angle controller to render the algorithm unstable if the third harmonic resonance was approached too closely. In his conclusions, he stated that there was significant uncertainty in the numerical solution for uncharacteristic harmonics, this being due to the inherent sensitivity to a wide range of parameters which were difficult to assess, or were of a time-varying, rather than steady-state nature.

Eggleston (1985) developed and extended the algorithm formulated by Harker, and in his investigations isolated the third harmonic as the root of many of the algorithmic instabilities. He also demonstrated that, at least in a particular case, the algorithmic instability exhibited behaviour characteristic of an harmonic instability in that it was independent of the system impedance unbalance, and could be removed by filtering or reducing the power of the convertor. Attempts at improving the numerical technique were also unsuccessful, which would also be characteristic of a true harmonic instability, since the instabilty would depend on the physical system parameters and not the simulation technique. However, he was unable (or unwilling) to state that there existed a complete isomorphism between algorithmic instability and harmonic instability. Partly this may have been due to the fact that IHA was compared favourably with a time domain simulation (TCS) and both were shown to be accurate. However, when the TCS algorithm was applied to an unstable IHA case, a steady state solution was reached, indicating that the system *didn't* suffer from an harmonic instability.

The purpose of this chapter, therefore, is to examine the possible causes and mechanisms of divergence in IHA, and to offer explanations which may help in distinguishing between the algorithmic instabilities, and the genuine harmonic instabilities. In more

general terms, it aims to unify the explanations into a theory which explains, in principle at least, *all* cases of algorithmic instability. The particular topics which will be addressed are :

- Uncharacteristic harmonic production.
- Growth of uncharacteristic harmonics.
- Representation of dynamics.
- Uncharacteristic harmonics with balanced systems.

3.2 UNCHARACTERISTIC HARMONIC PRODUCTION

It is a well documented fact that convertors under unbalanced operating conditions produce harmonics which are uncharacteristic of their 'ideal' operation (Phadke and Harlow, 1968; Reeve and Krishnayya, 1968). The basic building block of the convertor installation is the 6-pulse bridge, which normally produces harmonics of order $6k \pm 1$. If half wave symmetry is assumed, then even harmonics are not produced, and the remaining uncharacteristic harmonics are those odd multiples of 3 - the triplen harmonics.

The reason that the triplen harmonics are not produced under ideal conditions is explained by considering an idealised phase current waveform over one cycle, compared with an arbitrary third harmonic waveform over the same period, as shown in figure 3.1. The bottom waveform is obtained by multiplying the two upper waveforms together. The proportion of third harmonic in the phase current waveform is proportional to the total shaded areas of the composite waveform, since

$$b_3 = \frac{1}{\pi}\int_0^{2\pi} f(\theta)\sin(3\theta+\phi)d\theta$$

is the third harmonic component of the (arbitrary) function $f(\theta)$.

The problem is simplified by appealing to half-wave symmetry, so that the contribution of the second half cycle is equal to that of the first. Assuming the 1st and 3rd commutating-on current waveshapes to be governed by functions $i_{c1}(\theta)$ & $i_{c3}(\theta)$ respectively, and that the steady conduction current is I_d then the third harmonic component is :

$$\begin{aligned} b_3 &= \frac{2}{\pi}\int_0^{\pi} i(\theta)\sin(3\theta+\phi)d\theta \\ &= \frac{2}{\pi}\left[\int_{\theta_1}^{\theta_1+\mu_1} i_{c1}(\theta)\sin(3\theta+\phi)d\theta + \int_{\theta_1+\mu_1}^{\theta_3} I_d\sin(3\theta+\phi)d\theta + \right. \\ &\quad \left.\int_{\theta_3}^{\theta_3+\mu_3}(I_d - i_{c3}(\theta))\sin(3\theta+\phi)d\theta\right] \\ &= \frac{2}{\pi}\left[\int_{\theta_1}^{\theta_1+\mu_1} i_{c1}(\theta)\sin(3\theta+\phi)d\theta + \int_{\theta_1+\mu_1}^{\theta_3+\mu_3} I_d\sin(3\theta+\phi)d\theta + \right. \\ &\quad \left.\int_{\theta_3}^{\theta_3+\mu_3} -i_{c3}(\theta)\sin(3\theta+\phi)d\theta\right] \end{aligned} \tag{3.1}$$

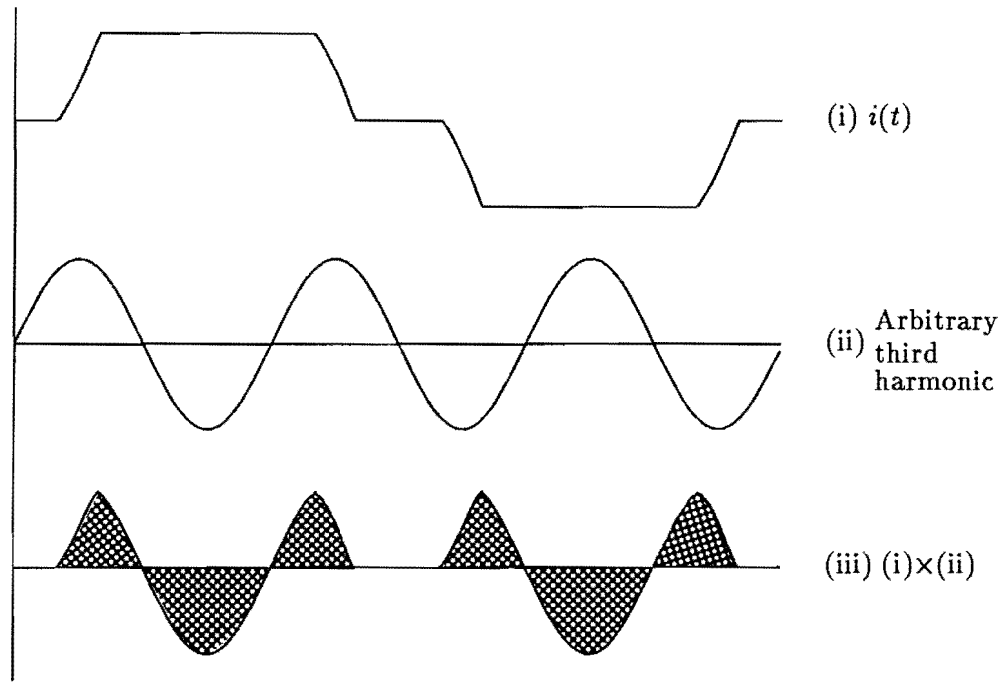

Figure 3.1: Third harmonic content in the idealised phase current waveform.

Noting that, in the ideal case, the shape of the first and third commutation are identical, then

$$i_{c3}(\theta) = i_{c1}(\theta - \frac{2\pi}{3})$$

and

$$\mu_1 = \mu_3$$

Also, the first and third firing instants (θ_1 & θ_3) are spaced by exactly $\frac{2\pi}{3}$ radians, so that :

$$b_3 = \frac{2}{\pi}\left[\int_{\theta_1}^{\theta_1+\mu_1} i_{c1}(\theta)\sin(3\theta+\phi)d\theta + \int_{\theta_1+\mu_1}^{\theta_1+\frac{2\pi}{3}+\mu_1} I_d \sin(3\theta+\phi)d\theta + \int_{\theta_1+\frac{2\pi}{3}}^{\theta_1+\frac{2\pi}{3}+\mu_1} -i_{c1}(\theta-\frac{2\pi}{3})\sin(3\theta+\phi)d\theta\right] \quad (3.2)$$

The first and third integrals in equation 3.2 cancel directly, while the middle term amounts to integrating an arbitrary third harmonic waveform over $\frac{2\pi}{3}$ radians, or exactly one third harmonic cycle. The contribution from this is therefore zero.

Thus, under completely idealised conditions, no third or (by similar argument) any other triplen harmonic is generated. Any deviation, however, from the ideal will result in immediate triplen production. Common physical causes of triplen generation are :

1. **Unbalanced Commutating Impedances :** If commutating impedances are unbalanced, then the commutations will be of different lengths, and therefore triplen harmonic contributions from the commutating-on and commutating-off periods in each phase (typified by the cancellation of the first and third integrals in equation 3.2 above) will no longer cancel.

2. **Unbalanced Commutating Voltages :** If the voltages at the terminal busbar of the convertor are unbalanced in any way, then each commutation will, in general, be driven by a different voltage to that driving the others. Therefore the commutations will again be of different lengths, and thus triplen harmonics will be generated.

3. **Unbalanced Supply Impedance :** The principal effect of unbalanced supply impedances can be seen in two different lights. Firstly, if the commutations are seen to be driven by the parallel combination of all the remote generator's internal emfs (which act as ideal voltage sources) then the supply impedances form part of the commutation circuit, and the effect of unbalance is really part of 1, above. If, however, the commutations are considered to be driven by the terminal busbar voltage waveforms, then the effect of the unbalanced supply impedance is to unbalance the terminal busbar voltages (at fundamental and/or harmonic frequencies) and the effect is that of 2, above.

4. **Unbalanced Firing Instants :** If the firing instants are unbalanced, then the middle term in equation 3.2 will no longer integrate to zero because the integration period will be greater or less than $\frac{2\pi}{3}$ radians. The most common cause of this phenomena is the earlier phase angle controller, in which each valve was fired a fixed angle after it became forward biased, i.e. after the zero crossing of its commutating voltage. If the zero crossings were unevenly spaced, then the firings were also unevenly spaced, and the results was introduction of triplen harmonics. One cure for this was the introduction of Equidistant Firing Control by Ainsworth (1968). This controller maintained a minimum delay angle on one phase, and produced a train of firing pulses exactly $\frac{\pi}{3}$ radians apart. Synchronisation with the supply frequency was by means of a phase locked loop oscillator. The effect of this controller was to eliminate triplen generation through firing angle unbalance, although other triplen generation mechanisms still remained.

3.2.1 Nature of the triplen harmonics produced

The principal causes of the triplen harmonic generation have now been enumerated, but the nature of the generated triplens has not been derived. To do this, the system of figure 3.2 will be used. The voltage source is assumed ideal (i.e. sinusoidal, balanced) and the d.c. current perfectly smooth. Under these conditions, the only triplen generation is due to the imbalance present in the commutating impedances. The impedances governing each commutation are given in table 3.1, from which it can be deduced that

Commutation number	1	2	3	4	5	6
Commutating reactance	0.20	0.21	0.21	0.20	0.21	0.21

Table 3.1: Commutating reactances governing each commutation.

μ_1 & μ_4 will be shorter than μ_2, μ_3, μ_5 & μ_6. In terms of the phase current waveforms then, phase 'a' will commutate on faster than it will commutate off, while phase 'c' will

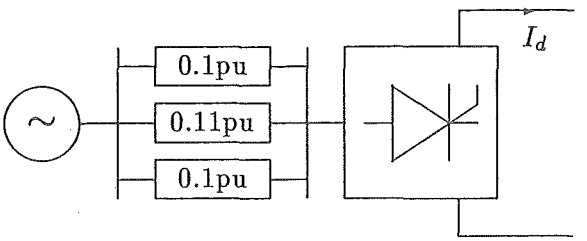

Figure 3.2: System for deriving typical third harmonic generation.

commutate off faster than it will commutate on. All of phase 'b's commutations will, however, be of equal length. Thus the area under the phase 'a' current waveform will be greater than in the purely balanced case, while the area under the phase 'c' current waveform will be less. The third harmonic components in the three phases are therefore those given in figure 3.3. As can be seen, the phase a third harmonic has a phase

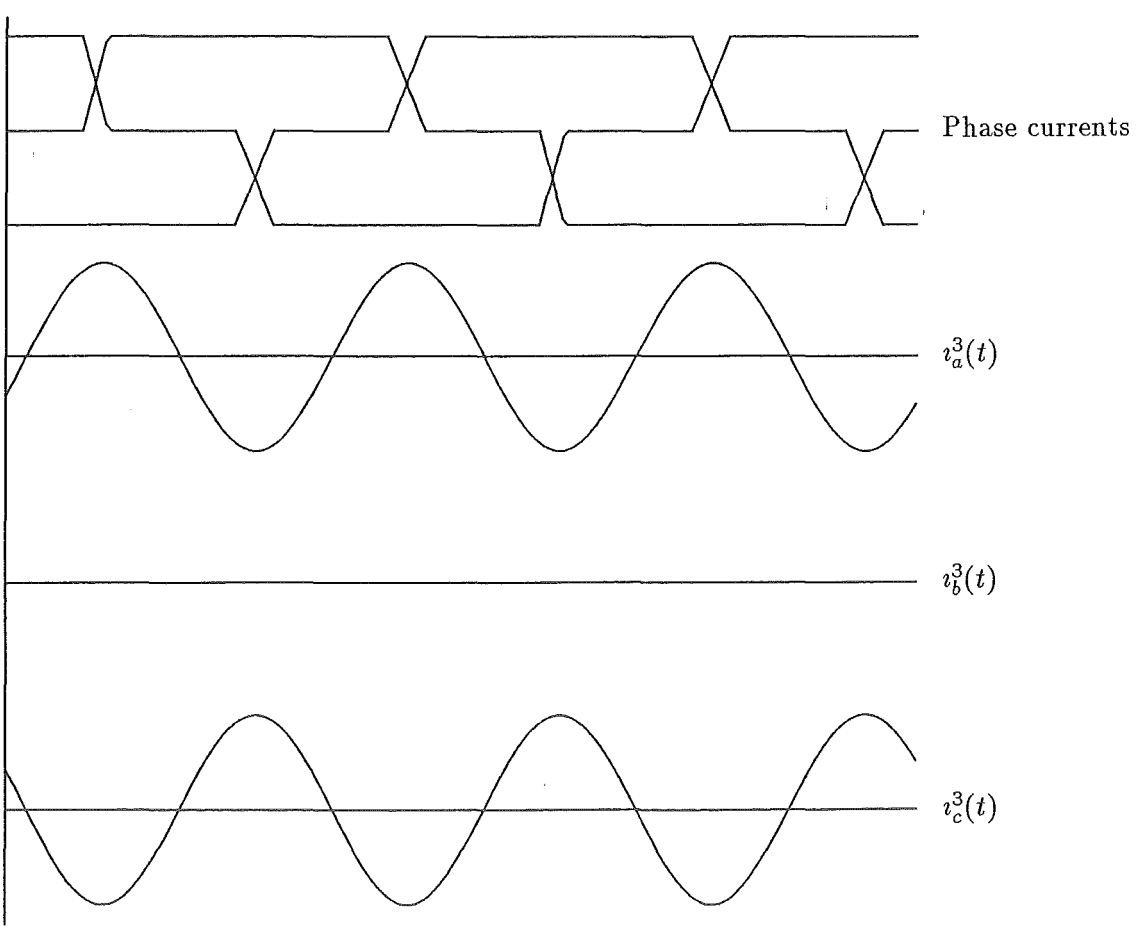

Figure 3.3: Third harmonic current generated by unbalanced commutations.

relationship such that it 'pads out the shoulders' of the phase 'a' current waveform, thus contributing to its increased area. Similarly, the phase 'c' third harmonic current is such that it 'thins out the shoulders' of the phase 'c' current waveform. Because phase 'b' is a balanced waveform, its third harmonic component is zero.

It is important to note that the phase 'a' & phase 'c' third harmonics sum to zero. This satisfies the condition that no zero sequence components can exist on the secondary of the convertor transformer. Approximately, the sequences of the third harmonic currents depicted here are given in figure 3.4. This type of third harmonic

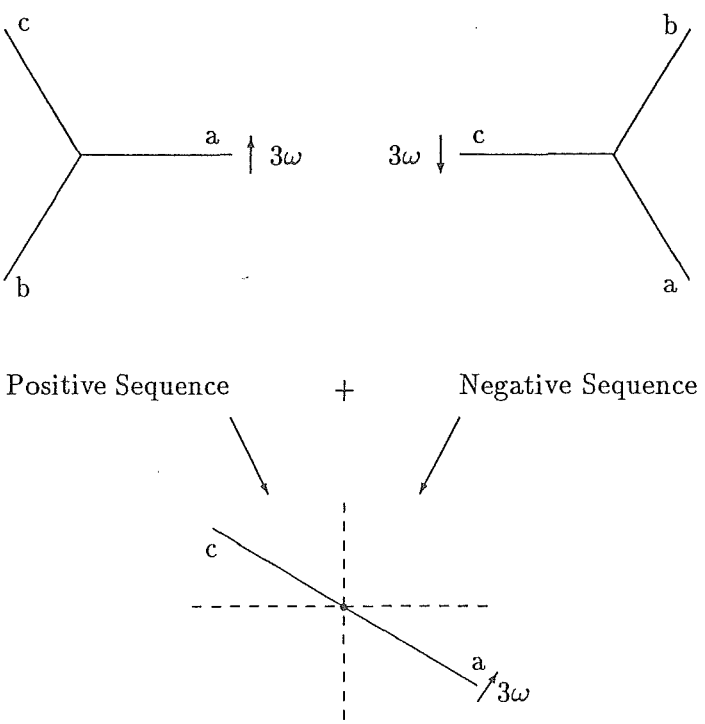

Figure 3.4: Third harmonic current sequences.

production is typical of that occuring in practice — a fairly even mixture of positive and negative sequence components.

3.3 MECHANISMS OF HARMONIC MAGNIFICATION

The mechanism of harmonic magnification within an algorithm such as IHA eludes simple or general description. The simplest situation in which it can readily be understood is that involving a convertor with an individual phase controller.

3.3.1 Phase Angle Control

With phase angle control, each valve is fired a fixed delay (α) after it becomes forward biased (i.e. at angle $ZC_i + \alpha$). In principle α can be different for each valve, but is generally the same for all. Thus the firing instants directly reflect the actual zero crossings.

In modelling phase angle control within IHA, the new zero crossings of the distorted commutating voltages are calculated, and the firing instants are calculated by adding the delay angle, i.e. $\theta_i = ZC_i + \alpha$.

Assuming that there is some initial cause of third harmonic production, and that there is a definite third harmonic impedance in the supply network, then the following steps occur.

(i) On the first iteration of IHA, some third harmonic current is produced, similar in form to that of figure 3.3.

(ii) This current results in third harmonic voltages appearing at the terminal busbar.

(iii) The zero crossings of the new (distorted) terminal voltages shift asymmetrically, due to the unbalanced nature of the third harmonic voltages. Other characteristic harmonics have a symmetrical effect on the zero crossings, and may be ignored for the purpose of explaining the harmonic magnification mechanism.

(iv) The (now) asymmetrical zero crossings are used to calculate the firing instants which are, therefore, also asymmetric, and are thus a source of third harmonic in their own right.

(v) The distorted voltages are used to recalculate the current waveforms, and now two possibilities exist. The triplen harmonics in the current waveforms will either increase with a similar phase to those of the previous iteration, or will be produced with a different phase relationship.

The mechanism by which triplen harmonic growth can occur is now clear. In the first possible case it is clear that larger triplen current with the same phase relationship as the previous iteration will produce even greater quantities of triplen voltage, and will serve to further displace the zero crossings in the same sense, resulting in unchecked growth of the triplen harmonics with subsequent iterations. This phenomena is clearly influenced by the phase of the third harmonic impedance of the supply network.

To demonstrate the effect of the phase of the third harmonic impedance, a simplified form of IHA was set up, in which the phase currents are represented by rectangular pulses with lengths determined solely by the intervals between firing instants. The fundamental supply voltages have a 1% -ve sequence component which ensures third harmonic generation in all waveforms. The third harmonic impedance magnitude is such that 5% third harmonic voltage appears on the second iteration. The phase of the third harmonic impedance is varied over the range ϕ_3 =90° to −90°, and with a delay angle of 20°, the conduction periods listed in table 3.2 were recorded for the first and second iterations. Over a range of ϕ_3 =90°→22.5° the tendency is for the triplen harmonics to work in the opposite sense to the source of unbalance, since the extended conduction period of phase 'a' is reduced to less than 120° over this range, while the

Phase	First Iteration Conduction Periods	Second Iteration Conduction Periods with ϕ_3 =				
		90°	67.5°	45°	22.5°	0.0°
a	120.987°	115.295°	114.529°	114.686°	115.756°	117.650°
b	119.506°	122.592°	122.805°	122.519°	121.852°	120.928°
c	119.506°	122.113°	122.665°	122.798°	121.392°	120.422°

Second Iteration Conduction Periods with ϕ_3 =			
−22.5°	−45°	−67.5°	−90°
120.129°	122.761°	125.056°	126.660°
119.863°	118.767°	117.746°	116.433°
119.008°	118.471°	117.198°	116.433°

Table 3.2: Conduction period behaviour with α =20°

contracted conduction periods on phses 'b' & 'c' are extended to beyond 120°. This will result in triplen harmonic currents of the opposite sense in the next iteration.

Over the range ϕ_3 =−45°→−90°, the tendency is for the triplen harmonics to extend the phase 'a' conduction period, and further contract the already contracted phase 'b' & 'c' conduction periods. This will produce, on the next iteration, triplen harmonics of greater magnitude, but with similar phases, and the effect will become self propagating.

It is clear, therefore, that if the third harmonic voltage resulting from a small imbalance serves to enhance the effect of that imbalance (insofar as uncharacteristic harmonic generation is concerned), then the situation will result in an algorithmic instability, and appears to depend strongly on the phase of the third harmonic impedance. If the effect of the third harmonic voltage is opposite to that of the initial imbalance, then an instability may still result, depending more strongly on other factors such as the third harmonic system impedance magnitude.

It is tempting to translate the preceding paragraph directly onto the physical system and state that should an algorithmic instability develop within IHA, then similar harmonic build up would be expected on the physical system. However, the development of an instability on the physical system is a dynamic phenomena, and cannot be directly linked to the IHA solution, which operates in the steady-state frequency domain. In other words, there is no direct isomorphism between successive iterations of IHA, and, say, successive cycles in a time domain simulation.

3.3.2 Equidistant Firing Control

The equidistant firing controller fires all the valves at 60° intervals, thus eliminating unequal conduction periods as a source of uncharacteristic harmonics. However other imbalances (such as unbalanced commutating impedances) still have an effect on (in particular) the length and shape of each commutation, and therefore triplen generation cannot be ruled out.

Within IHA, the equidistant firing controller is implemented by calculating the actual zero crossings, and, choosing one phase as a reference (typically phase 'a'), firing its valve after the delay angle α, and all other valves at 60° intervals with respect to the reference firing. Thus $\theta_i = ZC_{\text{ref}} + \alpha + (i - i_{\text{ref}})\frac{\pi}{3}$.

Two effects become significant in the context of the equidistant firing controller. The first is the effect of triplen harmonics on the commutations, and the second is the effect of subsequent zero crossing shifts on the firing instants and therefore the current waveforms.

Eggleston (1985) demonstrated the effects of a positive sequence third harmonic component of commutating voltage on the commutations of a zero-delay equidistant firing convertor when the phase 'a' third harmonic component was in phase with the phase 'a' fundamental voltage. Although that demonstration related to a very specific case, the conclusion generalises to the following statement :

If the triplen components of commutating voltage are positive over a positive going commutation, then that commutation will be accelerated. Conversely, if the triplen components are negative over a positive going commutation, then that commutation will be retarded.

The effect of accelerated & retarded commutations, as described in figure 3.3, is to produce triplen harmonics in the current waveform, causing, in turn, triplen harmonic voltages which further modulate the commutations. The worst case condition occurs when the modulations are such that they produce triplen harmonics which will modulate the commutations in the *same sense* on the next iteration. i.e. accelerated commutations become shorter, and retarded commutations become longer.

The waveforms derived in figure 3.3 can be extended further to include the third harmonic commutating voltages which result from injection of the third harmonic currents into a pure resistance via a star-star transformer. While a purely resistive system impedance at third harmonic is somewhat unrealistic (except when a parallel resonance exists at that frequency), it provides a basis for demonstrating the effects at other impedance angles, by simply sliding the third harmonic voltage waveforms through the appropriate angles.

The third harmonic voltage waveforms are obtained by inverting the third harmonic current components (so that they flow *into* the a.c. system) and multiplying them by the third harmonic resistance. This gives the primary third harmonic voltages, which are opposite in phase to the corresponding secondary currents, and which are used to determine the third harmonic components of the commutating voltage, as shown in figure 3.5.

In order to increase the quantity of triplen harmonics in the current waveform, the first and fourth commutations must be further accelerated, while the remaining commutations must be retarded. As it stands, the third harmonic voltages are in a position to *retard* the first and fourth comutations, because $v_{ac}^3(t)$ is negative over the first, and positive over the fourth, and similarly, the remaining comutations would be *accelerated* by the third harmonic components in their commutating voltages. This would result in third harmonic currents of opposite phase on each subsequent iteration, with the possibility of a limit cycle becoming apparent. To obtain the worst case effect, the third harmonic commutating voltages would have to be inverted with respect to the purely resistive case. In other words, a negative resistive third harmonic system

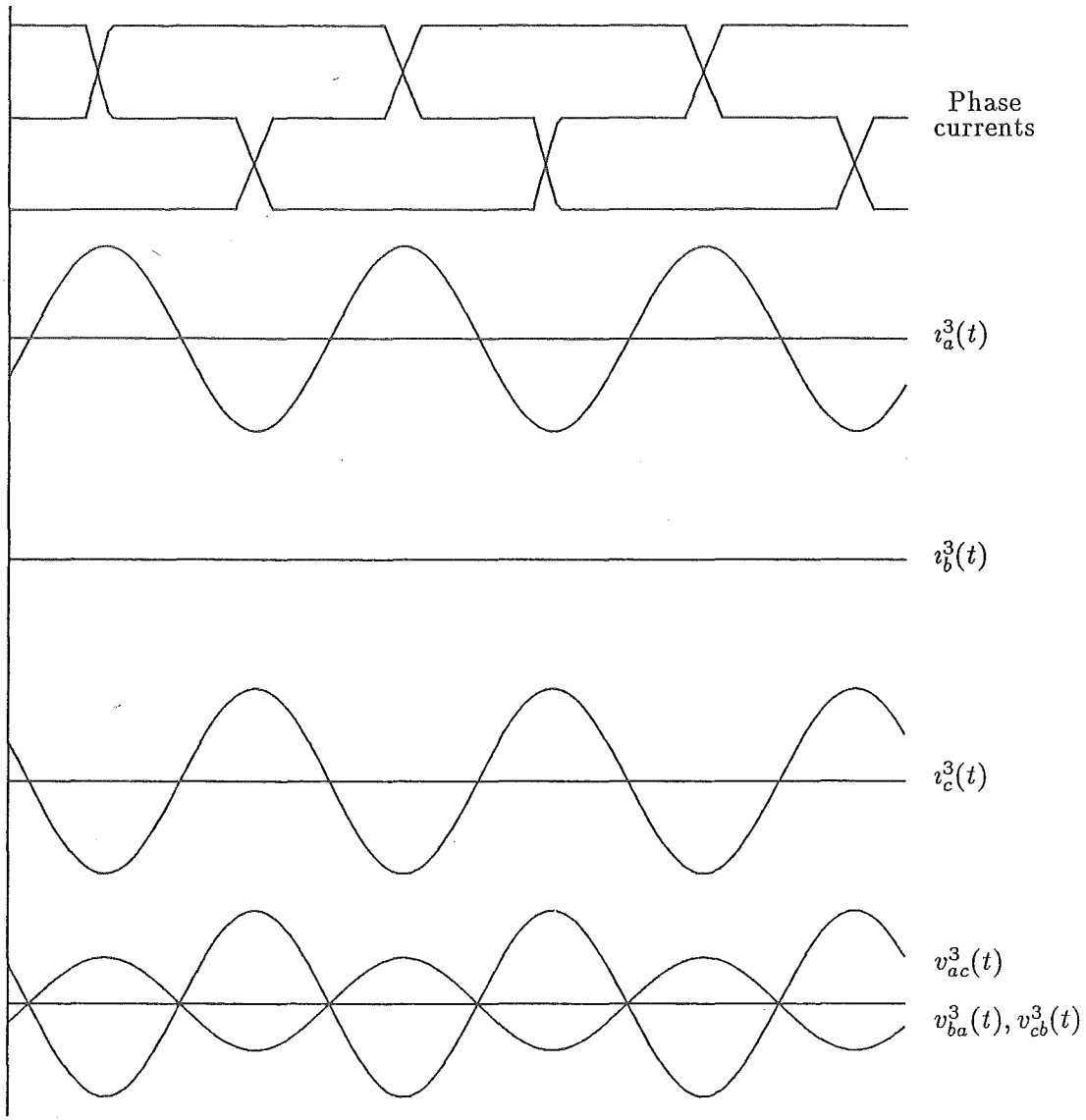

Figure 3.5: Third harmonic components with a star-star transformer.

impedance would be required.

If the system third harmonic impedance was purely reactive (i.e. $\phi_3 = \pm 90°$), then the zero crossings of the third harmonic components of the commutating voltages would align (approximately) with the commutations, and would have very little effect on the nature of the unbalance in the bridge, and would therefore produce ony small additional amounts of triplen harmonic currents on the next iteration, resulting in a fairly stable situation.

With a star-delta transformer, the third harmonic current must be referred back across the transformer before being injected into the system impedance. The conventions employed in figure 3.6 are used to analyze this situation.

The third harmonic current drawn above phase A flows into the convertor, and re-enters the transformer via phase C, flowing 2/3 in branch CA, and 1/3 in each of

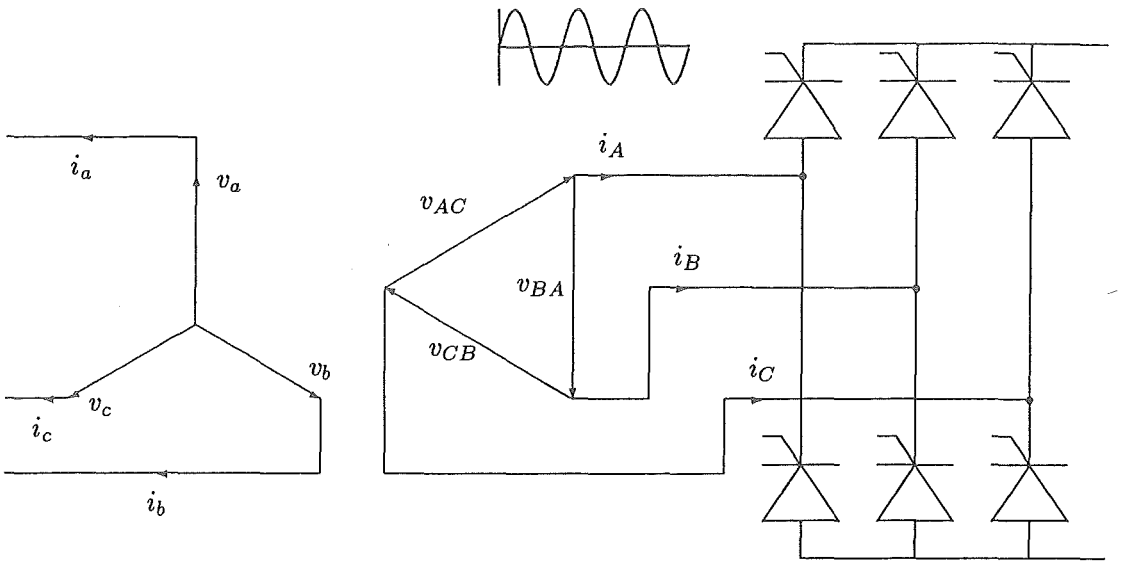

Figure 3.6: Third harmonic current flow in a star-delta transformer.

branches CB & BA as depicted in figure 3.7.

This allows the currents flowing in the branches of the primary windings to be established, (depicted as injections into the a.c. system in the figure), and therefore the primary phase voltages induced in a purely resistive network impedance. Finally, the commutating voltages, referred to the secondary of the convertor transformer can be found. Now it can be seen that $v^3_{ac}(t)$, which drives commutations 1 and 4 peaks near the first firing instant, and peaks in the negative sense near the fourth firing instant. This would result in a further accelerated commutation on the next iteration, thus enhancing the triplen harmonics generated by the existing unbalance. Similarly, $v^3_{ba}(t)$ & $v^3_{cb}(t)$ are both poised to retard their respective commutations further, because they are all negative (with respect to the positive-going commutations) near the firing instants. Thus a mechanism for a possible algorithmic instability becomes apparent.

An inductive or capacitive system impedance at third harmonic would result in the voltage waveforms being shifted to the left or right by 90°, thus aligning (approximately) the zero crossings of the third harmonic voltages with the firing instants of the valves. The contributions of the third harmonic voltages to the commutations would be considerably smaller, and therefore would not greatly affect the level of triplen harmonic currents in the current waveform. In both cases the IHA algorithm is likely to be stable.

Eggleston (1985) ran a series of test cases with varying phase angles of the third harmonic system impedance, and recorded the number of iteratons required for convergence. His results are given in figure 3.8.

From figure 3.8 it would seem that the greatest harmonic interaction actually occurs with a third harmonic impedance angle of 22.5° to 45°, which is somewhat offset from the prediction just made. This may be attributed to a number of factors omitted in the heuristic approach to the problem; in particular the shifts of the zero crossings (and

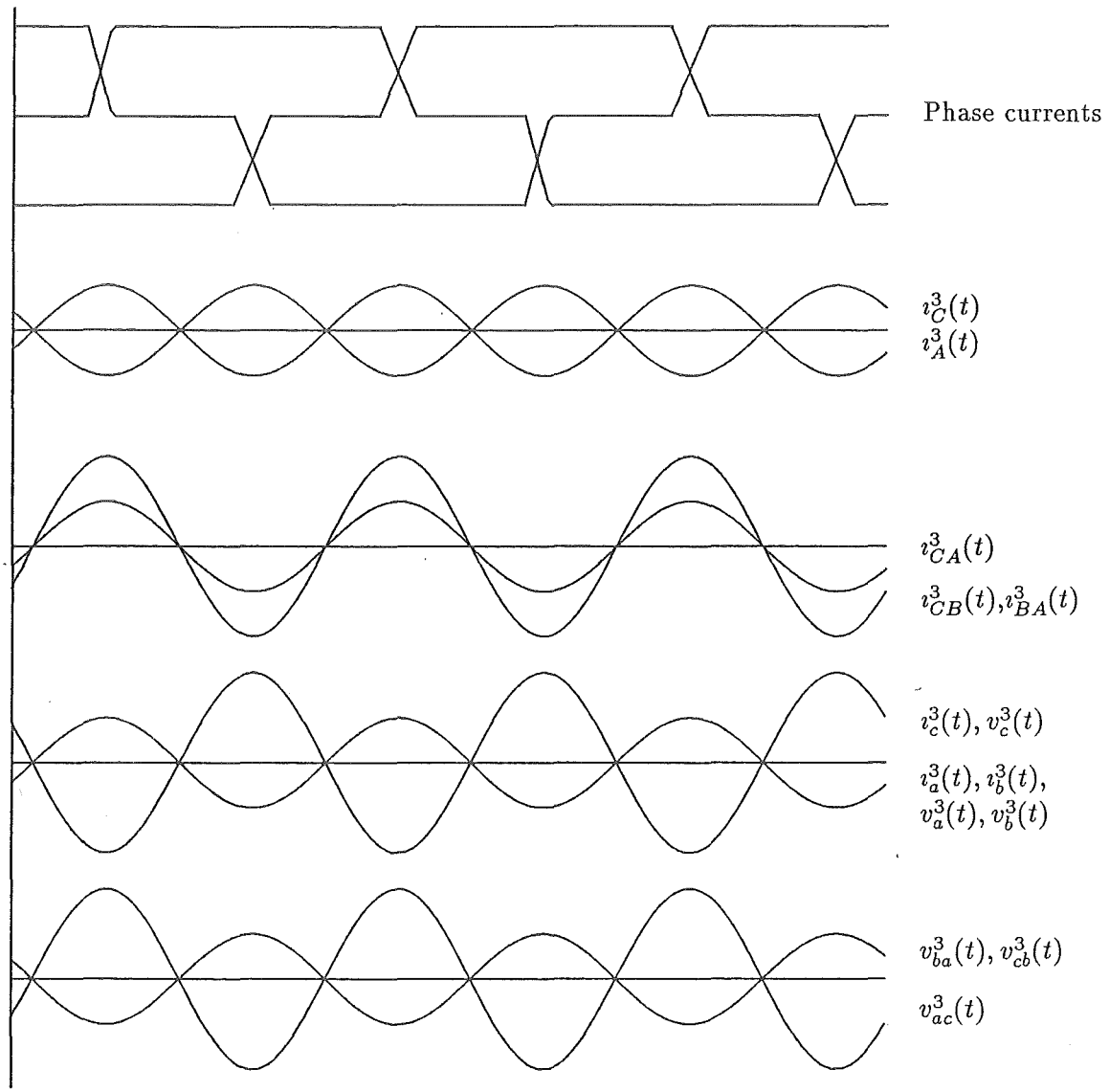

Figure 3.7: Third harmonic components with a star-delta transformer.

therefore firing instants) between iterations was not accounted for, and the nature of the imbalance is also likely to have been different, resulting in the discrepancy.

In the light of this, a identical study was performed for the star-star transformer case, with the results being given in figure 3.9.

The trend here is similar, except that the increase in the required number of iteratons occurs in the $-22.5°$ to $-90°$ range and peaks at $-67.5°$. This is somewhat surprising, since the worst case situation with the star-star transformer was predicted as being realisable only with a negative resistive third harmonic system impedance. However the disparity between the imbalance considered in the heuristic explanation and the case actually modelled is the most likely explanation for the observed behaviour.

Comparing figures 3.8 & 3.9, however, reveals that the least stable situations for each occur at (near) opposite phases of third harmonic impedance. This is consistent

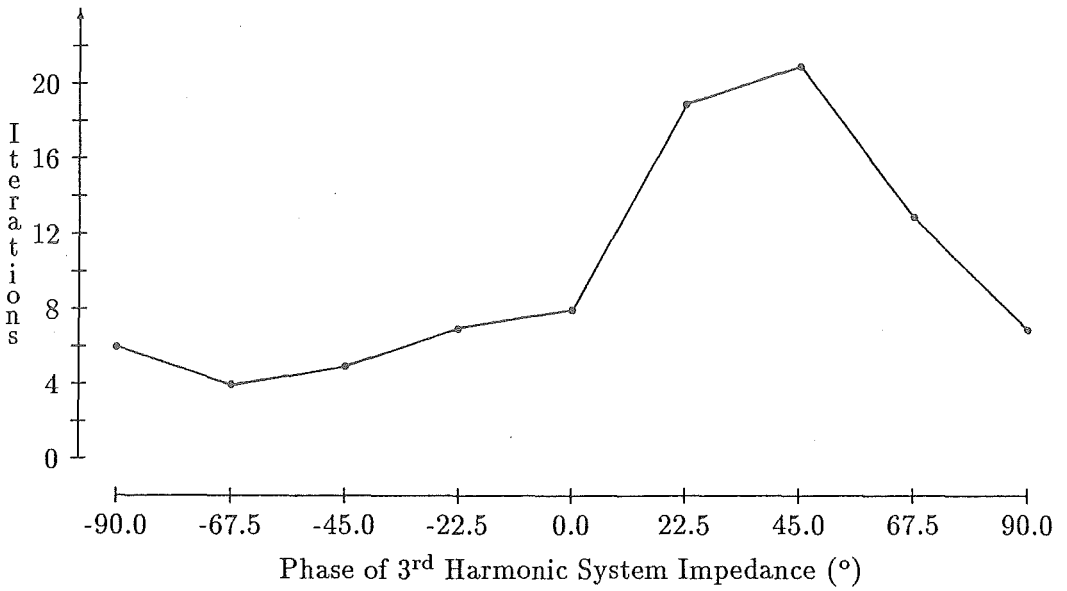

Figure 3.8: Iterations required for convergence with various ϕ_3 & a star-delta transformer.

with the prediction that instabilities would occur near ϕ_3 =180° and ϕ_3 =0° (i.e. 180° apart) respectively for the star-star and star-delta transformer connections.

3.3.3 The Representation of 'Dynamics'

The principal representation of 'dynamics' in IHA relates to the calculation of new firing instants based on the latest values of the actual zero crossings. With phase angle control, the firing instants follow exactly the shifts in commutating voltage zero crossings, and the potential problems with this have already been discussed.

With equidistant firing control, the dynamic shifting of zero crossings from iteration to iteration doesn't interfere with the harmonic interaction process to the same degree, since the firing instants are maintained at exactly 60° spacings. However, one effect that is possible is that a shift of firing instants changes the apparent phase of an interfering harmonic with respect to the commutation process. The worst case here occurs when the apparent phase shift results in the opposite effect to that which would otherwise occur. As a particular example, if the apparent phase shift slides a commutation across a third harmonic zero crossing, then the effect of the third harmonic commutating voltage on the commutation will be opposite to that which would otherwise have occurred. This could potentially result in a limit cycle, where the third harmonic on one iteration results in a third harmonic of opposite phase on the next iteration, or in an algorithmic instability, where the third harmonic continually reinforces itself with each iteration.

From the point of view of the characteristic harmonics there is also a potential problem, since the harmonic voltages present at the end of one iteration, due to a particular current waveform injection, are used on the next iteration to calculate a

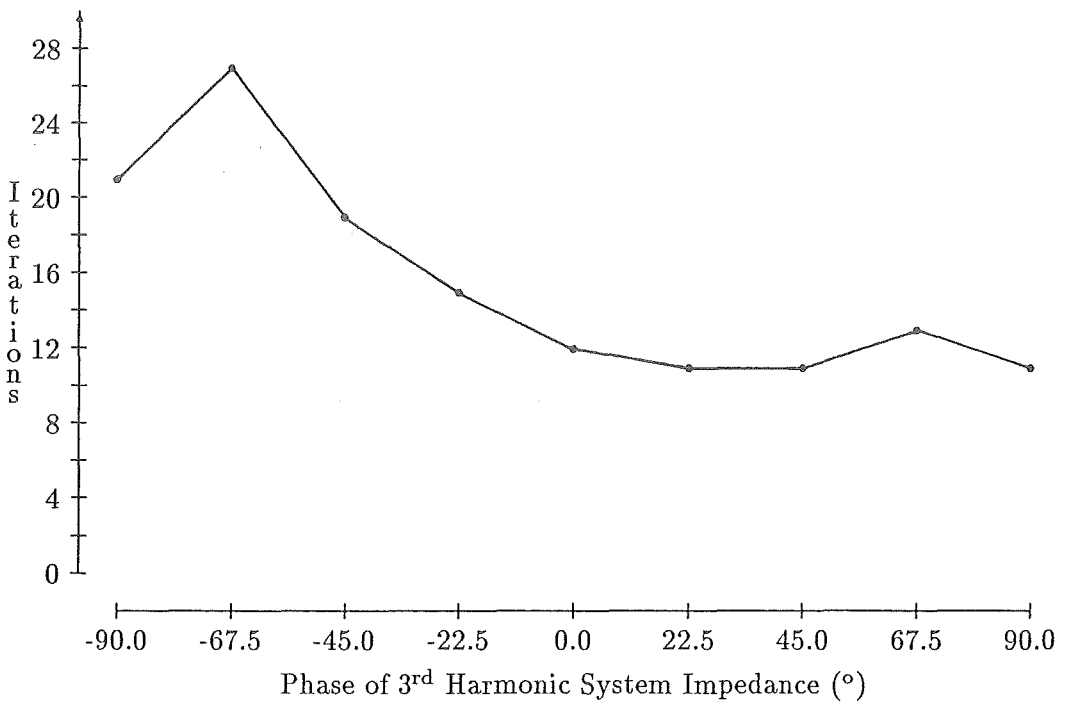

Figure 3.9: Iterations required for convergence with various ϕ_3 & a star-star transformer.

current waveform which is in a different position to the previous one. This phenomena is illustrated in figure 3.10. It is apparent that the commutations on the next iteration are initially unaffected by the notches in the commutating voltages, because of the shift in zero crossings. In the absence of uncharacteristic harmonics, it is unlikely that this (in itself) would result in algorithmic instability, but it will definitely degrade convergence.

One of the principal reasons for maintaining the firing instants with respect to the true zero crossings is to maintain integrity with the initial conditions specified by the loadflow. However, it must be remembered that, for reasonable levels of harmonic distortion, the d.c. voltage is still principally made up of the fundamental components of the a.c. commutating voltage waveforms, and that shifts in the firing instants with respect to the fundamental a.c. voltages will inevitably result in a change in the d.c. voltage - especially so at higher delay angles. Therefore, by maintaining integrity with the loadflow in one sense (i.e. retaining the specified delay angles), it is lost in some other sense (i.e. d.c. voltage level).

Therefore, it is true to say that complete integrity with the loadfow operating state is not possible, and that since the dynamics of following the zero crossings can lead to algorithmic instability (with uncharacteristic harmonics), or at least degrade performance in some way (with characteristic harmonics), it is permissible (and even

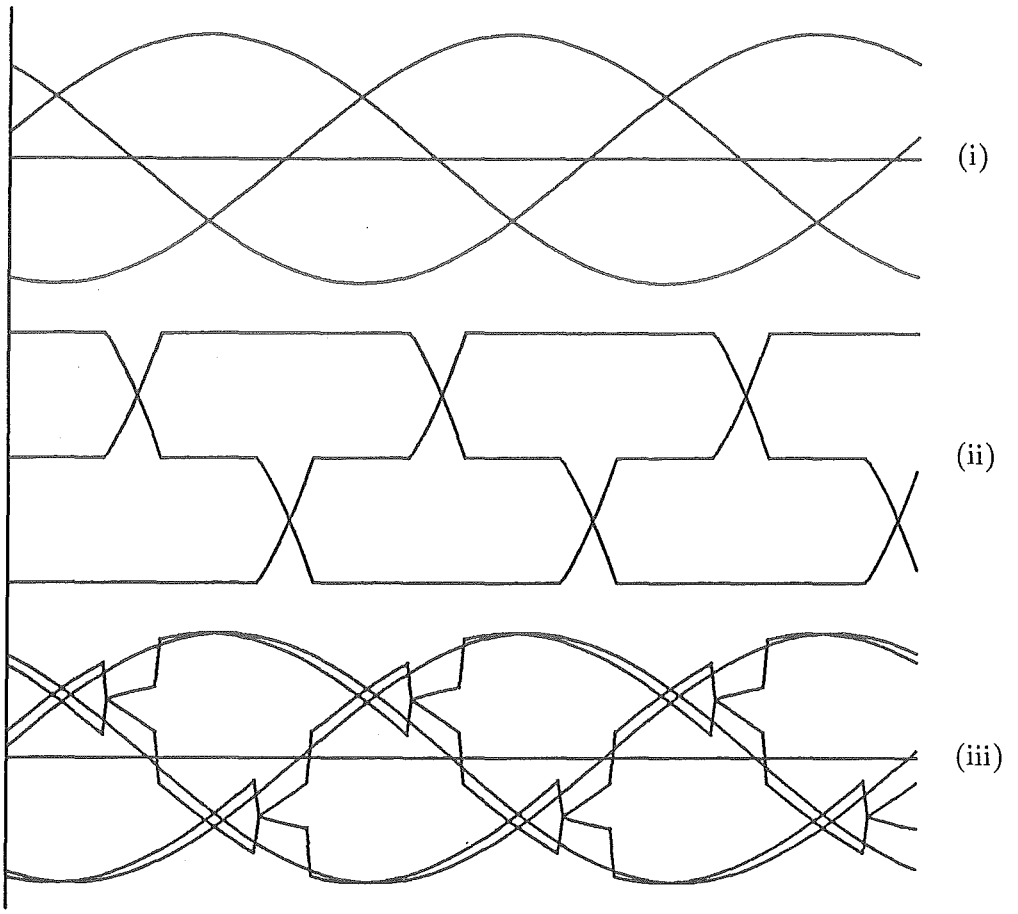

Figure 3.10: Nature of zero crossing shifts due to characteristic harmonics. (i) Original balanced sinusoidal voltages (ii) Balanced current waveforms (iii) Distorted waveforms with fundamental components added

advisable) to maintain the firing instants calculated by the loadflow.

However, if representation of (quasi) dynamics within IHA degrades performance, then how does the loadflow convertor model handle the dynamic changes that occur as the solution is approached ? The answer lies in the fundamentally different solution techniques of the two analyses. The loadflow convertor model is solved by a Newton Raphson technique, in which all variables are related to each other bilaterally via the Jacobian matrix. Thus, some variation from the set d.c. current level, for example, affects all the other variables such that the required value is eventually restored. The IHA convertor model, on the other hand, is solved sequentially, with a purely unilateral relationship between the input variables and those resulting at the final iteration. A change in those variables regarded as input will necessarily result in a solution different to that originally desired.

Therefore, it is not advisable to alter the firing instants as the solution proceeds, but to regard them as part of the convertor specification.

3.3.4 Numerical Noise

During validation comparisons of IHA with TCS (Arrillaga *et al.*, 1987), it was noted that a perfectly balanced system diverged with the IHA solution technique, but converged with the TCS solution technique, reaching a stable operating state after a few cycles. The IHA waveforms exhibited considerable quantities of third harmonic, and the supply network was resonant near this frequency, indicating a third harmonic problem similar to that described previously. The principal issue was that of determining the source of the third harmonic, since no triplen harmonics should be generated with the perfectly balanced operation modelled.

Close examination revealed that small amounts of non-characteristic harmonics were present from the very first iteration, but these were initially assumed to be numerical noise or aliasing errors within the FFT used to calculate the harmonic current phasors. Aliasing errors can arise when a non-band-limited signal is undersampled, which is always the case here, since the current waveforms sampled have, in theory, infinite spectra, although frequencies above the 50^{th} are generally ignored. In this range, then, 128 samples per cycle would provide all the necessary information, and the practical sampling rate of 512 or 1024 samples per cycle would provide accuracy up to the 256^{th} & 512^{th} harmonics respectively, thus reducing aliasing errors to a minimum.

Closer examination, however, revealed that the uncharacteristic harmonics consistently obeyed the constraint that no zero sequence components could exist on the secondary of the convertor transformer, which implied something more 'intelligent' than pure numerical noise.

The existence of these uncharacteristic harmonics is explained with reference to the diagram of figure 3.11, which depicts, in detail, one half-cycle of a perfectly balanced current waveform, showing also the sampling points arising with 128 samples per cycle.

From the diagram, it becomes clear that the events governing the convertor operation (valve turn-on and turn-off) are not clearly represented by the sampling process. For example, in the first waveform, the first commutation begins $2T_s/3$ after sample number 11, where T_s is the sampling interval, while the second commutation begins exactly 120° later, $T_s/3$ after sample number 54. Thus, the current waveshape seen by the FFT doesn't have symmetrical commutations (although they are), and the result is a generation of triplen harmonics by the FFT, which, as far as it is concerned, actually do exist.

The essence of the problem here is that evenly spaced events in the balanced operation of a convertor are separated by exactly 60°, or 1/6 of a cycle, whereas sampling by a power of 2 (256, 512, 1024...) can never represent the 60° spacings exactly. Thus, the FFT can be seduced into believing the balanced waveform to be slightly unbalanced, resulting in small but discernible quantities of uncharacteristic harmonics being produced.

The second part of the figure shows an identical waveform sampled with only 96 sample points - 2/3 of those of the previous waveform - but with the advantage that now the 9^{th} and 41^{st} sample points fall exactly on the beginnings of the commutations, and the 14^{th} & 46^{th} fall exactly $T_s/2$ short of the true ends of the commutations. Thus, the balanced nature of the waveforms has been retained, even though fewer samples have been used.

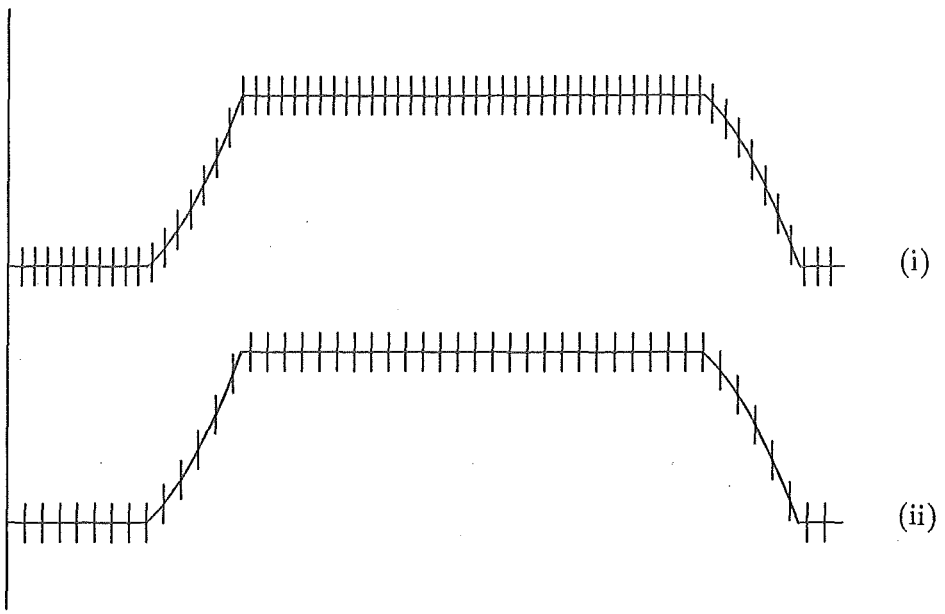

Figure 3.11: Different sampling regimes for a balanced current waveform. (i) 128 samples per cycle & (ii) 96 samples per cycle.

96 samples, however, are incompatible with the requirements of most standard FFT packages, and so a relatively uncommon one - the Mixed Radix FFT (Singleton, 1969) - is used instead. In principle, the MRFFT can handle an arbitrary number of sample points by forming the prime factors of the number of samples, and using these in the partitioning process. Accuracy is no different, and provided the prime factors are low, then there is little loss of efficiency. A useful number of samples in this case would include multiples of 6, since this will allow symmetry in the waveforms to be conserved. 768 samples ($= 3 \times 2^8$) is an excellent choice.

As an alternative to altering the number of samples, a thresholding technique can be applied. In this method, the spectra of the current waveforms are examined after Fourier transformation, and any phasors below a threshold level set to zero. Provided that the threshold level is appropriately set, then thresholding should not interfere with the normal process of harmonic interaction. More particularly it should not supress the generation of uncharacteristic harmonics where a genuine mechanism for their production exists.

In order to assess the likely levels of the triplen harmonics, a number of ideal balanced current waveforms were sampled with a varying number of sample points, and subjected to a standard (i.e. radix 2) FFT. The levels of triplen harmonics produced were recorded, and those of the third harmonic are given in table 3.3. All other triplen harmonics were found to have similar levels.

The first column may be ignored, since it represents the unfeasible situation of instantaneous commutations, and the first 2 rows may also be ignored, since the number of samples is too low for reasonable accuracy. The highest remaining error is 0.013%, which occurs with 2° commutations and 512 samples. Thus a threshold level of 0.015%

Number of Samples	Commutation Length			
	0°	2°	5°	10°
128	0.9	0.5	0.17	0.033
256	0.475	0.052	0.02	0.0081
512	0.235	0.013	0.0036	0.0042
1024	0.120	0.0067	0.002	0.0005
2048	0.060	0.0013	0.0002	0.0001

Table 3.3: Third harmonic levels with balanced current waveforms. (% of fundamental)

would be capable of screening out the purely 'noisy' uncharacteristic harmonics, while passing those which have a genuine cause.

It is important to recall, however, that triplen generation consists (typically) of equal amounts of positive and negative sequence components, and that, generally, two phases have (nearly) equal and opposite triplen harmonic phasors, while the remaining phase carries the remnant required to supress any zero sequence flow. This phase will therefore have only a small magnitude which is nonetheless essential to the correct representation of the convertor. If this magnitude falls below the threshold level and is eliminated, then it constitutes interference with the process of harmonic interaction. In one case this resulted in a limit cycle where convergence would otherwise have taken place. Therefore it is necessary to eliminate only those harmonics where all the phase magnitudes are below the threshold level.

It should also be noted that the above phenomena depends on the magnitude of the d.c. current, since this determines the magnitude of the a.c. harmonic current injections, including those of the uncharacteristic harmonics due to FFT error. This explains the apparent dependency of the algorithmic instability on Short Circuit Ratio with balanced resonant systems as demonstrated by Arrillaga *et al.* (1987). In this case, a 6-pulse rectifier was connected to a symmetrical supply network represented by its Thévenin equivalent and a set of characteristic harmonic filter branches corresponding to the single tuned filter branches on one pole of the NZ HVDC link, as depicted in figure 3.12.

The system reactance was chosen to resonate with the filter susceptance near the third harmonic, and the SCR was decreased by increasing the d.c. current, with the effect of this on the number of iterations given in figure 3.13.

From the diagram, it can be seen that without thresholding convergence could not be obtained below an SCR of about 1.8, whereas with thresholding, the solution was obtained in considerably fewer iterations. Thus thresholding is a useful technique for eliminating 'noisy' uncharacteristic harmonics and improving the convergence of IHA.

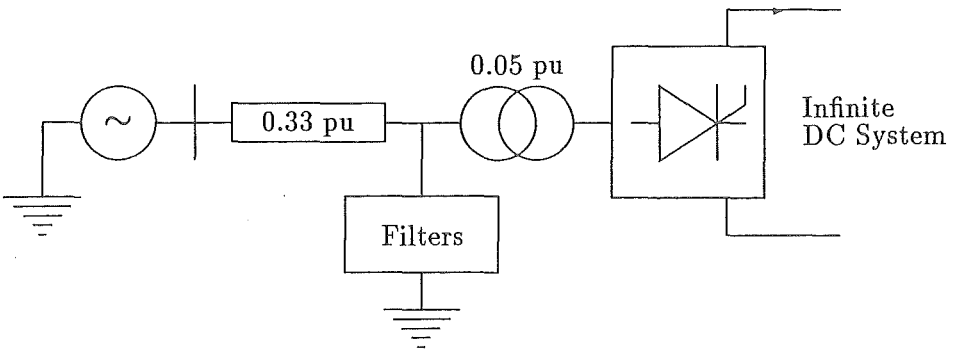

Figure 3.12: Symmetric system including filters.

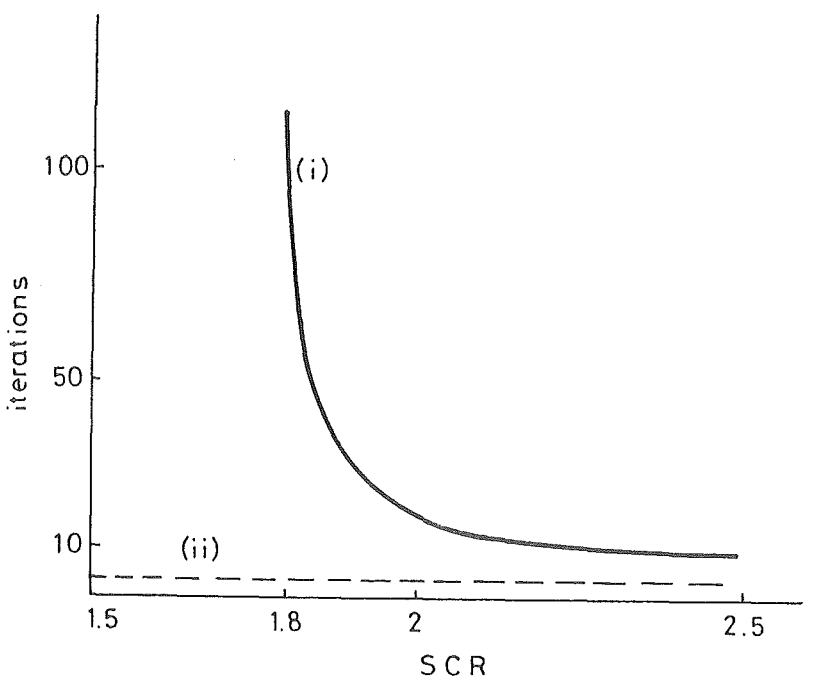

Figure 3.13: Effect of SCR on the convergence of IHA — (i) without thresholding (ii) with thresholding

3.4 DIVERGENCE UNRELATED TO UNCHARACTERISTIC HARMONICS

Thus far, attention has been focussed on the effect of uncharacteristic harmonics and the mechanisms by which divergence can occur. In the case to be discussed presently, however, uncharacteristic harmonics cannot be blamed for the divergence, since the system is symmetrical and non-resonant. The system under consideration is that of figure 3.14.

The system impedance is purely inductive, as is the transformer reactance, and the

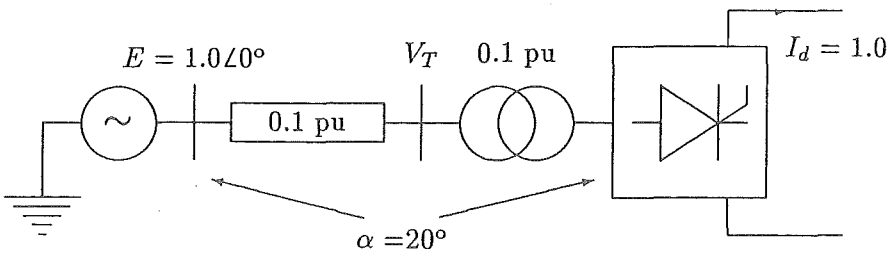

Figure 3.14: Analytically solvable test system

firing angle is measured with respect to the generator internal e.m.f. which is assumed to be perfectly sinusoidal. Thus the firing instants are fixed in time, and no amount of distortion at the terminal busbar (V_T) will shift them. It is clear that the harmonic distortion at the terminal busbar can be found by direct means if the system is redrawn as in figure 3.15.

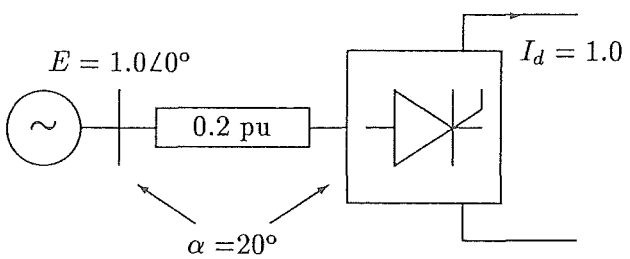

Figure 3.15: Figure 3.14 redrawn for clarity.

The a.c. current waveforms can be calculated using $E = 1.0\angle 0°$ as the commutating voltage, and since E is unaffected by the presence of either fundamental or harmonic currents, the solution is complete. The harmonic content of the current waveforms can be used to assess the distortion at V_T. This technique has already been used to cross-verify the results obtained by both IHA and TCS, and to validate the formulations of both (Arrillaga *et al.*, 1987), and yielded excellent comparisons up to the 15^{th} harmonic, as given in table 3.4.

However, subsequent attempts to repeat the study with higher harmonics (initially up to the 50^{th} - then the 25^{th}) failed because the IHA process failed to reach a solution. Inspection of the harmonics up to the 15^{th} revealed that they were essentially correct, and that the higher harmonics were the cause of the instability.

The problem was thought to stem from the fact that, due to the lack of filtering, the distortion levels were extremely high. The first iteration of IHA produced a current waveform with a commutation angle of 12°, compared with the value expected at the final solution of 19°. The reason for this is the presence of harmonics (in the form of

Harmonic Order	TCS	Exact	IHA
1	0.7666∠149.3°	0.7762∠149.5°	0.7658∠149.6°
5	0.1384∠−152.9°	0.1392∠−152.6°	0.1374∠−152.3°
7	0.0874∠145.8°	0.0887∠146.1°	0.0876∠146.4°
11	0.0381∠−159.3°	0.0386∠−158.3°	0.0383∠−157.8°
13	0.0246∠137.9°	0.0244∠137.7°	0.0243∠138.2°

Table 3.4: Comparison of the first 5 characteristic harmonic currents

the classical commutation 'notches') reduces the available commutating voltage over the commutation period, resulting in slower commutations. At the first iteration, with no harmonics present, the commutations are therefore fast. It seemed that, in this case, the initial error in commutation length was sufficiently large (7° is almost 1/2 cycle at the 25^{th} harmonic) that considerable error arose in the higher order harmonics, and that this induced error caused the IHA algorithm to fail.

The immediate approach to rectify this problem was to limit (initially) the number of harmonics considered, and gradually introduce them as the iterations proceeded. Thus the lower order harmonics (up to the 7^{th}) would be included from the beginning, followed later by those up to the 13^{th} and so on, so that, by the time the 23^{rd} and 25^{th} harmonics were introduced, the initial conditions for them would be much closer to the final solution. The method was tentatively labelled Binary Inclusion Relaxation Method (BIRM) since it is equivalent to assigning binary (0 or 1) weights to each harmonic. The inclusion scheme adopted is given in table 3.5.

Iterations	Highest Harmonic
1-3	7
4-6	13
7-9	19
10-12	25
13-15	31
16-18	37
19-21	43
22-24	49

Table 3.5: Inclusion scheme for BIRM.

This scheme corresponds to introducing the next 'set' of 6-pulse related harmonics at every third iteration.

When applied to the above problem, BIRM allowed the solution to proceed much further than before, with the reconstruction of the waveforms in figure 3.16 demonstrating the solution to be very close to the ideal solution.

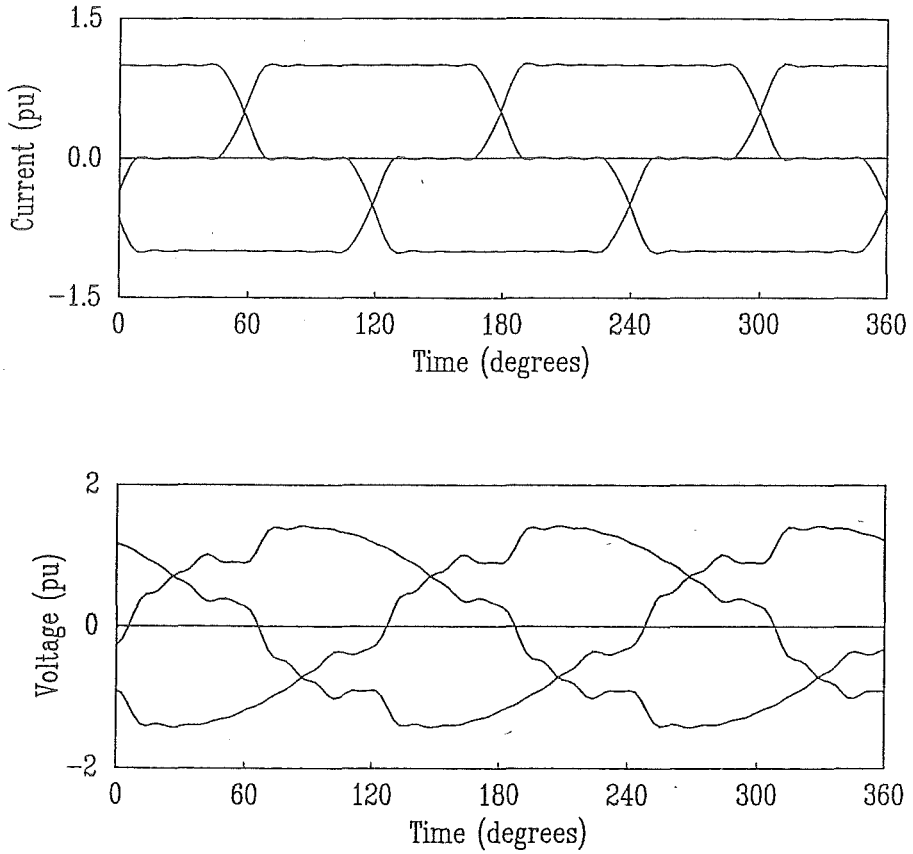

Figure 3.16: Reconstructed waveforms after applying the BIRM technique.

However, the fact that the IHA algorithm can still diverge in spite of ideal balanced and non-resonant conditions leads to the conclusion that there is some other factor, as yet unconsidered, which determines the course of the iterative procedure. The remainder of this chapter is therefore directed toward mathematical analysis of IHA in an attempt to isolate this unknown.

3.5 ANALYSIS OF IHA

The IHA process is a mathematical algorithm, based on the Gauss-Seidel method, for determining the harmonics which satisfy the constraints of the particular non-linear device. As such, it may be expected to suffer from the usual inferiority of the Gauss-Seidel methods with respect to other solution techniques.

3.5.1 Gauss-Seidel Nature of IHA

The fundamental definition of IHA for a general non-linear device is :

$$\begin{aligned} \mathbf{I}^{(k+1)} &= \mathbf{f}(\mathbf{V}^{(k)}) \\ \mathbf{V}^{(k+1)} &= [\mathbf{Y}]^{-1}\mathbf{I}^{(k+1)} \end{aligned}$$

where $\mathbf{f}(\mathbf{V})$ is a vector-valued function giving the harmonic currents produced by

the device for a particular set of harmonic voltages V, thus representing the device's non-linearity in the harmonic domain, and k is the iteration number. These equations simply state that the vector of harmonic currents depends on the applied set of harmonic voltages, which, in turn, depend on the system impedance and the injected currents. The currents can be eliminated between the two equations, giving :

$$\mathrm{V}^{(k+1)} = [\mathrm{Y}]^{-1}\mathrm{f}(\mathrm{V}^{(k)}) \tag{3.3}$$

which is clearly an equation of the form $x^{(k+1)} = g(x^{(k)})$, and is therefore Gauss-Seidel in nature. The convergence of the Gauss-Seidel or fixed-point (so called because the solution is a fixed point of the iterating function $x = g(x)$) iteration technique depends, in the single variable case, on the slope of the iterating function $g(x)$ (Traub, 1964). This dependence takes the form of a constraint on the slope of $g(x)$ in the interval containing the solution and the initial guess x^0 such that if the absolute value of the slope of $g(x)$ exceeds 1, then the method will diverge. This may be illustrated graphically for the single variable case as shown in figure 3.17.

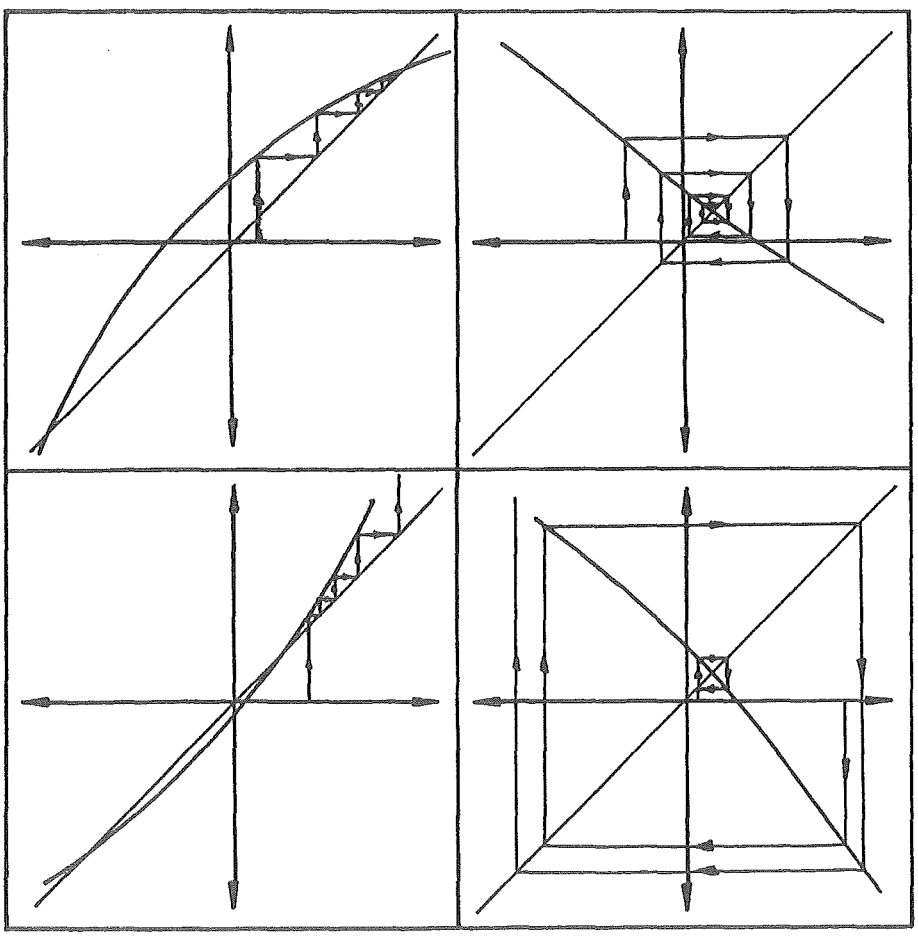

Figure 3.17: Gauss-Seidel convergence and divergence patterns. Clockwise from top left : Monotonic convergence, Oscillatory convergence, Oscillatory divergence plus limit cycle & Monotonic divergence.

If this is true in the single variable case, then it is likely that some analogous form

exists in the multivariable case, and may be applied directly to IHA, in order to obtain an understanding of the nature of divergence within IHA.

3.5.2 Multivariable Convergence Constraint

The multivariable convergence constraint given here is based on that given by Householder (1953).

Suppose that g(x) is a function with some constant vector a satisfying

$$\mathbf{a} = \mathbf{g}(\mathbf{a}) \tag{3.4}$$

and considering the sequence defined by $\mathbf{x}^{(0)}$ and

$$\mathbf{x}^{(k+1)} = \mathbf{g}(\mathbf{x}^{(k)}) \tag{3.5}$$

under what circumstances will the sequence converge onto **a** ?

A sufficient condition for this can be given by means of a Lipschitz condition. Letting big(x) represent the magnitude of the numerically greatest element in x, then the sequence of 3.5 will converge onto the vector **a** provided that for some $\epsilon < 1$ and on some suitable interval ρ :

$$\mathrm{big}[\mathbf{g}(\mathbf{x}^{(k+1)}) - \mathbf{g}(\mathbf{x}^{(k)}] < \epsilon\, \mathrm{big}[\mathbf{x}^{(k+1)} - \mathbf{x}^{(k)}] \tag{3.6}$$

for every $\mathbf{x}^{(k)}$ and $\mathbf{x}^{(k+1)}$ satisfying

$$\mathrm{big}(\mathbf{x}^{(k)} - \mathbf{a}) < \rho \;\&\; \mathrm{big}(\mathbf{x}^{(k+1)} - \mathbf{a}) < \rho \tag{3.7}$$

Noting that $\mathbf{x}^{(k+1)} = \mathbf{g}(\mathbf{x}^{(k)})$, then 3.6 can be rewritten

$$\mathrm{big}[\mathbf{g}(\mathbf{x}^{(k+1)}) - \mathbf{x}^{(k+1)}] < \epsilon\, \mathrm{big}[\mathbf{g}(\mathbf{x}^{(k)}) - \mathbf{x}^{(k)}] \tag{3.8}$$

The physical interpretation of this is that at every iteration, the greatest perturbation to the vector x *must* be less than that of the preceding iteration, which is a guarantee of convergence, although it does not guarantee to which solution (if there are more than one) the sequence will be directed.

3.5.3 Application to the Convertor

With particular reference to the static convertor formulation of IHA, the iterating function may be written as :

$$\begin{pmatrix} \mathbf{V} \\ \theta \end{pmatrix}^{(k+1)} = \begin{pmatrix} [\mathbf{Y}]^{-1}\mathbf{f}(\mathbf{V}^{(k)}, \theta^{(k)}) \\ \Theta\,([\mathbf{Y}]^{-1}\mathbf{f}(\mathbf{V}^{(k)}, \theta^{(k)}), \alpha) \end{pmatrix} \tag{3.9}$$

where Θ is a function which gives the new firing instants from the current voltage distortion. The dimension of the space (IHA-space) required to represent the problem considered here is $2N$ where N is the number of independent variables. $N = N_V + N_\theta$, N_V is the number of independent voltages, and N_θ the number of independent firing instants. Further, $N_V = 3(N_h - 1)$ where N_h is the highest harmonic considered on each phase. N_θ is 6 for phase angle control, and 1 for equidistant firing control. If the

$N_h =$	7	13	19	25	50
Phase Angle Control	48	84	120	156	306
Equidistant Firing Control	38	74	110	146	296
Constant Firing Instants	36	72	108	144	294

Table 3.6: Dimensions of the IHA-space for various cases.

firing instants are held constant with respect to some fixed external reference, $N_\theta = 0$. The dimensions of the harmonic spaces required for some typical cases are listed in table 3.6.

For the sake of simplicity, the firing instants will be excluded from the following derivation, accepting therefore the heuristic arguments presented in section 3.3.3. Their inclusion, however, is a straightforward but cumbersome extension of the following.

The iterating function for the convertor is :

$$\mathrm{V}^{(k+1)} = [\mathrm{Y}]^{-1}\mathrm{f}(\mathrm{V}^{(k)}) \tag{3.10}$$

It is assumed that the function $\mathrm{f}(\mathrm{V})$ returns the phase currents on the secondary of the convertor transformer, and that multiplication by $[\mathrm{Y}]^{-1}$ gives the voltages appearing on the primary side of the convertor transformer. In this case, then, V represents the voltage on the primary side of the transformer, which implies that the transformer winding arrangement must be included in the function $\mathrm{f}(\mathrm{V})$. This can be avoided if the voltage V is considered to be the commutating voltage of the convertor, referred to the secondary of the convertor transformer. In this way, $\mathrm{f}(\mathrm{V})$ is the same for all winding arrangements, and all that is required is a connection matrix [C] to refer the primary voltages back across the transformer to the secondary winding arrangement. The iterating function is therefore :

$$\mathrm{V}^{(k+1)} = [\mathrm{C}][\mathrm{Y}]^{-1}\mathrm{f}(\mathrm{V}^{(k)}) \tag{3.11}$$

where [C] and $[\mathrm{Y}]^{-1}$ are block diagonal matrices with the diagonals of [C] being :

$$[\mathrm{C}] = \begin{bmatrix} \frac{1}{a_1} & 0 & \frac{-1}{a_3} \\ \frac{-1}{a_1} & \frac{1}{a_2} & 0 \\ 0 & \frac{-1}{a_2} & \frac{1}{a_3} \end{bmatrix} \tag{3.12}$$

for a star-star transformer, and :

$$[\mathrm{C}] = \begin{bmatrix} 0 & 0 & \frac{-\sqrt{3}}{a_3} \\ \frac{-\sqrt{3}}{a_1} & 0 & 0 \\ 0 & \frac{-\sqrt{3}}{a_2} & 0 \end{bmatrix} \tag{3.13}$$

for a star-delta transformer connection.

The diagonals of $[\mathrm{Y}]^{-1}$ are obtained by inverting the 6×6 $[Y]_h$ matrix at each harmonic frequency to obtain :

$$\begin{bmatrix} Z_{PP} & Z_{PS} \\ Z_{SP} & Z_{SS} \end{bmatrix}_h = \begin{bmatrix} Y_{PP} & Y_{PS} \\ Y_{SP} & Y_{SS} \end{bmatrix}_h^{-1} \tag{3.14}$$

and noting the the primary side harmonic current injections are always zero, so that :

$$V_P = [Z_{PS}]I_S \tag{3.15}$$

and so the $[Z_{PS}]$ submatrices form the diagonals of $[\mathrm{Y}]^{-1}$.

In order to deal with the function f(V), it is necessary to simplify it by linearising it in the harmonic domain. Following the method of Semlyen *et al.* (1987), the form of the harmonic space equation of the convertor is :

$$\mathrm{I} = \mathrm{I_N} + [\frac{\partial \mathrm{f}}{\partial \mathrm{V}}]\mathrm{V} \tag{3.16}$$

where $\mathrm{I_N}$ has the physical interpretation of a Norton harmonic current source, V is the applied voltage, I is the resulting harmonic current vector, and the matrix $[\partial \mathrm{f}/\partial \mathrm{V}]$ is the Jacobian of the nonlinear function f(V) in the harmonic domain, in which each term $\partial f_i/\partial V_j$ represents the linear dependence of the i^{th} harmonic current on the j^{th} harmonic voltage. Practically, the terms within the Jacobian, which are partial derivatives in the frequency domain, would be evaluated by Fourier transforming the derivatives of $i(t)$ with respect to $v(t)$ in the time domain.

For the convertor, there are three time domain current waveforms, and three commutating voltage waveforms, so that, in principle, nine derivative waveforms are possible, and, again in principle, all of them are significant. To simplify the matter, it is assumed that the d.c. current is perfectly smoothed, so that during steady conduction of each phase, the current waveforms are independent of any of the voltages, and the derivatives are therefore zero. This removes three of the possible derivative waveforms, and simplifies the remaining six. The current waveforms still depend, however on the voltages driving their respective commutations. Each phase current depends on two commutating voltages : the voltage which turns the phase on, and the voltage which turns the phase off, as listed in table 3.7.

Phase Current	$v_{on}(t)$	$v_{off}(t)$
i_a	$v_{ac}(t)$	$v_{ba}(t)$
i_b	$v_{ba}(t)$	$v_{cb}(t)$
i_c	$v_{cb}(t)$	$v_{ac}(t)$

Table 3.7: Dependence of phase currents on commutating voltages.

However, since the d.c. current is perfectly smoothed, there is redundancy in the derivatives. For example, during the commutating on period of phase 'b',

$$i_a(t) + i_b(t) = I_d$$

where I_d is constant, so that

$$\frac{di_a}{dt} = \frac{-di_b}{dt}$$

Since $i_a(t)$ and $i_b(t)$ are both driven by the same commutating voltage ($v_{ba}(t)$) during the turn on of phase 'b', the derivatives of $i_a(t)$ and $i_b(t)$ with respect to the

commutating voltage $v_{ba}(t)$ are equal in form, but opposite in sign. By a similar argument,

$$\begin{aligned}\frac{di_a(t)}{dv_{ba}(t)} &= \frac{-di_b(t)}{dv_{ba}(t)} \\ \frac{di_b(t)}{dv_{cb}(t)} &= \frac{-di_c(t)}{dv_{cb}(t)} \\ \frac{di_c(t)}{dv_{ac}(t)} &= \frac{-di_a(t)}{dv_{ac}(t)}\end{aligned}$$

Thus, only three derivatives are unique, and the remaining three are accounted for by simple sign changes. The forms of the three unique derivatives are obtained by applying the chain rule to the time domain current and voltage derivatives. For example,

$$\frac{di_a(t)}{dv_{ac}(t)} = \frac{di_a(t)}{dt} \cdot \frac{dt}{dv_{ac}(t)}$$

From analysis of the commutating circuit, it is known that :

$$\frac{di_a(t)}{dt} = \frac{1}{l_{ac}} v_{ac}(t)$$

so that :

$$\begin{aligned}\frac{di_a}{dv_{ac}} &= \frac{1}{l_{ac}} \cdot \frac{v_{ac}(t)}{v'_{ac}(t)} \\ \frac{di_b}{dv_{ba}} &= \frac{1}{l_{ba}} \cdot \frac{v_{ba}(t)}{v'_{ba}(t)} \\ \frac{di_c}{dv_{cb}} &= \frac{1}{l_{cb}} \cdot \frac{v_{cb}(t)}{v'_{cb}(t)}\end{aligned}$$

with the 3 equations being valid during the commutation overlaps only. Figure 3.18 gives the form of each derivative function, and the three functions are then Fourier transformed and transferred into the Jacobian matrix of the function f(V). Of particular note is the fact that the magnitude of the derivative functions are inversely proportional to the commutating reactances, so that for small commutating reactance, the dependence of the harmonic currents on the harmonic voltages is considerable.

Having established the linearised form of the convertor equation, it may be substituted into equation 3.11 to yield :

$$\begin{aligned}\mathbf{V}^{(k+1)} &= [\mathbf{C}][\mathbf{Y}]^{-1}\left[\mathbf{I_N} + [\frac{\partial \mathbf{f}}{\partial \mathbf{V}}]\mathbf{V}^{(k)}\right] \\ &= [\mathbf{C}][\mathbf{Y}]^{-1}\mathbf{I_N} + [\mathbf{C}][\mathbf{Y}]^{-1}[\frac{\partial \mathbf{f}}{\partial \mathbf{V}}]\mathbf{V}^{(k)} \\ &= \mathbf{V_0} + [\mathbf{J}]\mathbf{V}^{(k)} \qquad (3.17)\end{aligned}$$

where [J] is the Jacobian of the iterating function. This may be inserted into the convergence contraint equation (3.6) to yield the following :

$$\begin{aligned}\text{big}\left([\mathbf{V_0} + [\mathbf{J}]\mathbf{V}^{(k+1)}] - [\mathbf{V_0} + [\mathbf{J}]\mathbf{V}^{(k)}]\right) &< \epsilon\,\text{big}\left(\mathbf{V}^{(k+1)} - \mathbf{V}^{(k)}\right) \\ \Longrightarrow \text{big}\left([\mathbf{J}](\mathbf{V}^{(k+1)} - \mathbf{V}^{(k)})\right) &< \epsilon\,\text{big}\left(\mathbf{V}^{(k+1)} - \mathbf{V}^{(k)}\right) \qquad (3.18)\end{aligned}$$

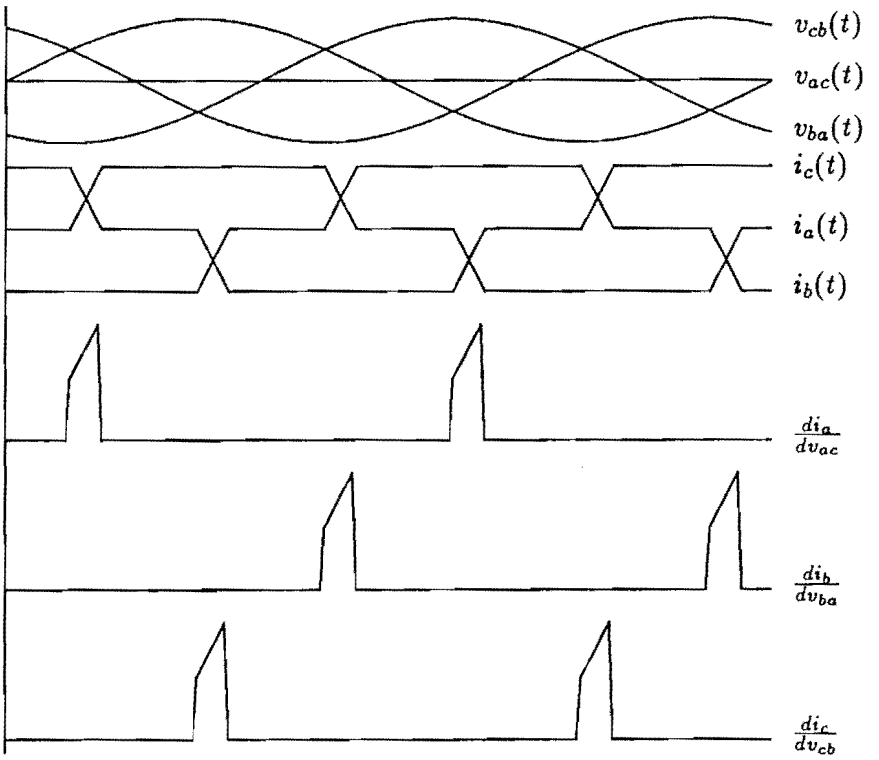

Figure 3.18: The three *unique* derivative functions.

This has the interpretation that the iterating function Jacobian matrix [J] should not be so large that the left hand side exceeds the right hand side. In other words, there is some norm (measure) of the matrix [J] such that the IHA process will diverge if the norm is exceeded. If steps can be taken to reduce the norm of [J] in a divergent IHA case, then the IHA process may be able to converge satisfactorily.

The factors affecting [J] for the static convertor are found by considering the equation for [J] :

$$[\mathrm{J}] = [\mathrm{C}][\mathrm{Y}]^{-1}\left[\frac{\partial \mathrm{f}}{\partial \mathrm{V}}\right] \tag{3.19}$$

from which it is clear that two actions may be taken to reduce the magnitude of [J].

(i) reducing the 'size' of $[\mathrm{Y}]^{-1}$.

(ii) reducing the 'size' of $[\partial \mathrm{f}/\partial \mathrm{V}]$.

In case (i), the magnitude of $[\mathrm{Y}]^{-1}$ can be decreased by introducing filters, or by strengthening the a.c. system - two approaches which are known to work. Alternatively, the derivative matrix may be reduced easily by *increasing* the values of the commutating inductances.

With reference to the unfiltered case of figure 3.14, both (i) and (ii) can be achieved simultaneously by shifting the terminal busbar electrically closer to the generator, while keeping the total impedance constant, so that the system impedance reduces and the commutating reactance increases. In line with this, the terminal busbar voltages also

have to be adjusted to reflect the reduced fundamental voltage drop along the reduced system impedance. This should have the effect of enabling the IHA algorithm to converge with the same physical system with which it diverged previously.

The results of several runs are summarised in table 3.8, which indicates that reducing the Jacobian of the iterating function has the desired effect of allowing the algorithm to converge.

X_{SYS}	X_C	Iterations to Convergence
0.05	0.15	8
0.07	0.13	14
0.08	0.12	20
0.09	0.11	36
0.10	0.10	Stagnated
0.12	0.08	Stagnated
0.15	0.05	Diverged
0.18	0.02	Converged to nonsense solution

Table 3.8: Convergence patterns with varying [J].

Therefore, by adjusting the parameters of the simulation, the same physical situation may be made to converge or diverge at will. This contradicts the widely held belief that divergence of IHA (or algorithmic instability) necessarily implies harmonic instability in the physical system.

This idea is also applicable to the heuristically derived causes of divergence in section 3.3.1, if the Jacobian of the iterating function contains information about the shifts in firing instants, and section 3.3.2, where interaction between firing instants & triplen harmonics on successive iterations would be determined by the off-diagonal elements in [J] linking the two, resulting in divergence when these elements exceed certain bounds.

3.5.4 A case with filters

The divergent case studied in depth by Eggleston (1985) was resurrected here to investigate the effect of changing the simulation parameters without changing the physical situation. The principal parameters of the divergent case are :

- 6-pulse convertor operating at 378 MW, with a d.c. current of 5.29 pu, connected to the Tiwai 220kV bus of the NZ South Island system.
- One set of pole filters from the Benmore end of the NZ HVDC link, including 5^{th}, 7^{th}, 9^{th}, 11^{th} & 13^{th} harmonic tuned branches and a 17^{th} harmonic high-pass branch.
- Realistic representation of the lower South Island (NZ) 220kV system, including the effects of distributed & frequency dependent line parameters and imbalance & mutual couplings between phases.

- Star-delta connected transformer with a 0.05 pu leakage reactance.
- Equidistant firing controller with $\alpha_{\min}$ =5.0°.

The previous case offered no resistance to shifting the point of observation electrically further from the convertor, but it should be clear that, in a case with filters, the point of observation cannot be shifted beyond the shunt elements that make up the filters without destroying the simplicity of the commutation model. Thus, the new observation point must always lie between the filters and the primary of the convertor transformer. This can be achieved by inserting a pair of equal and opposite reactances between the filters and the convertor transformer, so that their series combination is equivalent to a 'piece of wire'. This arrangement, depicted in figure 3.19, ensures that the physical system is preserved. The reactances will be referred to as an *inserted reactance pair*, and their value, X, will refer to the 50 Hz value of one of them.

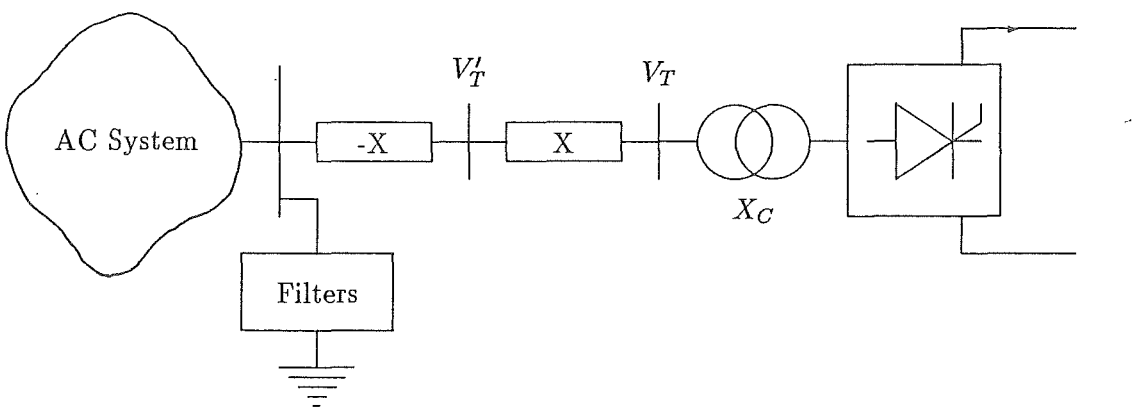

Figure 3.19: Position of the inserted reactance pair.

It is important to note that the negative reactance has no physical realisability, and that is certainly *not* a capacitor, which would have the wrong impedance/frequency characteristic for the application.

The positive reactance is then absorbed into the commutating reactance, while the negative reactance is absorbed into the parallel combination of the a.c. system impedance and the filter impedance. Thus V'_T becomes the new terminal busbar voltage.

The initial conditions at the original terminal busbar were obtained from a three phase a.c.-d.c. loadflow, with the terminal power flows given in table 3.9.

These were used to calculate the fundamental voltage magnitudes and angles at the fictitious terminal busbar V'_T with an inserted reactance pair of 0.05 pu, so that :

$$\begin{aligned} V'_a &= 1.164\angle 19.91^\circ \\ V'_b &= 1.184\angle -100.3^\circ \\ V'_c &= 1.182\angle 138.8^\circ \end{aligned}$$

Phase	Voltage (pu)	Real Power (MW)	Reactive Power (MVAr)
a	$1.0561\angle 10.58°$	132.95	65.4
b	$1.0762\angle -109.32°$	133.14	66.5
c	$1.0733\angle 134.81°$	134.81	66.1

Table 3.9: Terminal power flows at the original terminal busbar

Thus the angle difference is 19.91°−10.58°=9.33°, so that to retain the same firing *instants*,

$$\begin{aligned} \alpha' &= \alpha + 9.33° \\ &= 14.33° \end{aligned}$$

With the fictional busbar V_T' in place, the IHA algorithm converged in 12 iterations, indicating that a solution did in fact exist. To gain confidence in the accuracy of the method, the d.c. system resistance was increased, giving rise to a d.c. power of 278 MW, which is well within the normal convergent range of the IHA algorithm for this particular case, as shown by Eggleston (1985), and was in fact found to converge in 13 iterations.

An inserted reactance pair of 0.05 pu was then added to the normally convergent case, new initial conditions were calculated, and the algorithm run. This time, however, convergence took 81 iterations. The 0.05 pu inserted reactance pair were then replaced with a 0.01 pu pair, and the run repeated, but this time a limit cycle was entered, and convergence was not attained. Finally, with an inserted reactance pair of 0.005 pu, convergence was rapidly achieved in only 10 iterations, and the agreement between this case and the original in terms of the harmonic current magnitudes was found to be good.

Therefore the technique of changing the simulation parameters to achieve convergence without altering the physical system works with both the simple balanced and unfiltered case, as well as with the more complex unbalanced and filtered situation. However it seems that care must be exercised in the selection of the inserted reactance pair values to obtain the best result.

3.5.5 Interpretation in terms of continuation methods

The principal idea behind continuation methods is to deform a problem by introducing a parameter τ such that at some value of τ (τ_0) the problem is easily solvable, and at some other value of τ (τ_1) the problem is the one which is required to be solved. The desired solution is then found by integrating the parametricised problem solution with respect to τ along a path leading from τ_0 to τ_1, with initial conditions provided by the (easily found) solution to the problem with $\tau = \tau_0$. Details of the method and application to a wide range of engineering and related problems are given by Richter and DeCarlo (1983).

The inserted reactance pair technique may be visualised as a continuation method by considering the reactances to be always present with a weighting factor τ determining

the *actual* value present. Thus, with an appropriate inserted reactance pair which results in straightforward convergence, $\tau_0 = 1$ gives the easily solvable problem, and $\tau_1 = 0$ gives the required problem, since it removes the inserted reactance pair.

The process of integrating along the path from τ_0 to τ_1 is simplified by the fact that the true solution does not depend on the actual value of τ, since τ does not affect the physical system - just the simulation parameters. The true solution is found by integrating $dV'_h/d\tau$ with respect to τ from $\tau_0 = 1$ through $\tau_1 = 0$ with the initial condition $V'_h(\tau_0)$, noting that the harmonic currents flowing in the branch are independent of the particular value of τ. The function $V'_h(\tau)$ at harmonic frequency h is given by :

$$V'_h(\tau) = V_h - h\tau X I_h$$

where V_h is the h^{th} harmonic voltage at the primary of the convertor transformer, or that at the filter busbar, X is the value of the inserted reactance pair, and I_h is the h^{th} harmonic current injection. The derivative of this function is :

$$\frac{dV'_h(\tau)}{d\tau} = -hXI_h$$

since I_h & V_h are independent of τ. The integral from τ_0 to τ_1 is :

$$\begin{aligned} \int_{\tau_0}^{\tau_1} \frac{dV'_h(\tau)}{d\tau} d\tau &= \int_1^0 -hXI_h d\tau \\ &= [-h\tau X I_h]_1^0 \\ &= hXI_h \end{aligned}$$

Thus, the final solution at $\tau_1 = 0$ is given by :

$$\begin{aligned} V'_h(\tau_1) &= V'_h(\tau_0) + \int_{\tau_0}^{\tau_1} \frac{dV'_h(\tau)}{d\tau} d\tau \\ &= V'_h(\tau_0) + hXI_h \end{aligned}$$

It is noteworthy that the solution in terms of the continuation method is equivalent to adding the voltage drop along either of the inserted reactances to the voltage at the fictitious busbar V'_h, to give the voltage at the filter busbar or the primary of the convertor transformer, which is the more intuitive approach, and would be adopted in practice. This results from the extreme simplicity and linearity of the deformation of the original problem, and the fact that the deformation doesn't actually change the solution — just the point of obervation.

3.6 CONCLUSIONS

This chapter has been concerned with investigating the causes and nature of divergence within IHA, with a view to distinguishing between algorithmic instability and harmonic instability.

A review of the literature surrounding the topic revealed that opinion is divided on the matter, with some saying that algorithmic instability is completely equivalent to harmonic instability & others implying that it is simply a matter of poor numerical technique.

Past research in this department had indicated that divergence of IHA was not necessarily accompanied by instability in an equivalent time-domain (TCS) simulation, providing motivation for the thesis that divergence of IHA was simply a matter of algorithmic instability, and as such could be assisted or amended in some way to enable convergence.

Two heuristic arguments were advanced to explain the divergence of IHA with the phase angle controller and the equidistant firing controller in terms of triplen harmonic magnification between iterations and the phase of the third harmonic system impedance. Although, for the equidistant firing controller, the predicted impedance phases at which instability should occur were offset from those observed in the computational examples, the *difference* between the unstable 3^{rd} harmonic impedance phases observed for the star-delta and star-star transformer connections was consistent with that predicted i.e. 180°. It was also predicted that under otherwise similar conditions, the case with a star-delta transformer is likely to be more prone to divergence than with a star-star transformer.

Triplen harmonic generation in symmetrical systems by numerical noise was analysed and shown to be an artefact of the sampling technique used to sample the current waveforms, resulting in *apparently* unbalanced waveforms being presented to the FFT. Two techniques were proposed to deal with this situation. The first consisted of sampling with 3×2^N sampling points (where N is an integer) and using a Mixed Radix FFT to calculate the harmonic current phasors, while the second consisted of thresholding the harmonic current phasors (calculated in the normal way), such that harmonics less than 0.015% of the fundamental were set to zero. Both solutions have been found to be useful.

On the basis that IHA is essentially Gauss-Seidel in nature, a constraint equation was written and applied to IHA with reference to the static convertor. This showed that divergence of IHA could be traced to 'large elements' in the Jacobian of the iterating function, and demonstrated mathematically for the first time that divergence of IHA need not be representative of true harmonic instability. It was shown that the size of elements in the Jacobian could be reduced by shifting the terminal busbar (point of observation) at which the harmonic voltages are calculated such that the effective commutating reactance increases and the reactive component of the system impedance decreases. This was achieved by the addition of an 'inserted reactance pair' which combine electrically to equate to a single piece of wire, thus not affecting the physical system in any way. However, by picking the terminal busbar to be at the midpoint of the reactance pair, convergence of the algorithm was achieved in cases where it otherwise would not have been. Finally, the inserted reactance pair technique was shown to be a member of the class of solution techniques known as continuation methods, although in this case the deformation of the function is such that it leads to a trivial integral.

If, with *no* amount of adjustment to the simulation parameters (by the inserted reactance pair technique or any others) can the IHA process be made to converge, then (and only then) is it reasonable to assume that a true harmonic instability exists. Needless to say, the investigation must be thorough (and therefore tedious).

CHAPTER 4

INTEGRATED LOAD AND HARMONIC FLOWS

4.1 INTRODUCTION

Historically, load and harmonic flow algorithms have been separated by the fundamental assumption that they are disjoint : that is the fundamental operating conditions are not significantly affected by (reasonable) levels of distortion. However, the increasing levels of harmonic distortion brought about by higher powered non-linear devices in ever increasing numbers questions the validity of this assumption.

The single phase a.c.-d.c. load flow (Arrillaga and Bodger, 1977) was among the first attempts to integrate a representation of the convertor (other than as a purely fixed load) into the loadflow solution. As such, it not only provided real & reactive power injections into the a.c. network, but also yielded the operating state of each convertor in the system. The logical extension of the single phase a.c.-d.c. load flow was the three phase a.c.-d.c. load flow (Harker and Arrillaga, 1979), which took into account the effect of unbalance in supply voltages, commutating reactances and firing instants, as well as transformer connections. However, the three phase loadflow solution still assumed perfectly sinusoidal supply voltages and perfectly smooth d.c. currents. In order to more accurately assess the convertor operating state, the IHA technique described in chapters 2 & 3 was introduced, providing a three phase steady state harmonic operating snapshot of the convertor. This was generally run subsequent to a three phase load flow, which provided the best possible set of initial conditions.

Integration of load and harmonic flows has, thus far, been approached by two different techniques which bear mentioning. The method of Xia and Heydt (1982) is formulated in a similar manner to the Newton Raphson load flow in that appropriate mismatch equations, describing the operation of the convertor with harmonics, are written for all convertors in the network. These mismatches are iteratively forced to zero by manipulating the network voltages (at fundamental and harmonic frequencies) according to the actual mismatch and the Jacobian of the mismatch function. The mismatch functions are extended to include harmonic current balances at all busbars and apparent voltampere balance at all non-linear load busbars. Solution is again similar to the Newton Rhapson load flow, with the appropriate correction terms (ΔU) being calculated from :

$$\Delta M = [J]\Delta U \tag{4.1}$$

where ΔM is the mismatch vector and [J] is the Jacobian of the mismatch equations.

The method is, on the surface, complete in the sense that it can handle any combination of non-linear devices of arbitrary complexity. However, thus far at least, it has

only been formulated for the line commutated convertor in terms of its characteristic harmonics. In other words, the formulation is single phase in nature. One possible explanation for this is the anticipated complexity of the convertor formulation when the interaction between phases is considered in unbalanced operation. Certainly the computational and storage requirements would increase dramatically.

The second method, that of Tamby and Johns (1988) was formulated during the design stages of the Vancouver Light Rapid Transit system, and it is interesting to note that its *raison d'etre* was a perceived shortfall in the Xia and Heydt (1982) package (commercially available as HARMFLO), as well as in a consultant's package CYMHARMO (Cyme International Inc.,). The structure adopted for Q'HARM is of a more sequential nature, as depicted in figure 4.1, and caters for 6-pulse convertors and Non Linear Resistors (NLRs) as the non-linear elements of the system.

The functions of the steps involved are fairly self-explanatory. The 'Input Data' module reads in the necessary data, the 'Transmission Line' module forms equivalent-π models of each of the transmission lines at each harmonic frequency, and assembles them into a preliminary admittance matrix at each frequency. The 'Power Flow' module performs a Gauss-Seidel load flow using the fundamental frequency admittance matrix, and considering all buses to be conventional. The reactive power at NLR buses is zero, and at convertor buses is given by $Q = P \tan \alpha$. The '$[\mathbf{Y_{BUS}}]$' module forms the harmonic admittance matrices including the effects of filters and generator impedances, and these are inverted to form the bus impedance matrix in the $[\mathbf{Z_{BUS}}]$ module. The 'NLR' and '6-Pulse Convertor' modules provide the models of the non-linear devices in terms of their harmonic current injections given the applied harmonic voltages. The Non Linear Resistor model is a power series model with a state variable B which determines the overall real power consumption of the load. The 6-pulse convertor model calculates the convertor harmonic injections for a specified d.c. power and delay angle α. The 'Harmonic Power Flow' module uses the standard fundamental real and reactive power balance equations to update the fundamental voltages and a harmonic current balance equation of the form $\mathbf{V_{BUS}} = [\mathbf{Z_{BUS}}]\mathbf{I_{BUS}}$ at each harmonic to calculate the harmonic voltages at the appropriate buses. The convergence criteria are that the harmonic voltages do not vary significantly between iterations and that the NLR state variable B likewise converges to a stable solution. Finally the 'Output' module writes the converged harmonic voltages and currents to a file.

The method of convertor modelling is of interest here, since it maintains a constant d.c. power and delay angle in the presence of distortion. This is accomplished by writing equations for the d.c. components of the d.c. current and voltage (and therefore the d.c. power) in terms of the (harmonic) terminal voltages, the specified delay angle, the commutating reactance and the commutation overlap angle μ. μ is assumed to be a free variable, and can therefore be found numerically such that the constraint $P_{spec} = V_d I_d$ is satisfied. The technique employed is given in figure 4.2.

Once a suitable value of μ has been found, the current waveform can be calculated and Fourier transformed to extract the harmonic current components. Thus the Q'HARM approach to convertor modelling requires two iterative loops : the one solving for a suitable value of μ, and the other solving $\mathbf{V_{BUS}} = [\mathbf{Z_{BUS}}]\mathbf{I_{BUS}}$ at each harmonic. Inherent in the equations for V_d and I_d (written as $f(\mu)$ and $g(\mu)$ in figure 4.2 are the

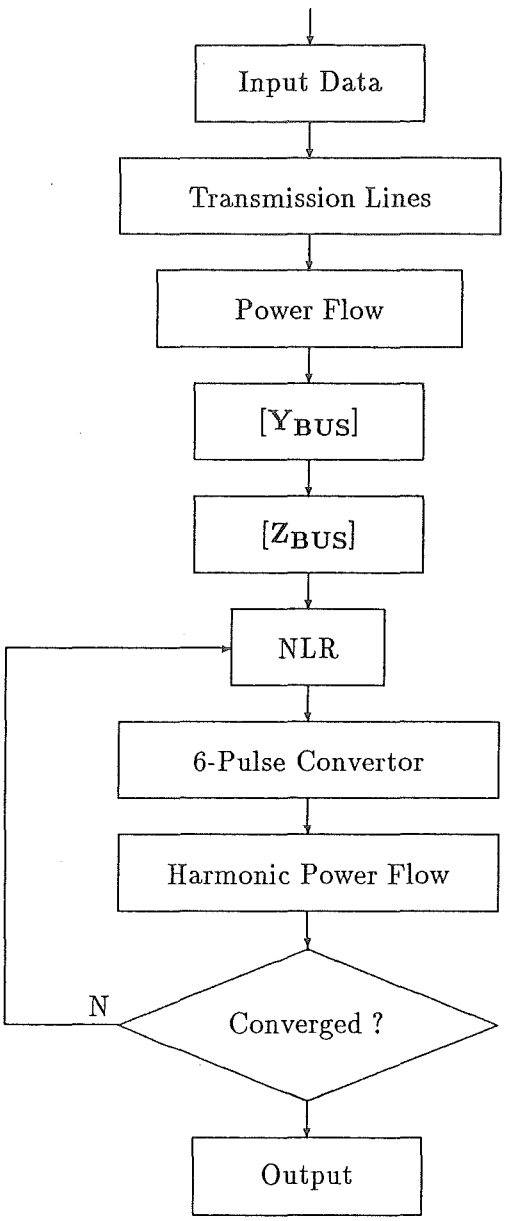

Figure 4.1: Flowchart of the Q'HARM algorithm.

assumptions that :

(i) Convertor losses are negligible.

(ii) I_d is perfectly smoothed.

(iii) Only characteristic harmonics are present.

While extension of the equations for V_d and I_d to encompass all three phases is possible in principle, this would be extremely cumbersome, as would the necessary

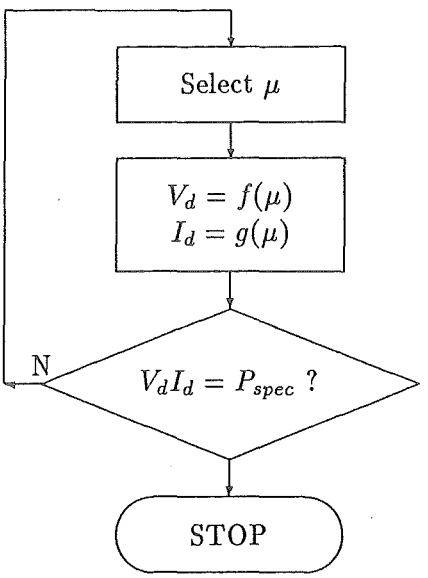

Figure 4.2: Convertor modelling within Q'HARM

modifications required to include d.c. current harmonics. However, the principal bar to the extension of the method is that with a three phase representation of the convertor, all six commutations are independent, and therefore all six commutation overlaps would have to be calculated from the single equation $P_{spec} = V_d I_d$. Thus the Q'HARM convertor modelling technique remains, as a single phase technique, ingenious in its conception, although somewhat limited in its scope of application.

However, the integrated load and harmonic flow algorithm, which will be developed in the next section, is nonetheless a distant cousin of Q'HARM in the sense that both have a similar double-iterative structure, and both solve for the fundamental and harmonic voltages at the non-linear load buses in a similar fashion.

4.2 THREE PHASE INTEGRATED LOAD AND HARMONIC FLOWS

The purpose of this section is to derive a three phase integrated load and harmonic flow algorithm. The existing tools for steady state convertor analysis have already been outlined in previous sections, and form the basis of the proposed algorithm. However, it is first necessary to review the operation of the three phase load flow, and, in particular, its convertor model. This will be used as a computational structure into which a more accurate harmonic model of the convertor can be subsequently inserted.

4.2.1 The Three Phase A.C.-D.C. Load Flow

In the three phase loadflow, the system admittance matrix includes the effect of each separate phase as well as the interphase mutual coupling in generators, transformers

and transmission lines. Moreover, the load active (P) and reactive (Q) powers are specified separately for each phase. The specified conditions are :

(a) at the all the generators' internal busbars (except the slack),

$$(\Delta P_{gen})_j = (P_{gen})_j^{SP} - (P_{gen})_j \tag{4.2}$$

$$(\Delta V_{reg})_j = f(V_j^1, V_j^2, V_j^3) = 0 \tag{4.3}$$

for $j = 1, ng - 1$, where ng is the number of generators.

(b) at the slack generator internal busbar,

$$(\Delta V_{reg})_{SL} = f(V_{SL}^1, V_{SL}^2, V_{SL}^3) = 0 \tag{4.4}$$

(c) at every generator terminal busbar and every load busbar,

$$\Delta P_i^p = (P_i^p)^{sp} - (P_i^p)^{ac} = 0 \tag{4.5}$$

$$\Delta Q_i^p = (Q_i^p)^{sp} - (Q_i^p)^{ac} = 0 \tag{4.6}$$

for $p = 1, 3$ and $i = 1, nb$, where nb is the number of busbars.

Equations 4.2 to 4.6 are written in terms of the unknown variables (normally V and θ). They may be solved by a 3-phase fast-decoupled Newton-Raphson algorithm (Harker and Arrillaga, 1979), as follows :

$$\begin{bmatrix} \Delta P_i^p/|V_i^p| \\ (\Delta P_{gen})_j/|(V_{gen})_j| \end{bmatrix} = [B'] \begin{bmatrix} \Delta\theta_i^p \\ \Delta(\theta_{gen})_j) \end{bmatrix} \tag{4.7}$$

$$\begin{bmatrix} \Delta Q_i^p/|V_i^p| \\ \Delta(V_{reg})_j \\ (\Delta(V_{reg})_{SL} \end{bmatrix} = [B''] \begin{bmatrix} \Delta V_i^p \\ \Delta(V_{gen})_j \\ \Delta(V_{gen})_{SL} \end{bmatrix} \tag{4.8}$$

where B' and B'' are the Jacobian matrices approximated to constants. The presence of an a.c.-d.c. convertor is manifest in two ways :

(i) an additional set of equations for each convertor, i.e.

$$[R] = [J][\Delta x] \tag{4.9}$$

which includes a further 26 variables per convertor.

(ii) modification of the constraint equations (4.5 and 4.6) at the convertor terminal busbars :

$$\Delta P_i^p = (P_i^p)^{sp} - (P_i^p)_{ac} - (P_i^p)_{dc} = 0 \tag{4.10}$$

$$\Delta Q_i^p = (Q_i^p)^{sp} - (Q_i^p)_{ac} - (Q_i^p)_{dc} = 0 \tag{4.11}$$

where $(P_i^p)_{dc}$ and $(Q_i^p)_{dc}$ are the convertor real and reactive power injections on each phase as functions of the a.c. terminal voltages and of the convertor variables.

The following convertor equations are developed from the three-phase variables illustrated in figure 4.3 with the convertor model being equally applicable to rectification and inversion. The assumptions made in the derivation of the equations are :

(i) No harmonic voltages exist at the terminal busbar.

(ii) No ripple component exists in the d.c. current.

(iii) The valve forward voltage drop while conducting is negligible.

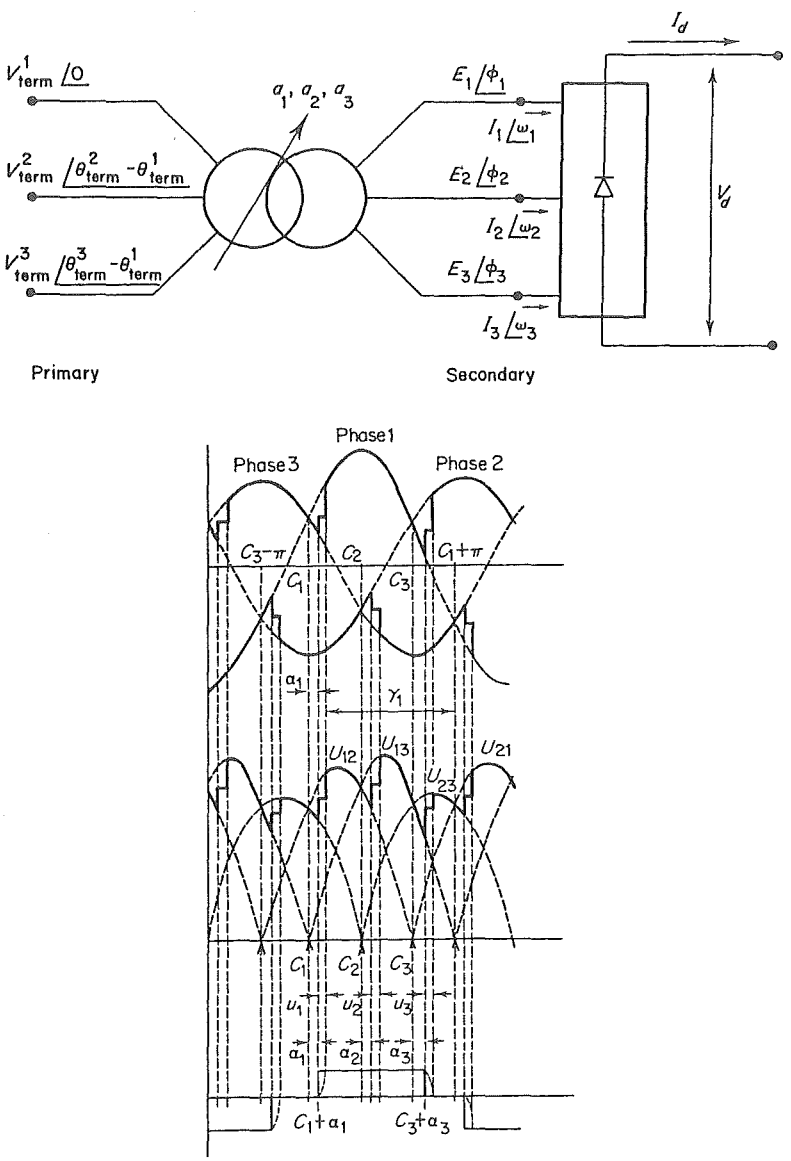

Figure 4.3: Assumed convertor connection and waveforms

The 26 equations which define the fundamental frequency operation of the convertor are as follows :

$$R(1) = \sum_{i=1}^{3} E_i \cos\phi_i = 0$$

$$
\begin{aligned}
R(2) &= \sum_{i=1}^{3} E_i \sin\phi_i = 0 \\
R(3) &= \sum_{i=1}^{3} E_i I_i \cos(\phi_i - \omega_i) - V_d I_d \\
R(4) &= I_1 - \frac{4I_d}{\sqrt{2}\pi} \sin(T_1/2) \\
R(5) &= I_2 - \frac{4I_d}{\sqrt{2}\pi} \sin(T_2/2) \\
R(6) &= I_3 - \frac{4I_d}{\sqrt{2}\pi} \sin(T_3/2) \\
R(7) &= I_1 \cos\omega_1 - \sum_{k=1}^{3} [b_{ss}^{1k} E_k \sin\phi_k + \\
&\quad b_{sp}^{1k} V_{term}^{k} \sin(\theta_{term}^{k} - \theta_{term}^{1})] \\
R(8) &= I_2 \cos\omega_2 - \sum_{k=1}^{3} [b_{ss}^{2k} E_k \sin\phi_k + \\
&\quad b_{sp}^{2k} V_{term}^{k} \sin(\theta_{term}^{k} - \theta_{term}^{1})] \\
R(9) &= I_3 \cos\omega_3 - \sum_{k=1}^{3} [b_{ss}^{3k} E_k \sin\phi_k + \\
&\quad b_{sp}^{3k} V_{term}^{k} \sin(\theta_{term}^{k} - \theta_{term}^{1})] \\
R(10) &= I_1 \sin\omega_1 - \sum_{k=1}^{3} [b_{ss}^{1k} E_k \cos\phi_k + \\
&\quad b_{sp}^{1k} V_{term}^{k} \cos(\theta_{term}^{k} - \theta_{term}^{1})] \\
R(11) &= I_2 \sin\omega_2 - \sum_{k=1}^{3} [b_{ss}^{2k} E_k \cos\phi_k + \\
&\quad b_{sp}^{2k} V_{term}^{k} \cos(\theta_{term}^{k} - \theta_{term}^{1})] \\
R(12) &= I_3 \sin\omega_3 - \sum_{k=1}^{3} [b_{ss}^{3k} E_k \cos\phi_k + \\
&\quad b_{sp}^{3k} V_{term}^{k} \cos(\theta_{term}^{k} - \theta_{term}^{1})] \\
R(13) & \\
\vdots \quad & \text{depend on the transformer connection.} \\
R(18) & \\
R(19) & \\
\vdots \quad & \text{depend on the control specifications.} \\
R(24) & \\
R(25) &= V_d\pi - \sqrt{2}U_{21}[\cos(C_1 + \alpha_1 - C_3 + \pi) - \\
&\quad \cos(C_2 + \alpha_2 - C_3 + \pi)] \\
&\quad -\sqrt{2}U_{13}[\cos(C_2 + \alpha_2 - C_1) - \\
&\quad \cos(C_3 + \alpha_3 - C_1)]
\end{aligned}
$$

$$
\begin{aligned}
& -\sqrt{2}U_{23}[\cos(C_3+\alpha_3-C_2)- \\
& \cos(C_1+\alpha_1-C_2+\pi)] \\
& +I_d(XC_1+XC_2+XC_3) \\
R(26) \;=\; & f(V_{di},I_{di}),\ \text{from d.c. system topology...}
\end{aligned}
$$

Mismatch equations 1 & 2 constrain the convertor transformer secondary voltages to have no zero sequence components, and equation 3 provides for continuity of real power across the convertor. Equations 4 to 6 define the fundamental current magnitudes on the secondary of the convertor transformer, and equations 7 to 12 govern the flow of (fundamental) current through the convertor transformer. Equations 13 to 18 refer the commutating voltages to the convertor transformer secondary voltage level and winding arrangement, while equations 19 to 24 are used to control specified quantities (usually off-nominal taps or delay angles). Finally equation 25 determines the average d.c. voltage level on the d.c. side and equation 26 relates the flow of d.c. current into the d.c. side network to the applied d.c. voltage.

These equations are solved according to the flowchart of figure 4.4.

With the sequential approach depicted in figure 4.4 the d.c. convertor power demands in equations 4.10 and 4.11 are considered as constant loads, and equations 4.7 and 4.8 are used without modification for the a.c. solution. For the solution of the d.c. link the terminal voltages V^i_{term} and θ^i_{term} are considered constant, and the standard Newton-Raphson technique is applied to equation 4.9. Thus there is not only (effectively) decoupling between the real and reactive power equations, but also between the convertor model equations and the rest of the loadflow, as shown in figure 4.5.

This decoupling allows the standard (fundamental frequency) convertor model to be easily replaced by *any suitable model*, and, in particular, with one which dispenses with the first and second assumptions made in the derivation of the standard loadflow model — the third is generally accepted at both fundamental and harmonic frequencies. However, in order to improve on the currently available integrated algorithms, the new model must be completely general — that is it must consider all harmonic frequencies on both sides of the convertor, as well as all causes of imbalance in the system. An eminently qualified model is, therefore, the IHA algorithm described in chapters 2 & 3.

4.2.2 Integration Of The Two Algorithms

The integration of the two algorithms is a relatively simple procedure - at the outermost level it consists of merely replacing the DC iteration of the loadflow with the IHA process. However the following considerations apply when merging the two algorithms.

4.2.2.1 Fundamental Power Flow

The fundamental real and reactive power flowing into the convertor is calculated in the three phase loadflow using the power flow equations across a three phase element — in this case the convertor transformer. This requires knowledge of the (equivalent) phase voltages on both the primary and secondary of the transformer : $V^i_{term}\angle\theta^i_{term}$ and $E^i\angle\phi^i$ respectively, and the relevant equations are (Arrillaga *et al.*, 1983) :

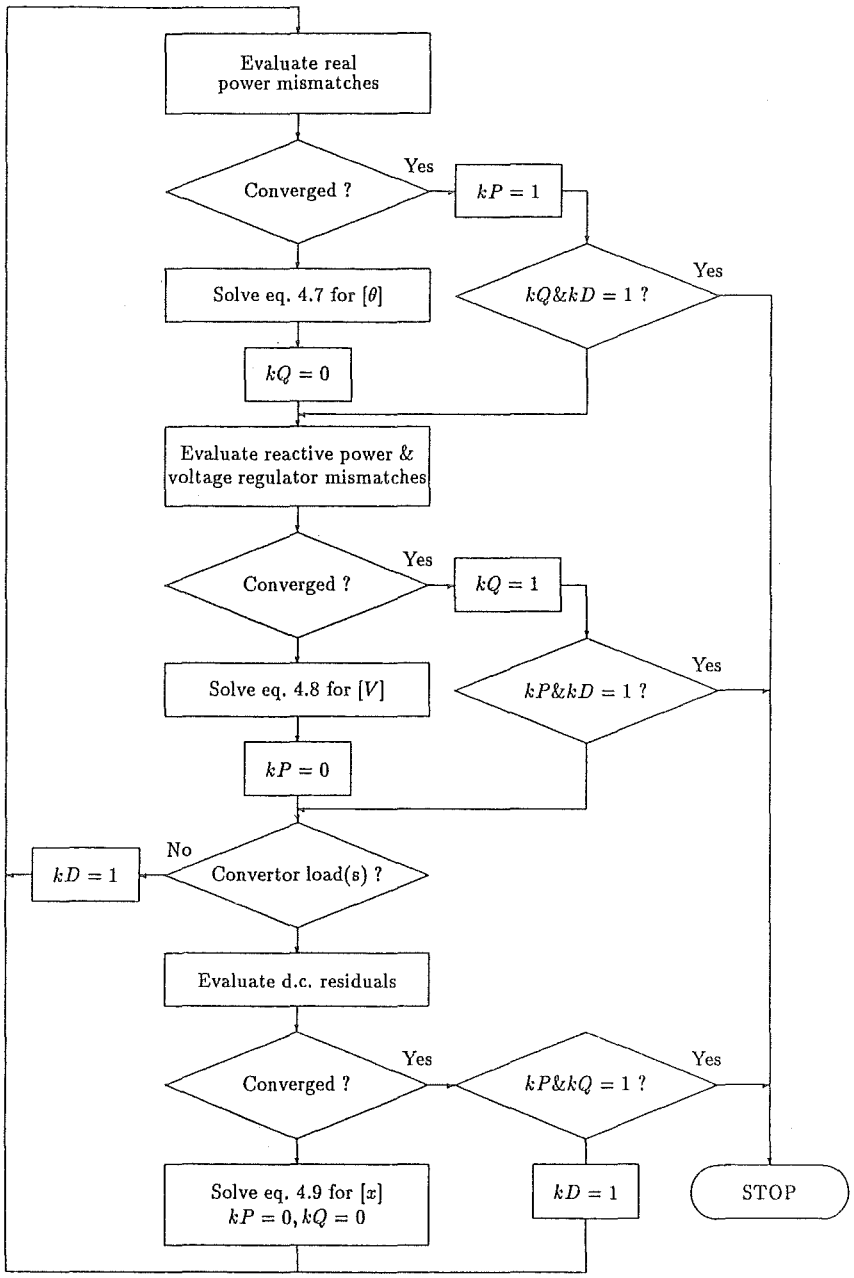

Figure 4.4: Detailed flowchart of the three phase a.c.-d.c. loadflow.

$$P_j = V_j \sum_{l=1}^{3} b_{ss}^{jl} E_l \sin\phi_l + b_{sj}^{jl} V_{term} \sin(\theta_{term}^{l} - \theta_{term}^{j}) \tag{4.12}$$

$$Q_j = V_j \sum_{l=1}^{3} b_{ss}^{jl} E_l \cos\phi_l + b_{sj}^{jl} V_{term} \cos(\theta_{term}^{l} - \theta_{term}^{j}) \tag{4.13}$$

This poses no problem in the loadflow, since both are part of the convertor solution, but $E^i \angle \phi^i$ are never used in the IHA algorithm, and must therefore be calculated. This is made possible by the fact that the fundamental phase currents on the secondary of the transformer (I_s) are known very accurately within IHA, and may be used with the

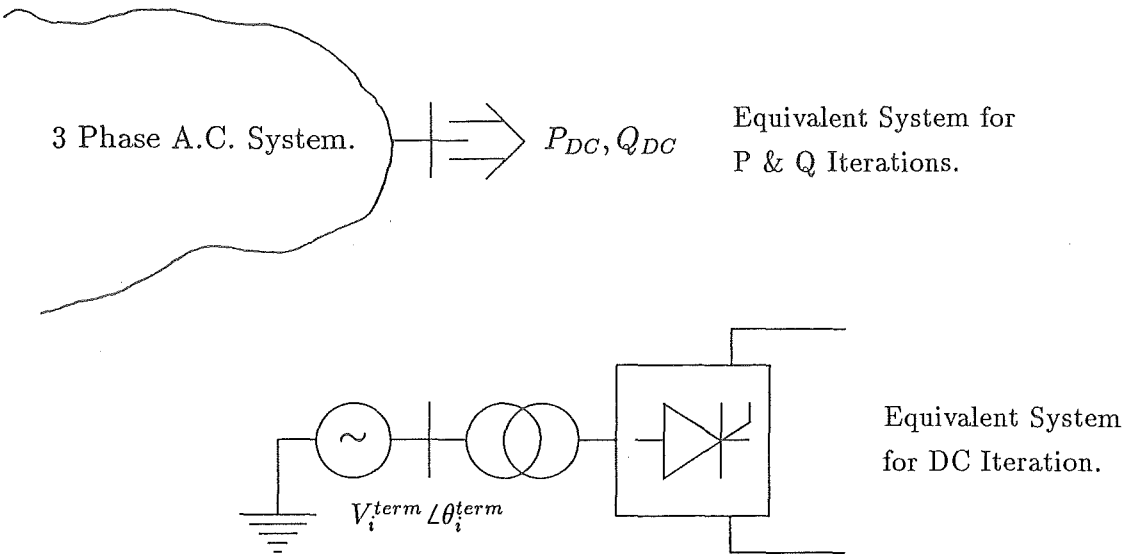

Figure 4.5: Decoupling between the convertor model and the real/reactive load flow.

known fundamental frequency terminal busbar voltages and transformer admittance matrix to calculate the effective secondary phase voltages, i.e.

$$\mathbf{E} = [\mathrm{Y_{SS}}]^{-1}(\mathrm{I_S} - [\mathrm{Y_{SP}}]\mathrm{V_{term}}) \tag{4.14}$$

The bracketed term represents the component of secondary current flowing to earth in the transformer, which is typically small, and, because it involves subtracting terms of similar magnitude, must be carried out with high arithmetic precision. The (sub)matrix $[\mathrm{Y_{SS}}]$ will be singular unless the transformer has some explicit reference point. This can be achieved by creating an artificial node to which all phases are connected via a large resistance. This new 'star' point can be eliminated from the matrix by earthing it, thus creating a mathematical reference equivalent to the zero sequence reference. The vector **E**, once calculated, can be further 'cleaned' by subtracting out any zero sequence components contained in it, thus ensuring the zero sequence reference is maintained.

4.2.2.2 Harmonic Power Flow

The harmonic power flows are, by contrast, never explicitly calculated in the program. This is because it is assumed that there are no sources of harmonic power in the network, and that the harmonic power dissipated in the network is due to harmonic conversion at the non-linear devices. By considering only the fundamental power flows at these devices, the network losses at harmonic frequencies are implicitly included, since the harmonic distortion at a non-linear device busbar is parasitic with respect to the fundamental component. Thus the real power available on the d.c. side of the convertor is given by :

$$P_d = P_1 + \sum_h P_h \tag{4.15}$$

and the individual terms P_h are given by summation of the individual phase harmonic powers over the three phases. Using the quantities defined in figure 4.6, the following equations result :

$$\begin{aligned} V_h &= -Z_h \angle\phi_h I_h \angle 0 \\ &= Z_h I_h \angle(\phi_h + \pi) \end{aligned}$$

from which :

$$P_h = -Z_h I_h^2 \cos\phi_h \tag{4.16}$$

and since, for ϕ_h in the range $\frac{-\pi}{2} - -\frac{\pi}{2}$, the $\cos\phi_h$ term is always positive, the harmonic powers are parasitic. Physically they represent the power dissipated at harmonic frequencies in the network impedance.

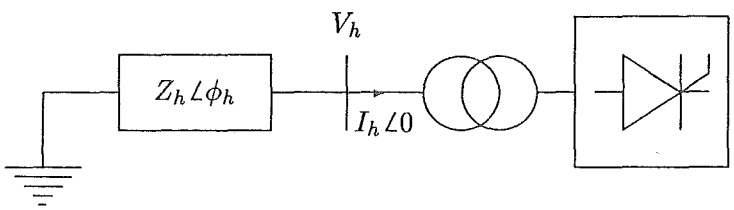

Figure 4.6: Harmonic voltage and current relationships at the terminal busbar.

The power balance equation (4.15) can now be rewritten as :

$$P_d = P_1 - \sum_h ||P_h|| \tag{4.17}$$

or as :

$$P_1 = P_d + \sum_h ||P_h|| \tag{4.18}$$

which states that the power in the fundamental waveforms at the terminal busbar equates to the useful power available on the d.c. side, and the harmonic losses in the network, and therefore the fundamental power requirement of the convertor realistically represents the actual real power load of the convertor with harmonics. This will be demonstrated by a practical example in chapter 5.

4.2.2.3 DC system consistency.

If the IHA algorithm is to be used within the context of the loadflow, then the d.c. voltage and current flows must remain consistent. However, as was discussed in section 3.3.3 it is not characteristic of IHA to maintain the required d.c. voltage on a bridge in the presence of harmonics. The residual equation in the fundamental frequency loadflow model which governs the d.c. voltage and current flows is :

$$[\mathrm{C}]\mathrm{V_d} + [\mathrm{D}]\mathrm{I_d} = 0 \tag{4.19}$$

Since an update of V_d is available at the end of each iteration of IHA, it is tempting to rearrange 4.19 to obtain a new set of d.c. currents, consistent with the latest d.c. voltages, for the next IHA iteration :

$$I_d = -[D]^{-1}[C]V_d \tag{4.20}$$

which is possible since [D] is rarely singular. By way of example, the [C] & [D] matrices for the simple loop of figure 4.7 are :

$$[C] = \begin{bmatrix} 1 & 1 & 1 & 1 \\ 0 & 0 & 0 & 0 \\ 0 & 0 & 0 & 0 \\ 0 & 0 & 0 & 0 \end{bmatrix}$$

$$[D] = \begin{bmatrix} -R_{loop} & 0 & 0 & 0 \\ 1 & -1 & 0 & 0 \\ 0 & 1 & -1 & 0 \\ 0 & 0 & 1 & -1 \end{bmatrix}$$

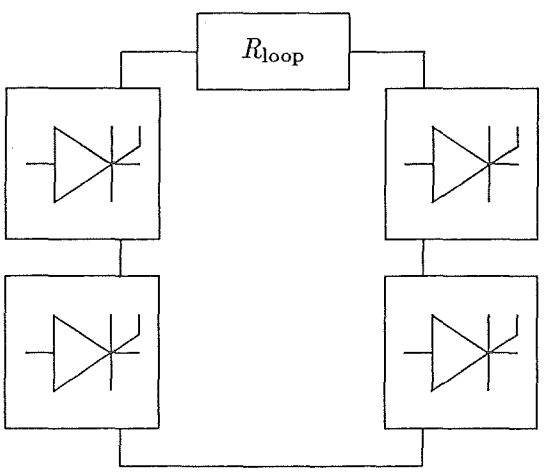

Figure 4.7: Simple loop configuration

While this is feasible when modelling convertors feeding passive resistive loads, it is not so where a rectifying/inverting loop is present, such as the one in figure 4.7, for the following reason. When the harmonics are initially introduced, the general effect is to reduce (slightly) the average rectifier voltage, and to increase (again slightly) the average invertor voltage, due to the notches which appear in the commutating voltage waveshapes. Thus, the total loop voltage, which represents the difference between the rectifier and invertor d.c. voltages, decreases significantly, resulting in a proportionally smaller loop current on the next iteration. On the next iteration, the commutations are shorter (due to the reduced d.c. current) and the d.c. voltages move in the opposite direction (i.e. the rectifier voltages increase slightly while the invertor voltages reduce),

resulting in a larger loop voltage, and a correspondingly larger d.c. current on the next iteration. With a realistic system, the swings in d.c. current become excessive within only a few iterations.

To combat this, the d.c. loop current must somehow be held constant, and this is achieved by maintaining the loop current constant at the value originally specified (or calculated) by the conventional loadflow, and adjusting the d.c. voltages to ensure consistency. However, since the average d.c. voltage for each bridge is a complex function of the fundamental and harmonic terminal voltages & firing instants, the simplest and most realistic method for adjusting it is to introduce an ideal, continuously variable tap changing transformer in series with the existing transformer, as depicted in figure 4.8. Since the transformer is ideal (i.e. without leakage), it takes no part in the commuta-

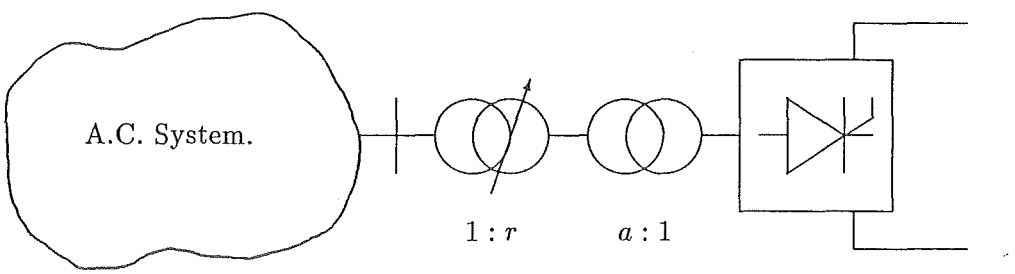

Figure 4.8: Position of the ideal tap-changing transformer.

tion process, and serves only to scale the effective commutating voltages such that the necessary loop voltage is attained. The tap ratio, r, of the new transformer is varied in the following manner to maintain the loop current at the 'pre-harmonics' value.

After each iteration, the total rectifier and total invertor voltages are calculated in each loop, and are added to form the total loop voltages. These are used to calculate the loop currents which would otherwise occur, from equation 4.20. A representative current from each loop is divided into the actual loop voltage, to give the effective loop impedance, which is then used to calculate the total loop voltage required to give the necessary (set-point) loop current. The strategy for applying tap control to the individual bridges contributing to the loop is based on the fact that, in typical convertor systems, the d.c. current is maintained by the rectifiers only, while the invertors are run under constant extinction angle control to maintain an adequate commutation safety margin on each valve. Therefore, the tap ratios are only applied to the rectifiers contributing to each loop.

An example of the generalised implementation is in order here to clarify the algorithm, using the d.c. system of figure 4.9, in which bridges 1, 2 & 3 are assumed to be rectifiers, and the remaining bridges the invertors.

The current to be controlled (I_d) flows entirely through bridges 1 & 6, so either I_{d1} or I_{d6} can be the representative loop current. The additional input required to the implementation is :

(i) the bridges contributing to the total loop voltage (i.e. bridges 1, 3, 4 & 6 in figure 4.9).

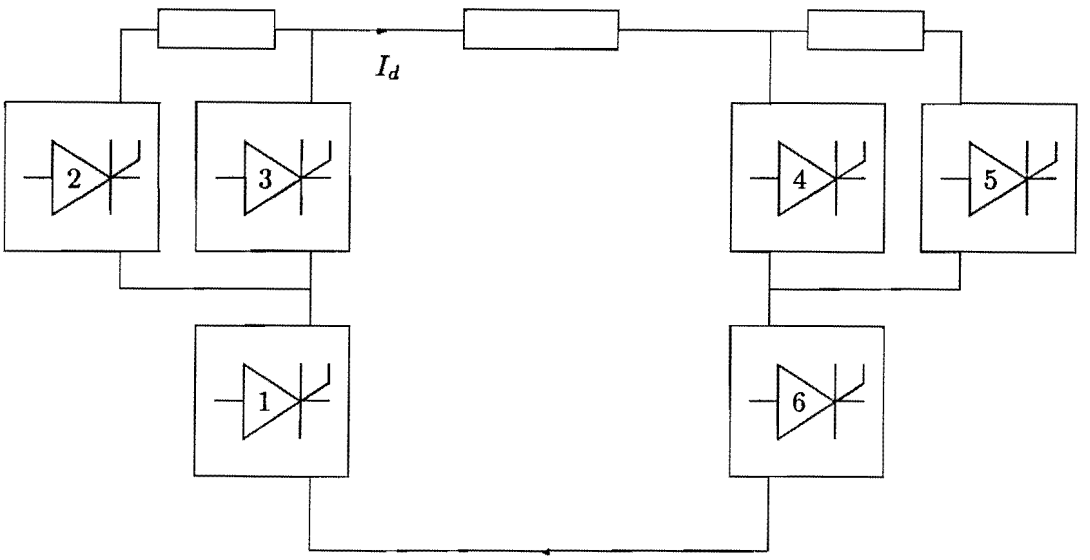

Figure 4.9: Example of application of the tap ratio algorithm.

(ii) bridges to which tap control must be applied (bridges 1, 2 & 3 in figure 4.9, since they are the rectifiers).

(iii) a bridge whose current is identical with the loop current (bridges 1 or 6 in figure 4.9).

The method for calculating r begins by calculating the rectifier and invertor components of the actual loop voltage, followed by the loop voltage itself.

$$\begin{aligned} V_{rect-actual} &= V_{d1} + V_{d3} \\ V_{inv-actual} &= V_{d4} + V_{d6} \\ V_{loop-actual} &= V_{rect-actual} + V_{inv-actual} \end{aligned}$$

The actual convertor currents are calculated using equation 4.20 and $I_{loop-actual} = I_{d6}$. From this, the loop voltage required to give the set value of I_d is :

$$V_{loop-req'd} = V_{loop-actual} \frac{I_{loop-req'd}}{I_{loop-actual}}$$

where $I_{loop-req'd}$ is the required loop current. Thus the required rectifier voltage in the loop is :

$$V_{rect-req'd} = V_{loop-req'd} - V_{inv-actual}$$

since the invertor voltages are assumed not to vary. Finally the required tap ratio for the rectifiers in the loop is :

$$r = \frac{V_{rect-req'd}}{V_{rect-actual}}$$

The resulting tap ratios are used in two ways :

(i) to scale the commutating voltages (fundamental and harmonics) on the next iteration such that the appropriate d.c. voltages are obtained.

(ii) to scale the secondary harmonic currents prior to their injection into the system impedance, so that consistency is maintained.

The deviation of r from unity at final convergence gives an indication of the departure of the integrated load and harmonic flow solution from that of the standard loadflow solution.

4.2.2.4 Zero Crossing Control

Notwithstanding the *caveat* of chapter 3, a limited form of zero crossing control is implemented such that at the beginning of each IHA process the current zero crossings are recalculated. A Newton-Raphson method is employed, taking the old zero crossing instants as initial conditions. Typically this requires 3–4 iterations when harmonics are initially introduced, but only 1–2 subsequently. The delay angle selected is the minimum α_i supplied by the loadflow convertor model. With the true zero crossings calculated, one must be selected as a reference crossing so that the equidistant firing template may be applied. The crossing point is selected such that :

(i) with equidistant firings NO violations of $\alpha_{\min}$ occur.

(ii) if more than one crossing point satisfies (i), the reference is selected such that the *maximum* deviation from $\alpha_{\min}$ on any other phase is *minimised*.

An example of the application of these constraints is illustrated in figure 4.10.

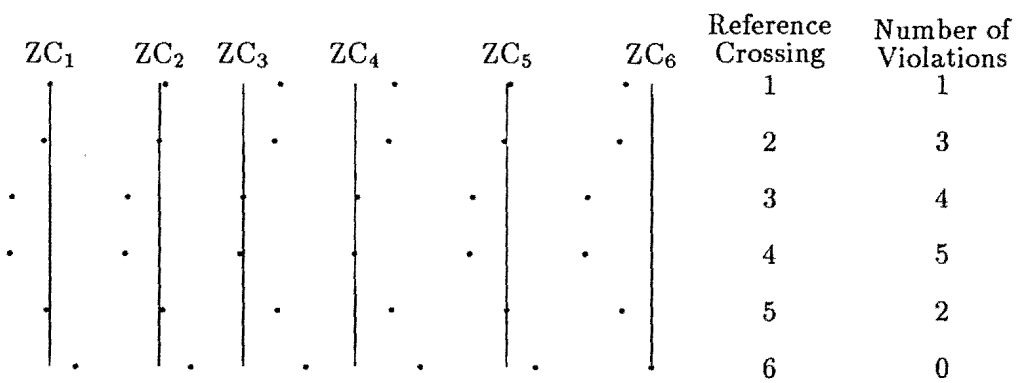

Figure 4.10: Selection of the reference zero crossing. The dots represent the (equidistant) firings which would occur at zero delay angle for the given reference phase. Any firing occuring before a zero crossing represents one violation of the minimum α constraint.

4.2.3 Form of the combined solution.

The most obvious form of the combined solution is obtained by simply replacing the DC iteration of the loadflow with the IHA process, subsequent to convergence of the loadflow with the fundamental frequency convertor model. This is illustrated in figure 4.11. In this form, each P and Q iteration is followed by a complete IHA process until the P and Q mismatches fall below a tenth of the convergence tolerance of the fundamental loadflow. This convergence criterion reflects the fact that convergence of

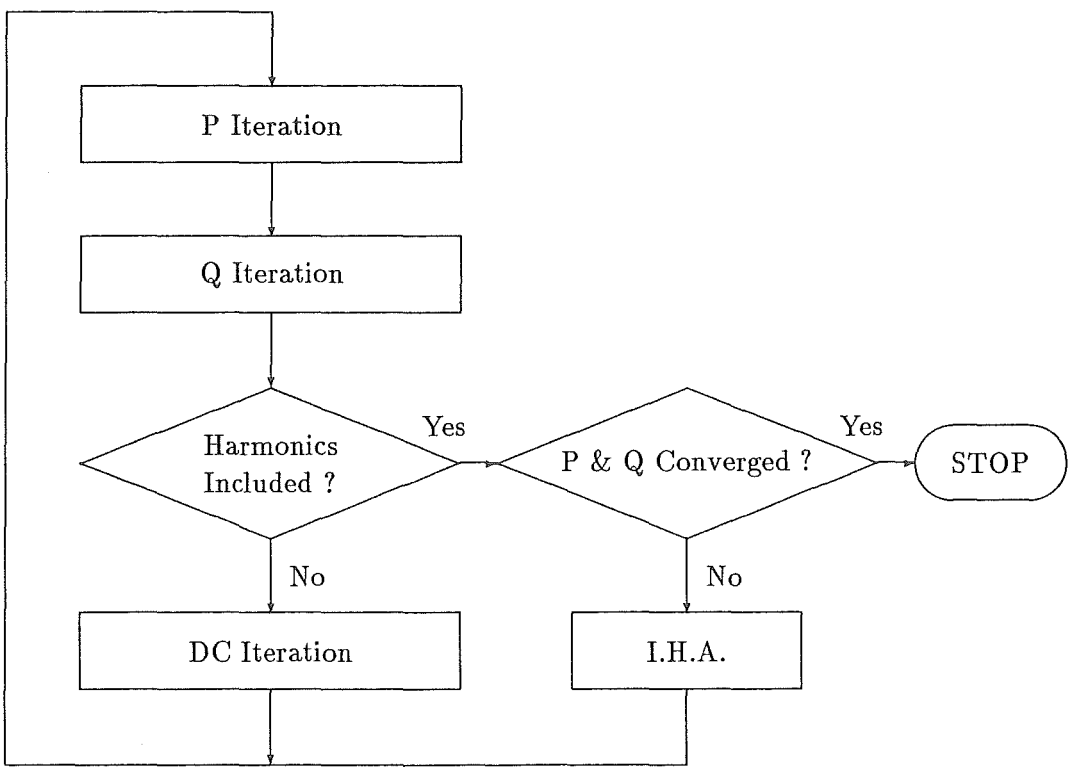

Figure 4.11: Obvious form of the integrated algorithm.

the IHA process always results in a self-consistent convertor solution, so there is no explicit convergence requirement for this in the outer loop as there is with the DC iteration. Therefore, if the P and Q mismatches are sufficiently small subsequent to a converged IHA process, then the integrated solution is consistent, and final convergence has been obtained.

For convenience, each excursion around the right hand loop (P iteration, Q iteration, IHA) of the integrated algorithm will be referred to as a PQH iteration, the IHA process will be known as an Harmonic iteration, and each iteration of the IHA process in the Harmonic iteration as an HA iteration.

4.2.4 Convergence Considerations

Convergence of the integrated algorithm depends on two distinct factors :

- The ability of the load flow algorithm to 'track' the small changes in convertor real and reactive demand due to the introduction and interaction of harmonics.
- Repeated convergence of the IHA process.

With regard to the first point, the anticipated changes in real and reactive demand are likely to be small, compared with those variations experienced during initial loadflow convergence with the fundamental frequency convertor model. Therefore, within the limits of arithmetic accuracy, this is not likely to become a problem.

The question of repeated convergence of IHA is less easily dealt with, and the considerations of chapter 3 apply. Observation of many simulations has indicated that, having converged once, IHA convergence is generally obtained in subsequent iterations. A guarantee of convergence on the first iteration cannot, however, be readily given. Thus, convergence of the integrated load and harmonic flow algorithm hinges primarily on the characteristics of the IHA process. Note that this is not necessarily a detrimental feature of the integrated algorithm, since the principal alternative to it (in terms of three phase unbalanced steady state harmonic analysis) is the IHA algorithm.

4.3 INITIAL TEST RESULTS

In order to gain an initial 'feel' for the performance of an algorithm, it is often useful to implement a very simple test system, such as the system here depicted in figure 4.12.

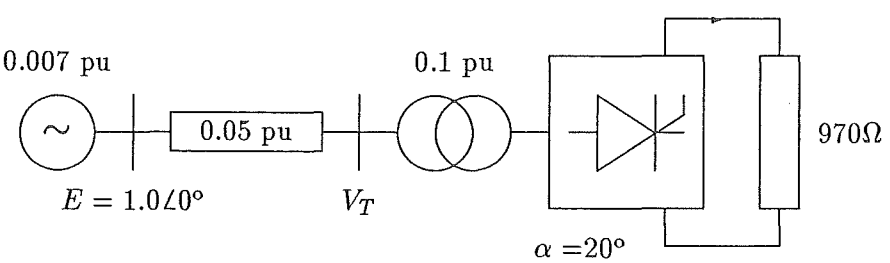

Figure 4.12: Integrated load and harmonic flow — initial test system.

Three variants of this test system are considered : exactly as in figure 4.12, the same with a 9.4μF capacitor connected to the terminal busbar (V_T), and again, with the capacitor replaced by a typical set of harmonic filters corresponding to those used on one pole of the Benmore end of the HVDC link.

The algorithm performance is considered in terms of the numbers of PQH and HA iterations required subsequent to the convergence of the fundamental loadflow convertor model, and a comparison is also drawn with the case where the zero crossing controller is disabled (i.e. the firing *instants* specified by the loadflow are maintained).

4.3.1 Unfiltered Case

The performance parameters of the integrated algorithm in the unfiltered case are given in table 4.1. In the absence of filters it is apparent that the presence of harmonics

PQH iterations	HA iterations	ΔZC°_{MAX}	HA iterations without ZC control
1	10	—	10
2	7	-2.645	2
3	3	0.142	1
4	1	-0.0207	1
5	1	0.000	1
6	1	0.000	—

Table 4.1: Performance of the integrated algorithm without filters.

has a significant effect on the zero crossings and the harmonic interaction process, as witnessed by the numer of extra HA iterations required with the zero crossing controller enabled. This is expected, however, since the initial changes in zero crossings (and therefore firing instants) are large & have a significant impact on the harmonics — especially at the higher orders. This effect, however, decays as the subsequent ZC shifts become smaller. It is therefore due to this initial perturbation to the harmonics that the ZC controlled case requires one extra PQH iteration over the uncontrolled case.

4.3.2 Shunt Capacitor Case

The presence of the 9.4μF capacitor has a significant effect on the whole process, as shown in table 4.2. Because the parallel combination of the capacitor (9.4μF) and the

PQH iterations	HA iterations	ΔZC°_{MAX}	HA iterations without ZC control
1	4	—	4
2	3	1.924	2
3	2	0.140	1
4	1	-0.00027	1
5	1	0.0000	—

Table 4.2: Performance of the integrated algorithm with capacitive reactive support.

system inductance (0.057 pu $\equiv$87.8 mH) is resonant at 175 Hz, the impedance seen by nearly all of the harmonics is capacitive, and this results in an entirely different set of ZC shifts. The shifts are now positive, so that the firing instants are now delayed by nearly 2° with respect to those of the fundamental loadflow. However, because the magnitude of the harmonic impedances decreases with frequency, being essentially capacitive in nature, the distortion at the terminal busbar is considerably lower than in the unfiltered case, explaining the low number of HA iterations required, which differs only slightly from those of the uncontrolled ZC case.

4.3.3 Filtered Case

In this case the distortion is again considerably lower than in either of the two previous cases, due to the design of the filters and the symmetry of the convertor operation, resulting in a greatly reduced degree of harmonic interaction. Thus the ZC shifts are much smaller than in the previous cases, although still obviously significant relative to the reduced levels of harmonic distortion, since the first and second PQH iterations both require the same number of HA iterations, as shown in table 4.3. By contrast the uncontrolled ZC case displays significant harmonic interaction only on the first PQH iteration.

PQH iterations	HA iterations	ΔZC°_{MAX}	HA iterations without ZC control
1	3	—	3
2	3	-0.335	1
3	1	-0.01	1
4	1	0.025	1
5	1	0.000	—

Table 4.3: Performance of the integrated algorithm with filters.

4.4 CONCLUSIONS.

An integrated algorithm for solving both load and harmonic flows for the static convertor in the general unbalanced three phase case has been derived in this chapter.

In contrast with other 'state of the art' proposals, the method proposed here is completely general in the sense that no assumptions are made concerning the degree of imbalance or the presence/absence of any harmonics, and is sufficiently flexible to allow various extensions such as d.c. system harmonic modelling. Integrity of real power flow is also maintained.

A method of absorbing the descrepancies which occur between the initial fundamental frequency operating state and the new harmonic operating state has been developed such that consistency is maintained in the d.c. side interconnection equations. A simple form of zero crossing control has also been developed which perturbs the IHA algorithm on the first HA iteration of each PQH iteration only, thus not continually interfering with the harmonic interaction process, but ensuring that, at final convergence, all the firing angles obey the minimum-α constraint with respect to the true zero crossings. This is borne out by the fact that in the three cases presented in section 4.3, the zero crossing shifts always decay to zero by the final PQH iteration. However, initial introduction of the ZC shifts (at the beginning of the second PQH iteration) incurs a penalty in the form of a significant increase in the number of HA iterations in this PQH iteration with respect to the uncontrolled ZC case.

The next chapter will present the application of the integrated load and harmonic flow algorithm to more realistic test systems, and will demonstrate on a practical system the integrity of real power flows.

CHAPTER 5

PRACTICAL APPLICATIONS

5.1 INTRODUCTION

It should be clear that the principal application of the integrated load and harmonic flow algorithm derived in chapter 4 is in the planning stages of a project or system, where accuracy and thoroughness are of primary importance. Operational load & harmonic flows, by contrast, seldom require such accuracy for the simple reason that, by then, it is often too late. This chapter, then, is devoted to some practical examples of planning stage studies of the type it is likely to be used for in practice. All examples refer to the New Zealand system, which has three major convertor loads. Briefly, they are :

(i) An aluminium smelter (Tiwai Point) in the south of the South Island. Operation here is by way of a 48-pulse rectiformer plant, which is slightly different in construction to a thyristor rectifier plant, although the steady state operation is identical. The total convertor power is some 450 MW.

(ii) A (normally) rectifying convertor station of 600 MW at Benmore, where four mercury-arc bridges are connected to form a 12-pulse bipolar convertor station. Benmore is situated about 400 km from the bottom of the South Island, and feeds a bi-polar transmission line of about 500 km, followed by an undersea cable of about 37 km, and a further 36 km of overhead line in the North Island.

(iii) A (normally) inverting convertor station at Haywards, in the south of the North Island. This is the receiving end of the transmission path from Benmore, and inverts into a fairly weak system dominated by a local municipal load (Wellington city) with more distant generation in the north.

Thus, with the wide spacing of nonlinear loads in the network it is clear that there are plentiful opportunities for interplay between harmonics from the various centres, especially given the possibility of resonances existing within the network.

5.2 TIWAI ALUMINIUM SMELTER

The first example given here is that of the Tiwai Aluminium Smelter considered in isolation, and the principal purpose is to demonstrate facets of the integrated algorithm with reference to a meaningful example. For practicality's sake, the South Island 220 kV system is reduced in this case to a seven bus system surrounding Tiwai, and is equivalent to that used by Harker (1980) and Eggleston (1985), as well as in chapter 3 of this thesis. The system is depicted in figure 5.1.

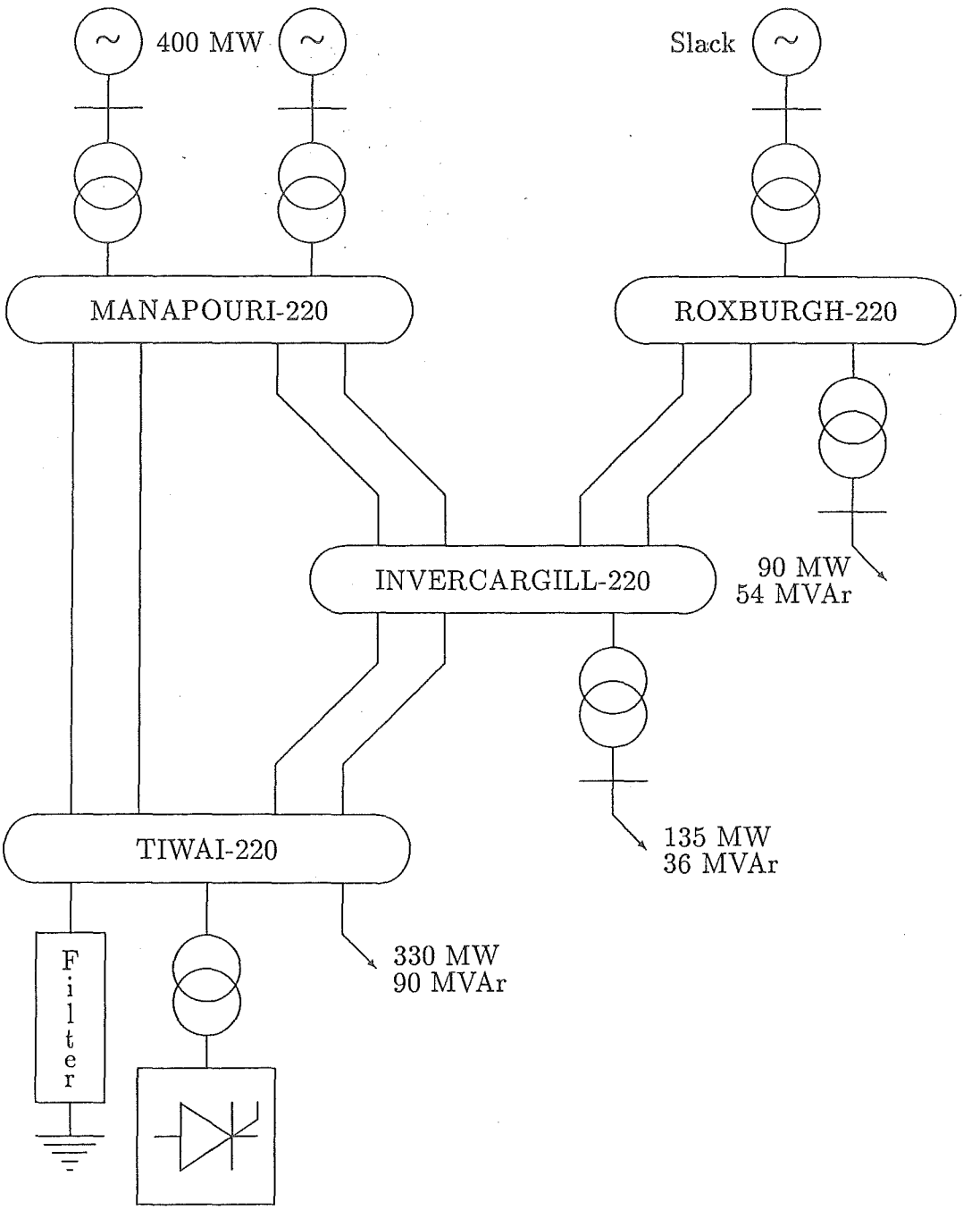

Figure 5.1: Tiwai seven bus system.

Representation of complete 48 pulse operation at Tiwai would be very difficult for the following reasons :

(i) Additional transformer models would be required to give the necessary phase shifts (7.5° for each bridge (Yacamini and de Oliveira, 1980)) for 48-pulse operation.

(ii) The resulting characteristic harmonics (from the 48-pulse operation) would include only the 47^{th} and 49^{th} harmonics in the range governed by the New Zealand limitation of harmonics notice (New Zealand Electricity, 1983). The next pair of characteristic harmonics would be the 95^{th} and 97^{th}, or 4750 and 4850 Hz respectively.

In addition to the second point, the magnitudes of the harmonic injections would be relatively small. Assuming worst case conditions, (i.e. quasi-square wave current injections) the magnitude of the 47^{th} and 49^{th} harmonic current injections would be low : 0.021 and 0.0204 of the fundamental respectively, and given that the network impedances (dominated by the capacitance of the filters at these frequencies) would be very low, then the resulting voltages will almost certainly be insignificant.

By contrast, however, if one of the rectiformer units is removed from service, then the resulting harmonics for the remaining units equate (essentially) to those of a 6-pulse unit with rating equal to 1/8 of the station rating. This is a relatively common occurence, since coarse control of the rectiformer units is maintained by on-load tap changing (OLTC) transformers, and the tap-chainging units require regular maintenance. In addition to the 6-pulse generation, there are also some remnant 48-pulse related harmonics, although these are ignored for the reasons given above. The remaining 6-pulse operation is modelled by a 75 MW 6-pulse bridge, representing a worst case situation of unbalanced load sharing among the remaining rectifiers. The remaining 330 MW is represented by a static PQ load of 330 MW & 90 MVAr, and two extremes of operation are considered : with filters and without filters.

The filter configuration at Tiwai is given in figure 5.2, although the bank was not installed until 1983, when harmonic interference in the network forced legislative measures to be taken.

The components used in the filters are given in table 5.1.

h	R (Ω)	L (mH)	C (μF)	r (Ω)
5	0.606	19.3	21.0	—
7	0.424	9.63	21.5	—
11	1.66	14.4	5.8	1.0
13	2.34	17.2	3.49	—
18	0.2526	1.34	23.3	—

Table 5.1: Physical component values in the Tiwai filters.

There are three filters of this configuration at Tiwai, all of which are connected at 33 kV, so that account may be taken of all three by simply adjusting the voltage base at which their pu admittances are calculated, and considering only one. A voltage base

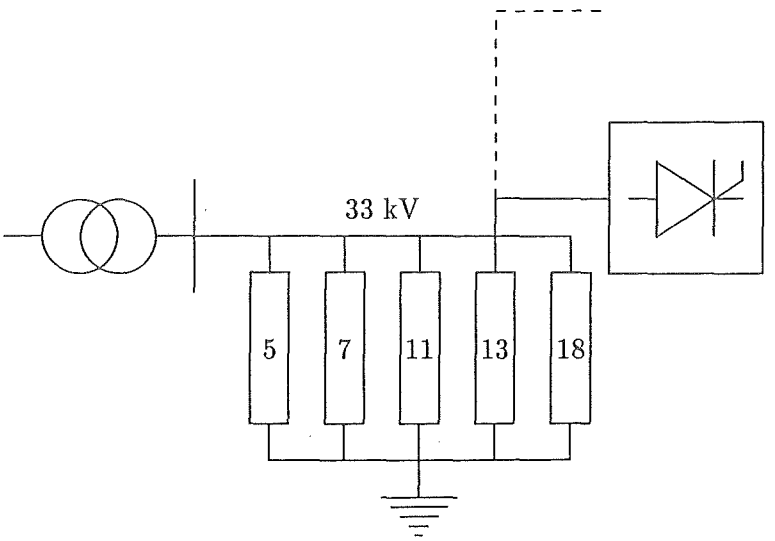

Figure 5.2: Filter arrangements at Tiwai.

of 57.16 kV ($= \sqrt{3} \times 33$) increases the impedance base by a factor of 3, proportionally reducing the pu impedance.

The total reactive power supplied by the filters at fundamental frequency is 79.8 MVAr, corresponding to a fundamental filter susceptance of 0.798 pu/phase. The somewhat unfamiliar practice of designing a damped 11^{th} harmonic branch while having an 18^{th} harmonic tuned branch arose when the consultant recommended leaving the shunt resistor out of the 18^{th} harmonic tuned filter, and including the 1Ω resistor in the 11^{th} harmonic filter to dampen a resonance occuring between the filters and the system impedance at 10^{th} harmonic (Simmons, 1983).

To demonstrate the utility of the integrated algorithm, the results obtained are compared with those obtained with the two-step analysis consisting of a fundamental loadflow followed by one IHA process. Recalling the convention that each major loop of the integrated algorithm (after preliminary convergence) in which first P & Q are solved, followed by an IHA process is referred to as a PQH iteration, the two-step analysis mentioned above is equivalent to performing only *one* iteration of the integrated algorithm.

5.2.1 Unfiltered Case

The unfiltered case is considered useful here for two reasons : firstly it represents the pre-1983 situation where no filters existed, and secondly it allows the balance of real powers to be demonstrated to best effect.

The effect of the addition of harmonics to the loadflow solution is found by comparing the results of the fundamental loadflow with those of the integrated algorithm after both one and many PQH iterations. This effect, in the unfiltered case, is tabulated in table 5.2, where the bracketed percentages represent the variation of each result from

the standard loadflow results in column one.

Quantity	Loadflow	One PQH iteration		Many PQH iterations	
P_1	23.61785	23.82989	(0.9%)	23.80600	(0.8%)
P_2	24.15014	24.38379	(0.97%)	24.37133	(0.92%)
P_3	24.35127	24.61566	(1.1%)	24.59098	(0.98%)
Q_1	11.85277	11.90798	(0.47%)	11.50974	(-2.9%)
Q_2	12.24333	12.25691	(0.11%)	11.85316	(-3.2%)
Q_3	11.88724	11.93320	(0.4%)	11.51017	(-3.2%)
V_d	2.00606	2.00618	(0.006%)	2.00645	(0.02%)
I_d	1.07853	1.07853	(-)	1.07853	(-)
P_d	2.163596	2.163725	(0.006%)	2.164017	(0.02%)

Table 5.2: Variations in fundamental frequency variables at Tiwai for the unfiltered case.

The solution required a total of 4 PQH iterations, requiring, in turn, 4, 3, 2 & 1 HA iterations respectively. The tap ratio 'audit trail' (a list of the tap ratios calculated at each iteration) is as follows :

$$\left.\begin{array}{l} 0.999954 \\ 1.001779 \\ 1.003911 \\ 1.003848 \end{array}\right\} \text{PQH} = 1$$

$$\left.\begin{array}{l} 0.996041 \\ 0.997794 \\ 0.997671 \end{array}\right\} \text{PQH} = 2$$

$$\left.\begin{array}{l} 0.996171 \\ 0.996269 \end{array}\right\} \text{PQH} = 3$$

$$\left.\begin{array}{l} 0.996071 \end{array}\right\} \text{PQH} = 4$$

The tap ratios in the first PQH iteration (with the exception of the very first) are greater than 1, but are thereafter less than 1. The reason for this is that, on entering the second PQH iteration, the zero crossings are re-calculated, and the nett shift is to the left. The firing instants, therefore, also shift to the left with respect to the fundamental component, which is equivalent (as far as the fundamental is concerned) to a reduction in the firing angle α. The result is, therefore, a small increase in the average d.c. voltage (notwithstanding the commutation notches), which is countered by the sudden change in tap ratio behaviour. This effective change in firing delay also explains the 3.1% nett decrease in fundamental reactive demand observed after 4 PQH iterations, which contrasts with the small increase after only 1 PQH iteration.

The 0.9% increase in the real power demand recorded in the first PQH iteration is not matched by a similar or even near similar increase in the d.c. side power. This

is due to the extra (0.9%) real power being converted into harmonic I^2R losses in the supply network. This figure can be easily verified because a star-star transformer was assumed, thus making the primary & secondary current waveforms identical apart from the transformer tap ratios (r/a). Therefore, by reconstructing the phase voltage and current waveforms, scaling appropriately by r/a, multiplying the waveforms and extracting the d.c. component, the real powers flowing into the convertor in each phase may be calculated. If only the fundamentals are used in the reconstruction process, then the resulting power is the fundamental real power requirement calculated by the loadflow. In this case, the powers in the distorted and fundamental waveforms are given in table 5.3.

	Real Power (PU)	
Phase	Fundamentals Only	All Harmonics
1	0.715610	0.708306
2	0.732504	0.726081
3	0.739132	0.729403
Totals	2.187336	2.163792

Table 5.3: Power in the convertor waveforms : with and without distortion.

The real power in the distorted waveform represents that power which flows into the convertor, and is therefore available on the d.c. side of the bridge. The real power in the fundamental waveforms represents that power which must be supplied by the generators in order to satisfy the load on the d.c. side and the I^2R losses in the supply network.

Here $P_{N_h=1}$ is greater than $P_{N_h=25}$ by about 0.9%, which corresponds to the nett real power increase calculated by the integrated algorithm as necessary to supply the additional losses incurred by the addition of harmonics. Thus it can be seen that the integrated algorithm, with no special constraints, maintains a balance of real power at the convertor (or other nonlinear load) busbar. This observation is consistent with the diagram (after Tschappu (1981)) of figure 5.3.

In summary, both the real and reactive power requirements of the convertor are affected by the presence of harmonics at the terminal busbar, with an almost 1% increase in real power requirement, and the zero crossing shifts in the presence of distortion resulting in a reactive power decrease of more than 3%. In particular, the results obtained with the integrated algorithm differ from those obtained with PQH=1 in terms of the reactive power requirements, which *increase* slightly on the first PQH iteration.

In terms of the harmonics, the characteristic harmonics (the most important in the unfiltered case) all reduce slightly when compared with the one PQH case, by the amounts given in table 5.4.

The mechanism of the harmonic reduction in this instance is the parasitic effect of the harmonics on the commutating voltages combined with the effective leftward shifts of the firing instants, resulting in longer commutations, and therefore slightly more

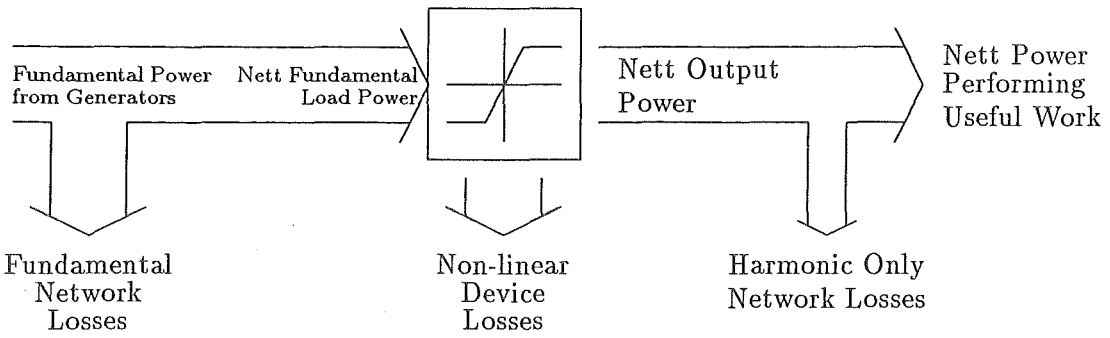

Figure 5.3: Distribution of real power in the network.

Harmonic Order	5	7	11	13	17	19	23	25
% Variation	-1.0	-1.3	-2.1	-2.7	-4.3	-5.6	-9.0	-13.0

Table 5.4: Percentage changes in the unfiltered harmonics, with respect to the one PQH case.

'rounded' current waveforms. This results in a reduced harmonic injection at Tiwai - a factor which may have been influential in the days when Tiwai was negotiating its obligations with respect to the New Zealand harmonic legislation with (then) New Zealand Electricity. Significant swings in the phases of the harmonics were also observed, which is also very important, especially when considering interactions with other harmonic sources.

5.2.2 Filtered Case

With the appropriate filters represented at Tiwai, the comparison of fundamental frequency variables given in table 5.5 results. It is apparent that the real power demand does not change as significantly in this case, since much of the harmonic current now flows in the filter branches, rather than in the system, and therefore the harmonic I^2R losses are no longer incurred.

The solution required three PQH iterations, requiring, in turn, 3, 2 & 1 HA iterations respectively. The tap ratio 'audit trail' is as follows :

Quantity	Loadflow	One PQH iteration		Many PQH iterations	
P_1	25.05528	25.00768	(-0.2%)	25.00981	(-0.18%)
P_2	25.58454	25.59162	(0.03%)	25.60453	(0.08%)
P_3	25.81526	25.82508	(0.04%)	25.83125	(0.06%)
Q_1	12.53121	12.86461	(2.7%)	12.92755	(3.2%)
Q_2	12.95704	13.26729	(2.4%)	13.33289	(2.9%)
Q_3	12.65987	13.03627	(3.0%)	13.08327	(3.3%)
V_d	2.06548	2.06547	(-)	2.06522	(-0.01%)
I_d	1.11048	1.11048	(-)	1.11048	(-)
P_d	2.29367	2.29366	(-)	2.29338	(-0.01%)

Table 5.5: Variations in fundamental frequency variables in the filtered case.

$$\left.\begin{matrix}0.999957\\1.000664\\1.000666\end{matrix}\right\}\ \text{PQH} = 1$$

$$\left.\begin{matrix}1.001986\\1.001987\end{matrix}\right\}\ \text{PQH} = 2$$

$$\left.\begin{matrix}1.002109\end{matrix}\right\}\ \text{PQH} = 3$$

Here the opposite trend to that of the unfiltered case is observed. The tap ratios tend to increase after the first PQH iteration, rather than decrease, and this is due to the shifts in the zero crossings being to the right this time. This also accounts for the increase in reactive demand, which is significant in the PQH=1 case, and even more significant after many PQH iterations. It is also in contrast with results published by Arrillaga and Callaghan (1989), in which essentially the same case resulted in a similar increase in reactive power on the first PQH iteration, but this reduced to a nett decrease by the final PQH iteration. The only differences between the two cases are that here the true Tiwai filters are used (whereas the paper case substituted the Benmore pole filters - the Tiwai filter parameters being unavailable), and the static (PQ) load level at the Tiwai bus is a little more realistic. The a.c. systems are compared in figure 5.4.

It can now be seen that the actual Tiwai filters differ significantly from those assumed previously in terms of strength, particularly at the higher frequencies, which are dominated by the Tiwai 18^{th} harmonic filter. Of importance, too, are the phases of the admittances, and it is clear that the characteristic (and unfiltered) 17^{th} harmonic impedance is capacitive with the Tiwai filters, but inductive with the Benmore filters. Therefore, the effect of this harmonic is opposite in the two cases, and the nett effect is reflected in the shift in zero crossings - left in the case with the Benmore filters, but right in the case with the Tiwai filters. This accounts for the apparent anomaly in the results, and highlights an important point of the integrated algorithm. That is the

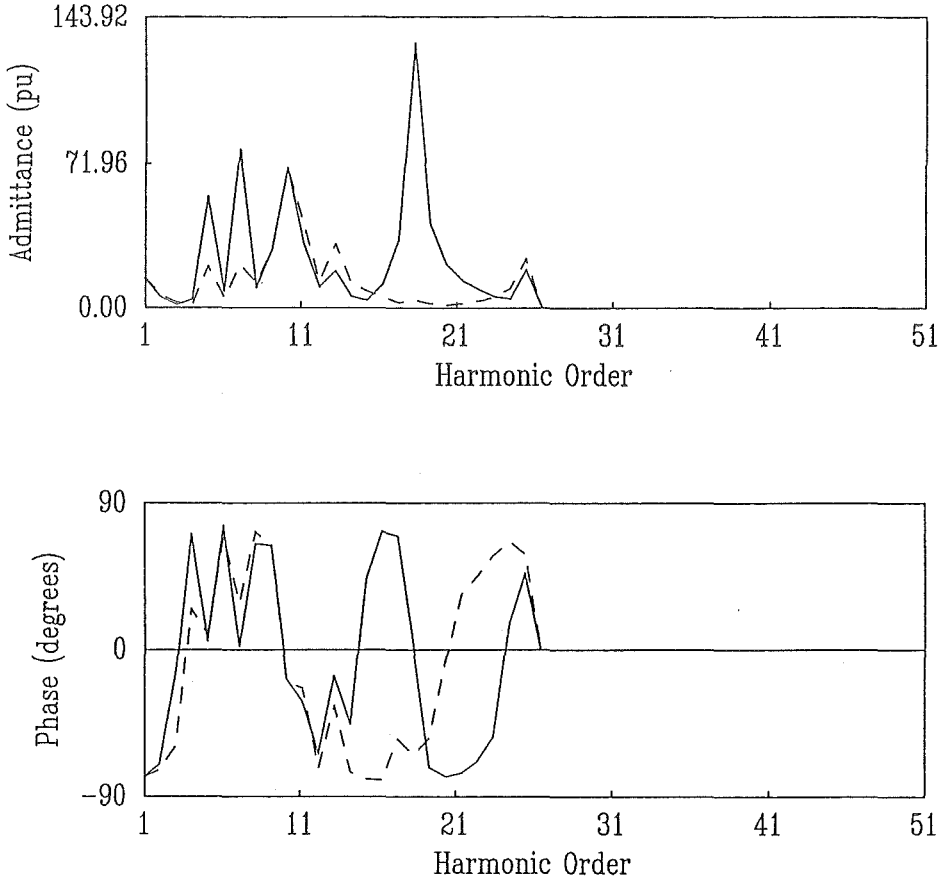

Figure 5.4: Comparison of the a.c. systems used in the two conflicting filtered cases
Solid line $\Longrightarrow$ Tiwai filters
Dashed line $\Longrightarrow$ Benmore filters

effect of the harmonics on the loadflow depends not only on the magnitude, but also on the phase of the system harmonic impedances.

With regard to the harmonics in the filtered case, the effect of further PQH iterations on the characteristic harmonics are not as significant as in the unfiltered case, with a maximum characteristic harmonic increase of approximately 2% occuring at the 25^{th} harmonic. More significant are the (unfiltered) uncharacteristic harmonics, and, in this case, the phase 'b' triplen harmonics are drastically modified, as shown in table 5.6.

Harmonic Order	3	9	15	21
% Variation	60.7	56.1	46.9	34.8

Table 5.6: Phase two triplen increases for the filtered case.

These indicate a significant change in the degree of imbalance in the bridge, which is due to the interaction of the fundamental and harmonic frequencies in continued PQH iterations of the integrated algorithm.

5.3 HARMONIC INTERACTION BETWEEN BENMORE AND TIWAI

With two major sources of convertor harmonics in the South Island, comprising a large proportion of the total South Island hydro generation, the interaction between the two must be assessed, if the harmonic limitation legislation (New Zealand Electricity, 1983) is to be effectively observed.

A system comprising the bulk of the South Island 220 kV network (below Islington) was assembled as a test bed for the investigation. Fundamental initial conditions included specified generation at Manapouri (600 MW), Benmore (540 MW) & Aviemore (200 MW), with the slack bus being Roxburgh. Other relevant system conditions and interconnections are given in figure 5.5.

Similarly, a series of harmonic admittance matrices (6×6) were formed to represent the interconnection of the two convertor load buses (Benmore and Tiwai) at harmonic frequencies.

The Tiwai convertor load was represented as per the previous example, while Benmore was represented explicitly by 4 6-pulse rectifiers each developing some 250 MW. This represents the order of injection magnitudes expected when the New Zealand HVDC expansion project is complete. The present filter ratings were retained, however, since the new filter parameters are, as yet, unknown, and it is uncertain as to what exact policy will be adopted in this regard.

5.3.1 Effect of Remote Harmonic Injections

Initially, the integrated algorithm was run with both convertor loads in place, in order to determine the exact real and reactive demands of each in the presence of their own distortion, and the distortion from the remote convertors. This run was repeated twice, alternately replacing the Benmore and Tiwai convertors by their equivalent demands (obtained from the first run), thus giving the harmonic operating state of each convertor with respect to the same fundamental conditions in each case, but with and without harmonic injections from the remote convertors. The fundamental frequency variables are given in table 5.7.

The results given in the Benmore columns are those obtained for one of the bridges only, since each of the four bridges was specified identically (except for the transformer winding arrangement) and was connected to the same busbar.

The effects of the remote Tiwai injections on the Benmore fundamental operating state are practically negligible, and although the converse is almost true, it is clear that the effects of the Benmore harmonic injections on Tiwai are somewhat more pronounced, especially with regard to the Tiwai reactive demand. Although the changes are smaller than those occuring in the previous section (when the effect of Tiwai's own harmonics on its fundamental operation were assessed) it is significant that, in this instance, they result from harmonic injections some 300 km distant.

The reason the Tiwai harmonic injections do not similarly affect the Benmore operating state is that the injections are of considerably smaller magnitude (75 MW compared with 1000 MW), and that the most significant of them (5^{th}, 7^{th}, 11^{th} & 13^{th}) are filtered at both ends of the transmission path. Also, partial or complete cancella-

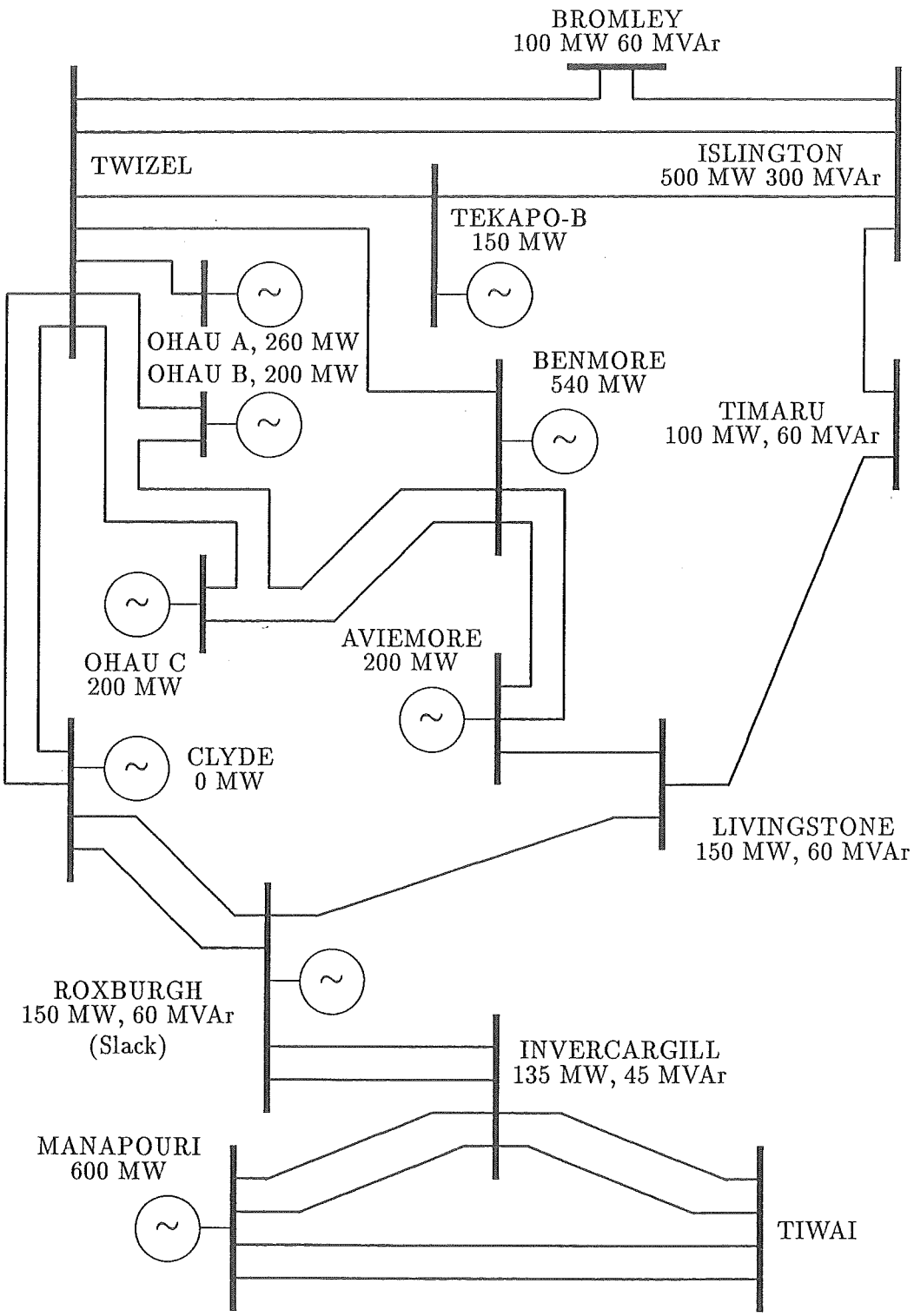

Figure 5.5: Interconnection of the South Island network for the harmonic interaction study.

tion of the Tiwai injections by the Benmore harmonics will occur if the conditions are

	Including Remote Harmonic Injections		Ignoring Remote Harmonic Injections			
	Tiwai	Benmore	Tiwai		Tiwai	
P_1	24.158	82.410	24.090	(-0.28%)	82.414	(0.005%)
P_2	24.317	82.481	24.298	(-0.08%)	82.484	(0.004%)
P_3	24.231	82.577	24.217	(-0.06%)	82.582	(0.006%)
Q_1	12.077	51.983	12.122	(0.37%)	51.985	(0.004%)
Q_2	12.010	52.089	12.075	(0.54%)	52.091	(0.004%)
Q_3	11.783	52.044	11.886	(0.87%)	52.046	(0.004%)
V_d	2.0141	1.9745	2.0122	(-0.09%)	1.9747	(0.011%)

Table 5.7: Fundamental variable behaviour with and without remote harmonic injections.

favourable.

The harmonics in the three cases are compared under the following three headings :

Globally Characteristic Harmonics - these are defined as the harmonics which are characteristic to both, or more generally all, convertor installations in the network. For the present case they include the 11^{th}, 13^{th}, 23^{rd} & 25^{th} harmonics, since these are characteristic of both the 6-pulse Tiwai operation, and also of the 12-pulse Benmore operation.

Locally Characteristic Harmonics - these are defined as those harmonics which are generated at only some of the installations - not at all of them. The remaining 6-pulse characteristic harmonics (5^{th}, 7^{th}, 17^{th} & 19^{th}) fit this category.

Globally Uncharacteristic Harmonics - these consist of the remaining harmonics which are characteristic of none of the bridges in the network.

5.3.1.1 Globally Characteristic Harmonics

At Benmore the effects on the globally characteristic harmonics are minimal, with the 11^{th} & 13^{th} harmonics being affected by less than 0.1%, and the 23^{rd} & 25^{th} by only about 1%. More significantly, reductions of 8% and 2.7% respectively were recorded for the 11^{th} & 13^{th} at Tiwai when the Benmore harmonic injections were incorporated, while the 23^{rd} & 25^{th} harmonics increase in a very erratic manner, as shown in table 5.8. The erratic nature of the increases is due partially to the fact that the Benmore harmonic currents are being transferred across an unbalanced transmission path, and partially due to the slight change in the imbalance of Tiwai's operation when the Benmore injections are introduced.

Therefore, significant increases in the 23^{rd} & 25^{th} harmonics at Tiwai can be expected as a direct result of explicit representation of the Benmore injections.

h	Phase A	Phase B	Phase C
23	36%	52%	39%
25	78%	34%	-16.5%

Table 5.8: Perturbation to the 23^{rd} & 25^{th} harmonics at Tiwai when the Benmore injections are introduced.

5.3.1.2 Locally Characteristic Harmonics

The 5^{th}, 7^{th}, 17^{th} & 19^{th} harmonics are characteristic of the Tiwai convertor only, and therefore the levels of these harmonics are not expected to vary much with the introduction of the Benmore injections. This is essentially true for the 5^{th} & 7^{th} harmonics, although the 17^{th} & 19^{th} harmonics both reduce by about 1%. This is, however, brought about by a similar change in the harmonic current injections at these frequencies by the Tiwai convertors, rather than any significant transfer of current from Benmore.

At Benmore, where the only mechanism for the existence of these harmonics is incomplete cancellation at the terminal busbars, the levels before the Tiwai injections are considered are very small. When the Tiwai injections are included in the solution, very large percentage increases occur at Benmore, as recorded in table 5.9. The per-

h	Phase A	Phase B	Phase C
5	421%	743%	555%
7	194%	217%	186%
17	688%	1993%	1170%
19	103%	234%	1231%

Table 5.9: Effect of Tiwai harmonic injections on the Locally Characteristic Harmonics at Benmore.

centage increases indicate that a significantly higher quantities of locally characteristic harmonics appear at Benmore as a result of the normal 6-pulse related injections at Tiwai. However, it must also be remembered that, in spite of the significant increases, the actual levels are still considerably lower in magnitude than those of the globally characteristic harmonics.

5.3.1.3 Globally Uncharacteristic Harmonics

Comparing the changes in uncharacteristic triplen harmonic levels is difficult because the symmetry of the system in the Benmore region precludes significant generation of triplen harmonics there. Therefore, apparently large percentage changes can occur, which are basically misleading because of the very low levels existing previously.

When the Tiwai injections are considered, the Benmore triplen harmonic levels increase only slightly, while at Tiwai the phase C triplen levels are those most affected

by the presence of Benmore injections. The reason for the effect on (essentially) only the one phase is because it is that phase which makes up the difference between the sum of phases A & B and the required zero-magnitude set of zero sequence triplen harmonic phasors. Given that the direct triplen harmonic contribution from Benmore to Tiwai is very small (because of the symmetry inherent in the Benmore operation), the explanation of the change in triplen levels at Tiwai lies in the change in the imbalance of the Tiwai bridge as a result of Benmore injections at other frequencies.

5.3.1.4 Summary

Examination of the effects of remote harmonic injections on local convertor operation has shown that two different mechanisms exist for bringing changes in harmonic generation. The most direct is that where the harmonic currents from one convertor flow through the network and result in a corresponding voltage at the remote bus. This appears to be the dominant effect, particularly with regard to the globally characteristic harmonics.

The second mechanism occurs when the harmonic levels from the remote bus are sufficient to affect the operation of the local bridge(s), bringing changes in locally generated harmonic current injections (and therefore the local voltages) even though the harmonics affected may not even be generated at the remote installation. This is the case with the changes in the locally characteristic and globally uncharacteristic harmonics at Tiwai.

5.3.2 Effect of Varying the Tiwai Delay Angle

The effects of the Tiwai injections on the Benmore harmonics have been examined at one delay angle : α_{TIWAI} =20°. In this section the Tiwai delay angle is varied from 20° up to 85° in 5° steps. Since the Tiwai convertor feeds a passive load, this has the effect of decreasing the d.c. voltage, and therefore the current, thus significantly altering the nature of the Tiwai harmonic injections. The results are plotted in figure 5.6 for the locally characteristic harmonics at Benmore as percentages of the harmonic magnitudes at α_{TIWAI} =20°, thus indicating the percentage changes in harmonic levels due to the changes in α_{TIWAI}.

From the graph of figure 5.6 it is apparent that some harmonics are more significantly affected than others, and all respond in different ways. The globally characteristic harmonic levels at Benmore are scarcely affected, but this is unsurprising given the relative magnitude of these injections at Benmore compared with the transferred current levels from Tiwai. Those harmonics characteristic of Tiwai only, however, are present at Benmore principally as a result of current transfer, and therefore vary considerably with the Tiwai delay angle. For an ideal (i.e. quasi square-wave) current waveform, the harmonic current magnitudes are (Arrillaga, 1983) :

$$I_h = \frac{\sqrt{6} I_d}{\pi h}$$

and for a convertor feeding a resistive load, as Tiwai is here :

$$V_d = V_{co} \cos(\alpha) - \frac{3 X_c I_d}{\pi}$$

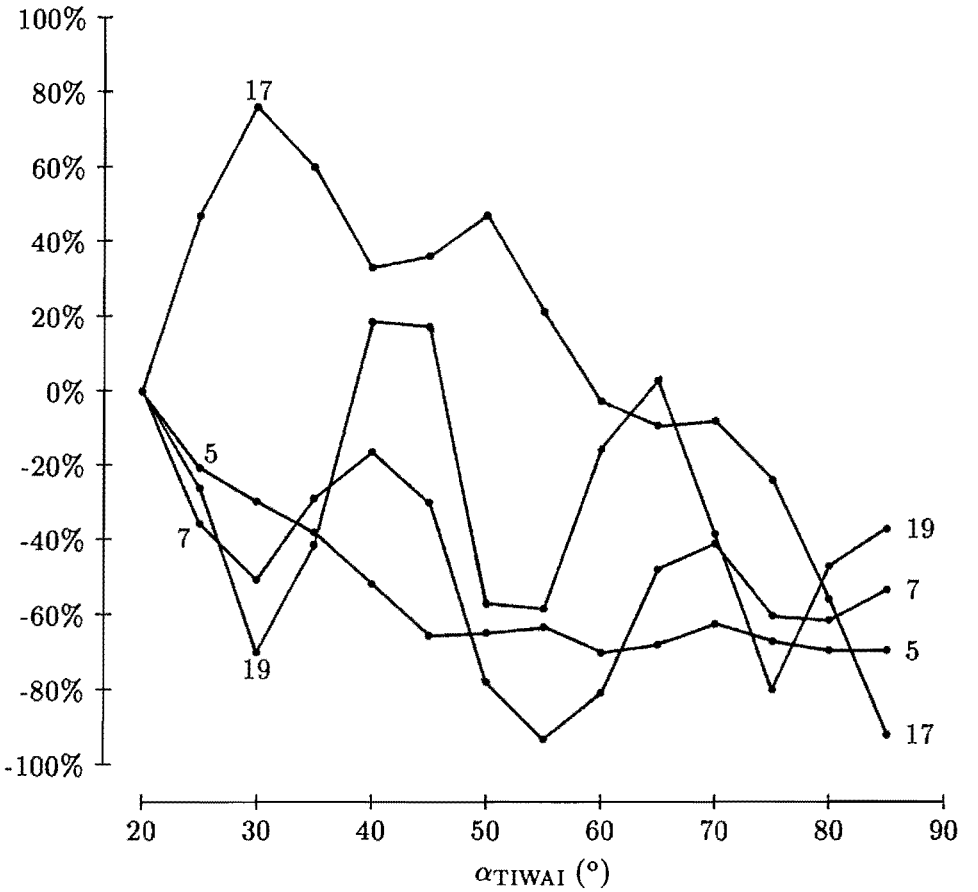

Figure 5.6: Percentage changes in Benmore harmonic voltages with varying α_{TIWAI}.

$$\Rightarrow I_d = \frac{V_{co}\cos(\alpha)}{R_d + \frac{3X_c}{\pi}}$$

so that :

$$I_h = \frac{\sqrt{6}V_{co}\cos(\alpha)}{(R_d + \frac{3X_c}{\pi})\pi h} \tag{5.1}$$

Given that all other quantities in 5.1 remain constant (which is not strictly true - the commutating voltage will vary a little as the load is decreased) the Tiwai harmonic current injection magnitudes may be expected to decrease cosinusoidally as α_{TIWAI} increases. However, this is inconsistent with the observed effect, whereby there is a general reduction in the levels of the locally characteristic harmonics, but definitely *not* cosinusoidal. The reasons for this phenomenon are twofold.

Firstly, the current waveforms at Tiwai are less than ideal. In particular, as the delay angle increases, the commutations become shorter due to the reduced d.c. current level, and to the increase in available commutating voltage. This has the effect of increasing the proportions of (especially) the higher order harmonics relative to the fundamental components, with respect to the α_{TIWAI} =20° case.

Secondly, incomplete cancellation of the locally characteristic harmonics in the Benmore convertor transformers results in slight background injections of these frequencies which are free to interact with currents transferred from Tiwai. This interaction takes the form of alternately constructive and destructive interference as the phase of the Tiwai injections changes. If the Benmore injections are assumed to be the same for all α_{TIWAI}, and the phases of the Tiwai injections are assumed to vary linearly with α_{TIWAI}, then one would expect an oscillatory behaviour in the harmonic voltages at Benmore, with period $2\pi/h$. This behaviour is approximated by the 17^{th} and 19^{th} harmonics, which have a much stronger presence at Benmore than the remaining locally characteristic harmonics, since they are not directly filtered at Tiwai. The 17^{th} is a particularly good example, oscillating with an apparent period of about 20°, which compares well with the expected period of 360°/17 =21.5°.

The background levels of globally uncharacteristic harmonics at Benmore are fairly low, given the symmetry of supply from the Benmore generators, and the lack of asymmetry in the convertors themselves. Therefore the bulk of the triplen harmonics appearing at Benmore are due to injections at Tiwai. The observed trend is for the 3^{rd} & 9^{th} harmonics to increase with α_{TIWAI}, while the 15^{th} & 21^{st} decrease. Note that this is not in contradiction with the characteristic harmonic case, where increasing delay angle results in decreased injection magnitudes, since the uncharacteristic harmonics are produced by a different mechanism (i.e. imbalance) to the characteristic harmonics. Therefore changes in their levels are more strongly related to changes in the imbalance of the bridge due, in turn, to the changes in the remote delay angle, rather than to the remote injections alone.

5.3.3 Improving the Efficiency of the Algorithm

The set of 14 comparison runs presented in the previous section required a total CPU time (execution time) of 9 hours and 15 minutes, which averages to about 40 minutes per case. This represents a considerable computing burden which would benefit from a little pruning.

It was noticed that the IHA process frequently converged at the Tiwai bus before convergence was obtained at the Benmore bus. In spite of this, the Tiwai current waveforms were still calculated (even though they were identical with those of the previous HA iteration). Since the sampling of the current waveforms is one of the most computationally expensive tasks in the IHA algorithm, considerable computational savings could be made by storing the current phasors from the previous HA iteration, and reusing them if the terminal voltages for the particular convertor have converged, as shown in figure 5.7.

However, by taking a wider view of the integrated algorithm as a whole, a much greater improvement in efficiency can be made.

The current iteration scheme is "P-Q-H-P-Q-H...", for the simple reason that it parallels the operation of the three phase a.c.-d.c. loadflow("P-Q-D-P-Q-D..."), which is already well established. However, the harmonic iteration is logically more separate from the P & Q iterations since it always (provided that it converges) produces a consistent harmonic operating state for the convertor. Moreover, it is computationally more expensive than either the P or Q iterations. It therefore makes little sense to

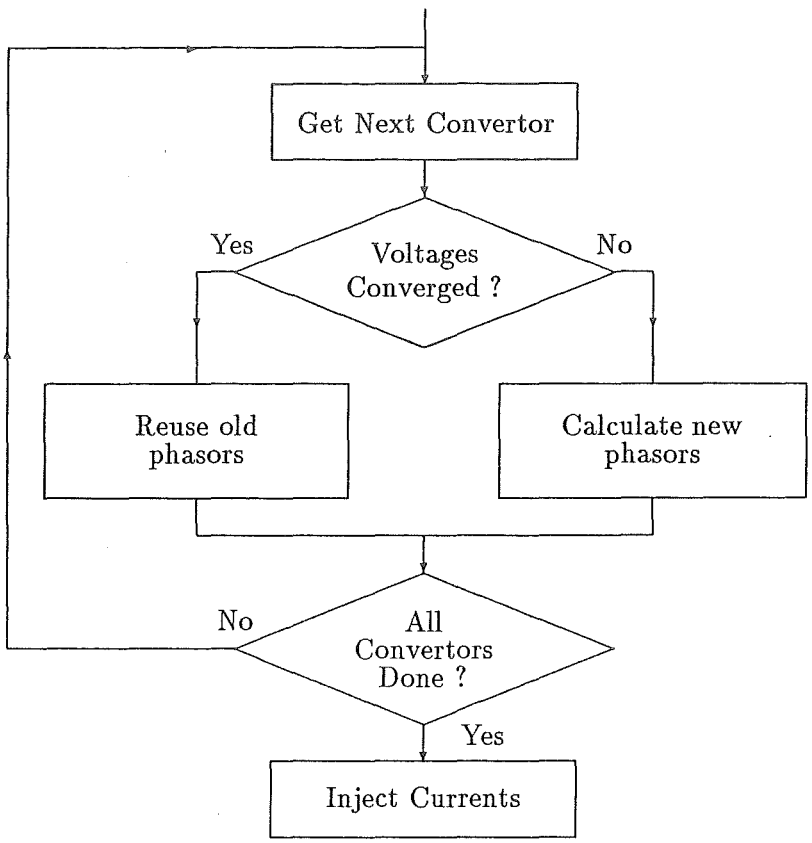

Figure 5.7: Efficiency improvement by reusing current phasors in IHA.

perform a harmonic iteration after each pair of P & Q iterations, unless convergence of real and reactive powers has been obtained, and so benefit should be obtained by adopting the fundamentally different structure depicted in figure 5.8, subsequent to convergence of the standard loadflow algorithm. Note that the previous convergence criteria of $\Delta P, \Delta Q < \epsilon$ is no longer applicable, since it is already used to control the (inner) PQ loop. A more suitable criterion now is that the harmonic iteration converge in 1 HA iteration. This implies that the harmonics have not been appreciably affected by the latest update of fundamental conditions, which further implies that the real and reactive injections of the convertors will not change, and that a consistent solution has been reached.

The savings made by implementing the two schemes were investigated in three cases.

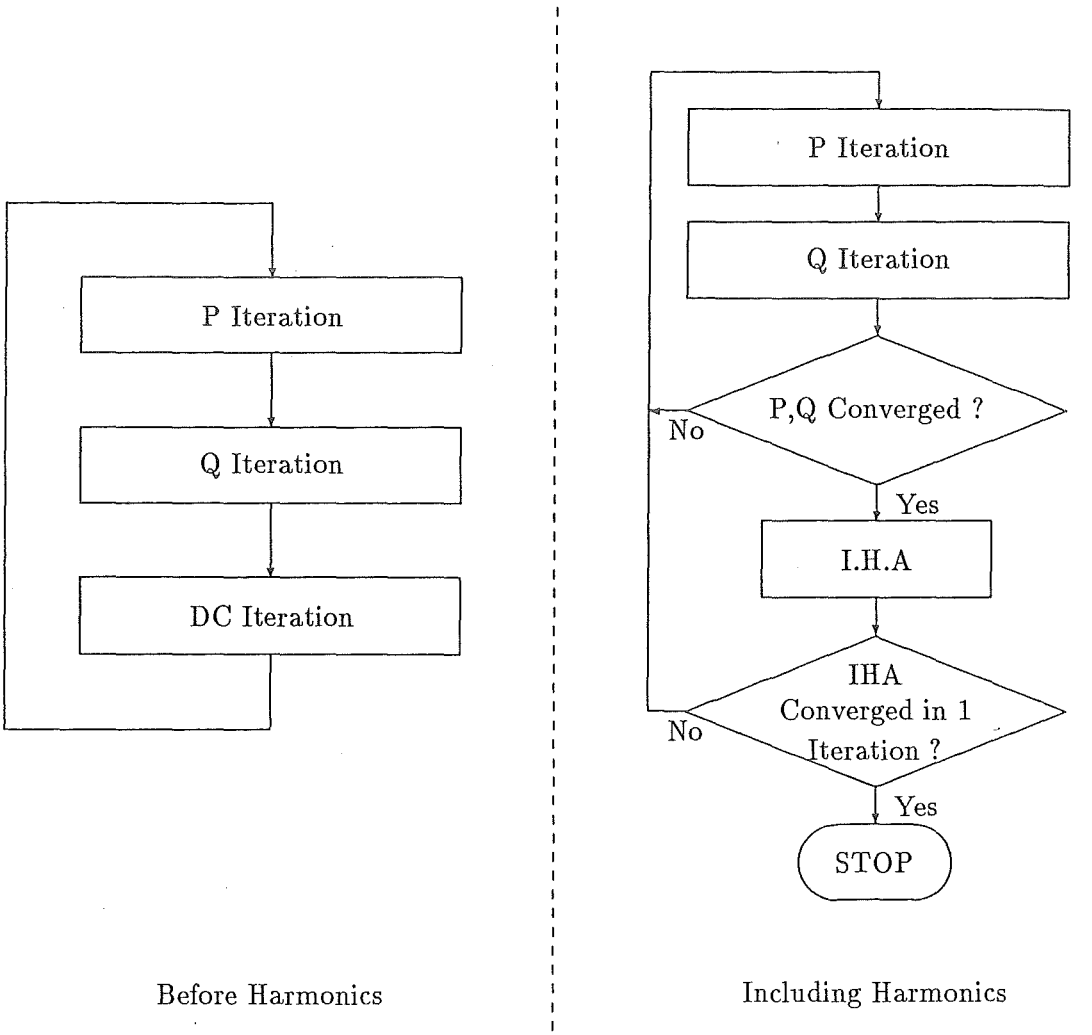

Figure 5.8: More efficient structure for the integrated algorithm.

5.3.3.1 One 6-pulse convertor at Tiwai

With only one convertor in the system, the only saving achieved is that due to the second idea. The CPU savings are given in table 5.10, and amount to about 11%.

Method	CPU seconds
Old way	102.85
New way	91.62
Saving	11.23

Table 5.10: CPU savings with one convertor.

5.3.3.2 6-pulse convertors at Tiwai and Benmore

With more than one convertor, both efficiency schemes contribute to the overall saving, as shown in table 5.11.

Method	CPU seconds
Old way	1300
New way	233
Saving	1067

Table 5.11: CPU savings with two convertors.

In percentage terms, the saving is 82% of the original CPU time. This turns out (in this case) to be directly related to the total number of times the current waveforms are sampled, as shown in table 5.12. This reduction is due to the fact that the Tiwai

Method	Current Sampling Processes
Old way	100
New way	28
Saving	82

Table 5.12: Current sampling processes with two convertors.

harmonics converged much faster than the Benmore harmonics, and highlights the computational intensity of the current sampling process, since an 82% reduction in the number of current sampling processes results in an equivalent CPU saving.

5.3.3.3 One 6-pulse convertor at Tiwai, four at Benmore

The savings in CPU time in this case are given in table 5.13. The savings in this case

Method	CPU seconds
Old way	3796
New way	1742
Saving	2054

Table 5.13: CPU savings with five convertors.

are not as significant as in the previous case, although the computational task is still more than halved, with a 54% saving in CPU time. However, the saving in current sampling processes for this case (given in table 5.14) is only 61%, which is lower than the previous example since convergence at the Benmore busbar is faster (relative to

Tiwai) because of the reduced inter-harmonic interaction with twelve pulse operation. This indicates that there is some significant computational overhead which prevents

Method	Current Sampling Processes
Old way	445
New way	174
Saving	271

Table 5.14: Current sampling processes with five convertors.

the 61% saving in current sampling processes being reflected in CPU time savings. However the saving of 54% is, nonetheless, very worthwhile.

5.3.3.4 Conclusions

Considerable savings in CPU time have been made by implementing two pertinent changes to the structure of the algorithm, neither of which detract from the overall nature or accuracy of the algorithm. In particular, the reduction in the number of current sampling processes was shown to be a significant factor influencing the efficiency of the algorithm. The changes made would still be worthwhile, however, (even if they did not greatly improve the efficiency) since fewer current sampling processes will result in less build up of numerical noise in the solution.

5.3.4 Effect of Varying the Benmore Delay Angle

Varying the Benmmore delay angle is likely to significantly affect the harmonic operation of the system, since it is not only the strongest source of harmonic injections, but also because it is a significant fundamental load in the system. For simplicity's sake, Benmore is modelled as a 4 bridge, 12-pulse convertor feeding a purely resistive load. Although this is in contrast with the actual system (in which Benmore feeds an invertor via a D.C. link), running the Benmore delay angle (α_{BENMORE}) through to 90° is similar to running the entire link into an idling state prior to a shutdown.

The range of Benmore firing angles covered in this case was from 20°, representing the full 1000 MW capacity of the link, through to 55°, representing a transfer of 360 MW. This range covers the upper (and therefore most significant) 64% of the Benmore rating.

The harmonics at Tiwai were observed, with particular attention to the globally characteristic harmonics (11^{th}, 13^{th}, 23^{rd} & 25^{th}), since these are generated at both stations, and considerable harmonic interaction is likely.

The 11^{th} & 13^{th} harmonics vary slowly as the Benmore delay angle increases, and increase by only about 3% over the entire range of α_{BENMORE}. This is due to the fact that these frequencies are filtered at both ends of the transmission path, making the interaction between them small.

The 23^{rd} & 25^{th} harmonics vary much more considerably, as shown in figure 5.9, and considerable variations are observed between phases. For example, the phase C

25^{th} harmonic has a local minimum at α_{BENMORE} =30°, and a local maximum at α_{BENMORE} =50°, while those points occur 5° later on phases A & B. It is clear, therefore, that unbalanced harmonic variations of up to ±40% (with respect to the nominal α_{BENMORE} =20° case) are possible with the 23^{rd} & 25^{th} harmonics, as a result of varying remote harmonic injections at Benmore.

The behaviour of the triplen harmonics at Tiwai is somewhat more dramatic, although, in terms of actual magnitudes, a little less significant. It is important to note, however, that the increasing nature of the triplens (as depicted in figure 5.10 indicates a change for the worse in the balance of the bridge, brought about by the changes in Benmore fundamental and harmonic injections. However, as noted previously, Benmore generates only small amounts of triplen harmonics (because of the symmetry of the surrounding network),and therefore the increased triplen harmonic generation is local to Tiwai and induced by the change in unbalance of (especially) the 23^{rd} & 25^{th} harmonics. In other words, the changes in these harmonics, due to varying injections at Benmore, interact within the Tiwai bridge and result in greater triplen harmonic production.

Finally, the locally characteristic harmonics (5^{th}, 7^{th}, 17^{th} & 19^{th}) are affected only mildly, although they do become a little less balanced as α_{BENMORE} approaches 55°. This is the anticipated result, since they are unlikely to be directly affected by current transfer from Benmore, but will still reflect the change in unbalance of the bridge.

5.4 CONCLUSIONS

This chapter has described the application of the integrated algorithm developed in chapter 4 to realistic and representative examples pertinent to the New Zealand system.

With only one source of harmonics considered, the differences between the fundamental results of the standard loadflow and the integrated load and harmonic flow algorithms were compared, and found to differ significantly, in terms of both real and reactive power. The reactive power variation was shown to be mostly due to shifts in zero crossings (and therefore firing instants), while the real power variations were linked to harmonic I^2R losses in the supply network. Significant changes in both the characteristic and uncharacteristic harmonics were also observed.

With two distant sources of harmonics (i.e. both Tiwai and Benmore) the interactions between the two become more complex. Benmore harmonic injections were shown to affect the fundamental operation of the Tiwai unit, although the converse was considerably less pronounced. Two mechanisms were shown to be instrumental in affecting the harmonic levels at the remote busbar. The more direct mechanism is that where harmonic currents flow through the network and bring about changes in harmonic levels at the remote busbar, and thus harmonics of order h affect only harmonics of order h. This phenomenon is most significant where harmonic generation at one busbar is considerably stronger than the equivalent generation at the remote busbar, and is most strongly observed when filters are not present at either ends of the transmission path. The less direct mechanism allows an injection at one frequency to affect a different frequency at the remote busbar by altering the operating state of the remote convertor. This is particularly evident when strong characteristic harmonic injections (such as those at Benmore) alter the balance of the remote bridge (i.e. Ti-

wai), and thus modify the generation of uncharacteristic harmonics there. The ability to observe and analyse such situations is a powerful application of the new algorithm.

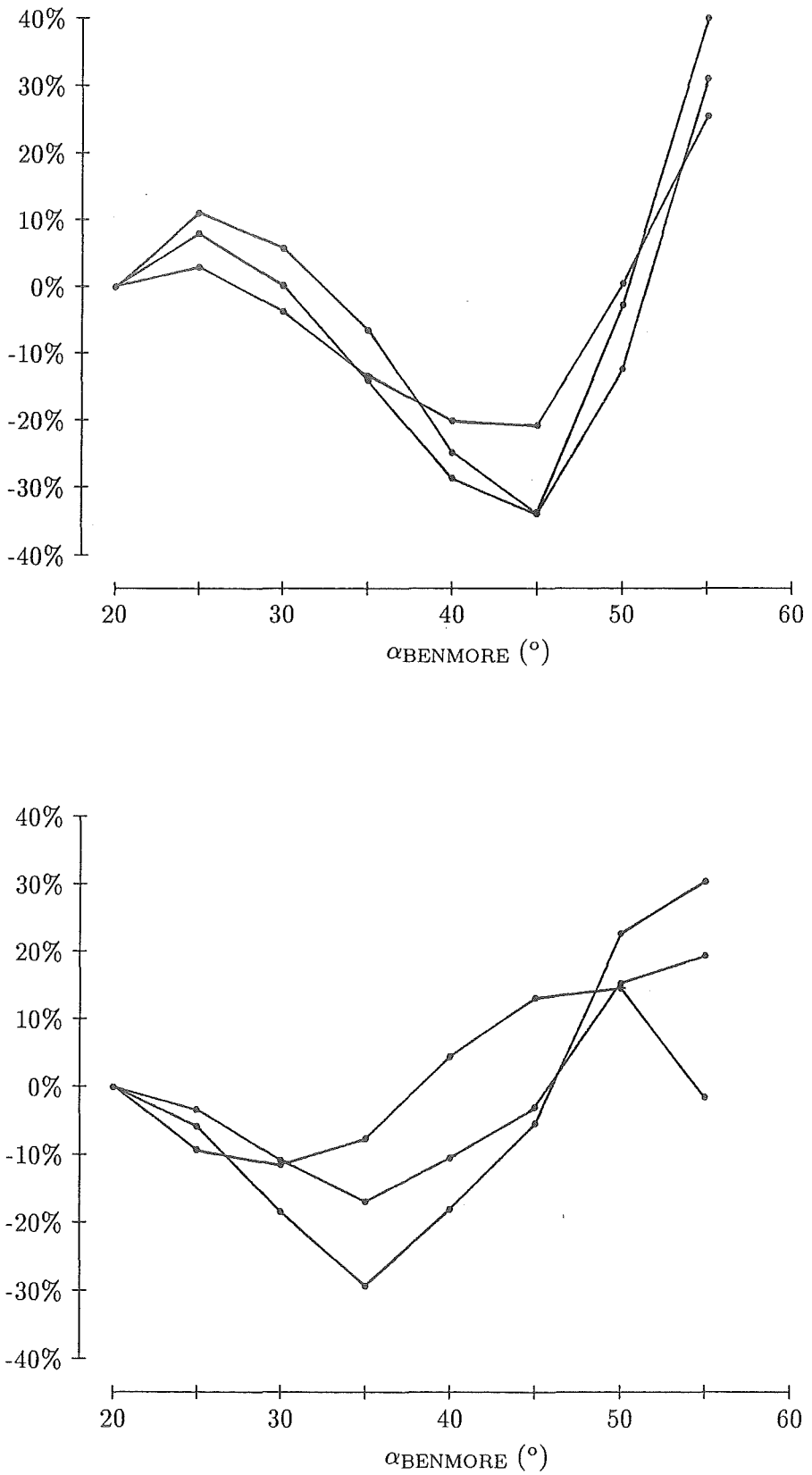

Figure 5.9: Variations in the 23$^{\text{rd}}$ & 25$^{\text{th}}$ harmonics with α_{BENMORE} — upper = 23$^{\text{rd}}$ harmonic, lower = 25$^{\text{th}}$ harmonic.

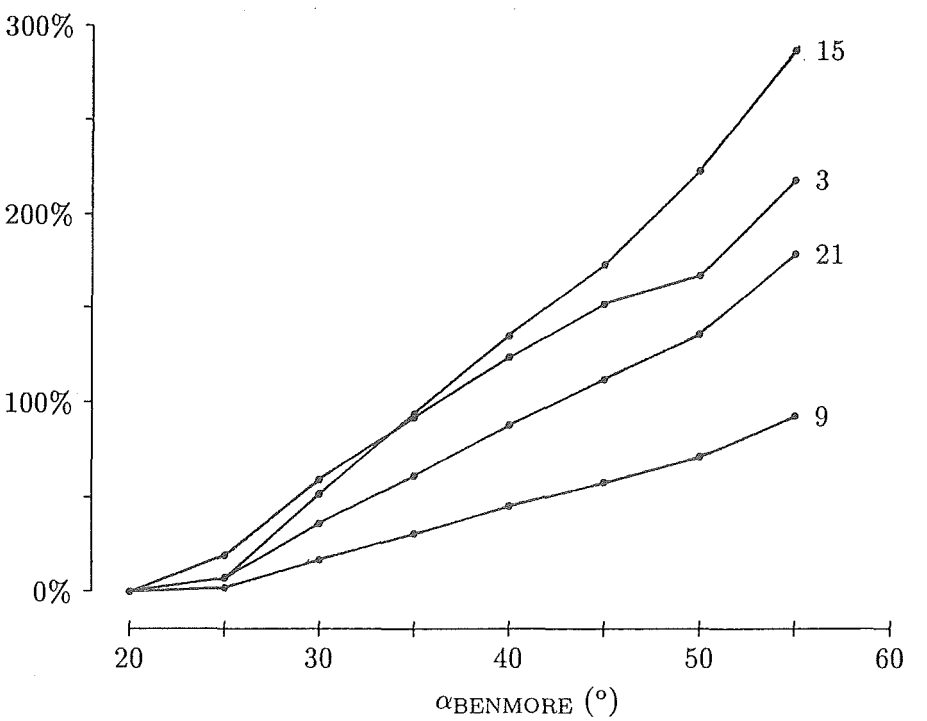

Figure 5.10: Variations in the triplen harmonics at Tiwai with α_{BENMORE}.

CHAPTER 6

CONCLUSIONS

6.1 DISCUSSION

The impending expansion of the NZ HVDC interconnection brings with it the possibility of harmonic generation and propagation problems over and above those due to the existing scheme. Previous contributions to the solution of these phenomena (Eggleston, 1985; Densem, 1983; Watson, 1987) have gone a long way toward providing satisfactory analysis tools, and it has been the aim of this thesis to round out the existing pool of expertise.

The existing convertor analysis algorithm, IHA, has been widely accepted as an accurate convertor model, provided that it converges. A cloud of uncertainty has hitherto surrounded the divergence of the IHA algorithm, with the question 'Does divergence of IHA indicate a physical harmonic instability ?' never being satisfactorily answered. Accordingly, chapter 3 examined the mechanisms of divergence within IHA, for both the phase angle controller and the equidistant firing controller in terms of triplen harmonic generation, with the dependence of convergence on the phase of the troublesome harmonic impedance being highlighted. Additionally, divergence in symmetrical cases attributable to triplens generated by numerical noise was analysed and two remedies suggested. However the crux of the whole convergence/divergence problem was best illustrated with respect to a system so simple that it could be solved analytically. This lead to the realisation that, whatever other factors were at work, divergence of IHA was somehow a fundamental property of the algorithm. Finally, IHA was analysed as a member of the Gauss-Seidel (fixed point) family of iteration techniques, revealing that, under certain conditions (relating to the Jacobian of the iterating function), divergence occurs for purely arithmetic reasons, and in no way indicates (in isolation) that a physical harmonic instability would occur in practice.

Integrated load and harmonic flow algorithms have been in use since 1983, but have been invariably single phase formulations, thus precluding the consideration of triplen harmonic generation, which arises purely as a result of asymmetries in the supply network. Therefore, chapter 4 derived an integrated three phase load and harmonic flow algorithm, based on existing analysis tools : the three phase a.c.-d.c. loadflow and IHA. The principal effort here was directed towards ensuring that consistency of the system was maintained in the final solution, despite the discrepancies which occur between the three phase a.c.-d.c. loadflow and IHA solutions considered in isolation from each other. The adopted method of absorbing these differences was to introduce an ideal, infinitely variable tap changing transformer, whose off-nominal tap ratio at final convergence indicates the departure of the integrated load and harmonic flow

solution from that of the standard loadflow solution. Simple test systems showed that the effect of the presence of harmonics on the loadflow solution depended on the degree and nature of the filtering present. Generally, unfiltered convertor operation has the greatest effect on the standard loadflow solution, although even with standard HVDC harmonic filters the effect is still noticeable.

The final chapter examined two practical test systems, both taken from the New Zealand South Island network. In the first, harmonics due to 75 MW 6-pulse operation at Tiwai point was shown to have a significant effect on the reactive power requirement of the convertor under both filtered and unfiltered operation. Real power consumption was seen to increase when harmonics were included in the loadflow solution under unfiltered operation, and this increase was shown to be directly related to harmonic dissipation in the supply network. However, with filtered operation, the flow of harmonic currents in the network is severely curtailed, and thus harmonic losses are reduced to a minimum. Additionally, the effects of the modified fundamental conditions on the harmonic generation of the convertor were shown to be significant in that the harmonics at final convergence of the integrated algorithm differed from those predicted by the IHA algorithm alone.

The second case dealt with the interaction between the previous convertor, and the NZ HVDC link at Benmore. It was shown that the Benmore harmonic injection (12-pulse, 1000 MW) was sufficient to affect the fundamental operation of the Tiwai convertor, although the converse was considerbly less pronounced. Two mechanisms were isolated as affecting harmonic levels at a remote busbar. The first was direct harmonic current transfer, whereby harmonic currents injected at the remote busbar resulted in corresponding harmonic voltages at the local busbar, and was particularly significant where the remote injection source was much stronger than the other & filters were not present at both ends of the transmission path. The second mechanism resulted from the effect of the directly transferred currents on the operation of the local convertor, altering the local generation of frequencies other than those transferred.

6.2 FUTURE WORK

Future endeavour in this field could be profitably focussed on two areas.

An harmonic domain model of the convertor, similar to that developed for transformer non-linearites by Acha (1987), may provide more reliable convergence than the IHA technique, despite the singular nature of the switching waveform (compared with, say, the transformer magnetising characteristic). Of principal importance in defining a harmonic domain model of any device is the linearisation of the device non-linearity into a Norton harmonic current source plus harmonic admittance matrix representation. This was essentially achieved in section 3.5.3, where the linearisation of the convertor non-linearity was used to derive the convergence constraint for IHA. Thus, all that is required is incorporation of this into a suitable algorithmic structure. Subsequent to the successful development of a Newton-like solution technique, the harmonic domain model could be substituted into the integrated load and harmonic flow algorithm to provide the industry with a very powerful steady state analysis tool.

One other area which could profitably be investigated is the interaction on the d.c. line, and in the a.c. systems, of HVDC links joining systems with different fundamental

tal frequencies. In this case, inter-harmonic frequencies are generated in each system since the convertors act essentially as ring-modulators (Yacamini, 1986). Analysis of this situation in the time domain has been hindered by the lack of suitable frequency-matched d.c. line models, but this is no problem with IHA. However, in order to fully represent all the frequencies present, extended sampling periods are required, so that both systems are sampled for identical periods of time, and both by an integral number of cycles. For example, considering an HVDC link connecting 50 Hz & 60 Hz systems, the sampling period would be 0.1 seconds, corresponding to 5 cycles of 50 Hz operation, and 6 cycles of 60 Hz operation. In general, the sampling period corresponds to the greatest common factor (GCF) of the two frequencies, so that investigating the interaction between two closely matched systems (say 49 and 50 Hz) would require an excessive computational effort (49 and 50 cycles of operation respectively) and would not warrant the work. However, for the more common interconnection (50-60 Hz), the method would be applicable.

REFERENCES

ACHA, E. (1987), *Modelling of Three Phase Transformers in the Complex-Conjugate Harmonic Space*, PhD thesis, University of Canterbury, New Zealand.

AINSWORTH, J.D. (1968), 'The phase locked oscillator - a new control system for static convertors', *IEEE Trans. on Power Apparatus and Systems*, Vol. PAS-87, No. 3, April, Pp. 859–864.

AINSWORTH, J.D. (1981), 'Harmonic instabilities', In *International Conference on Harmonics in Power Systems*, UMIST, Manchester.

AL-KHASHALI (1976), *Generalised Dynamic Modelling of High Voltage AC-DC Transmission Systems*, PhD thesis, University of Manchester Institute of Science and Technology, Great Britain.

ARRILLAGA, J. (1983), *High Voltage Direct Current Transmission*, Peter Peregrinus.

ARRILLAGA, J. and BODGER, P.S. (1977), 'Integration of h.v.d.c. links with fast decoupled load-flow solution', *IEE Proceedings*, Vol. 124, No. 5, Pp. 463–468.

ARRILLAGA, J. and CALLAGHAN, C.D. (1989), 'A double-iterative algorithm for the analysis of power and harmonic flows at HVDC convertor terminals', *IEE Proceedings, Part C.* (accepted for publication.).

ARRILLAGA, J., HARKER, B.J. and DENSEM, T.J. (1983), *Power Flow Program Operations Manual*, University of Canterbury, Private Bag, Ilam, Christchurch, NZ.

ARRILLAGA, J., WATSON, N.R., EGGLESTON, J.F. and CALLAGHAN, C.D. (1987), 'Comparison of steady-state and dynamic models for the calculation of ac/dc system harmonics', *IEE Proceedings*, Vol. 134, Part C, No. 1, January, Pp. 31–37.

CAMPOS-BARROS, J.G. and RANGEL, R.D. (1985), 'Computer simulation of modern power systems : the elimination of numerical noise caused by valve action', In 4^{th} *International Conference on AC and DC Power Transmission*, IEE Conf. Publ. 255, London.

Cyme International Inc. *CYMHARMO - Harmonic Analysis*, 1485 Roberval, Suite 204, St. Bruno, Quebec, Canada.

DENSEM, T.J. (1983), *Three-Phase Harmonic Penetration*, PhD thesis, University of Canterbury, New Zealand.

DOMMEL, H.W. (1969), 'Digital computer solution of electromagnetic transients in single and multiphase networks.', *IEEE Trans. on Power Apparatus and Systems*, Vol. PAS-88, No. 4, April, Pp. 388–399.

DOMMEL, H.W., YAN, A. and WEI, S. (1986), 'Harmonics from transformer saturation.', *IEEE Trans. on Power Delivery*, Vol. PWRD-1, No. 2.

EGGLESTON, J.F. (1985), *Harmonic Modelling of Transmission Systems Containing Synchronous Machines and Static Convertors*, PhD thesis, University of Canterbury, New Zealand.

HARKER, B.J. (1980), *Steady State Power System Analysis*, PhD thesis, University of Canterbury, New Zealand.

HARKER, B.J. and ARRILLAGA, J. (1979), '3-phase a.c.-d.c. load flow.', *IEE Proceedings*, Vol. 126, No. 12, December, Pp. 1275–1281.

HEFFERNAN, M.D. (1980), *Analysis of AC/DC System Disturbances*, PhD thesis, University of Canterbury, New Zealand.

HOLMBORN, H. and MARTENSSON, H. (1966), 'Experience with AC harmonics from HVDC installations', In *High Voltage DC Transmission*, IEE Conf. Publ. 22, London, Pp. 445–449.

HOUSEHOLDER, A.S. (1953), *Principles of Numerical Analysis*, McGraw-Hill Book Company.

KAUFERLE, J., MEY, R. and ROGOWSKY, Y. (1970), 'HVDC stations connected to weak AC systems', *IEEE Trans. on Power Apparatus and Systems*, Vol. PAS-89, No. 7, July, Pp. 1610–1617.

LAST, F.H., JARRETT, G.S.H., HUDDART, K.W., BREWER, G.L. and WATSON, W.G. (1966), 'Isolated generator-DC link feasibility trials', In *High Voltage DC Transmission*, IEE Conf. Publ. 22, London, Pp. 58–65.

MARTI, J.R. and LIN, J. (1989), 'Suppression of numerical oscillations in the EMTP', *IEEE Trans. on Power Systems*, Vol. 4, No. 2, May, Pp. 739–747.

NATALE, M., LANE, F.J. and CALVERLEY, T. (1966), 'The Sardinian-Italian Mainland HVDC interconnection', In *High Voltage DC Transmission*, IEE Conf. Publ. 22, London, Pp. 42–45.

New Zealand Electricity (1983), *New Zealand Limitation of Harmonic Levels Notice*, issue 2 ed.

PHADKE, A.G. and HARLOW, J.H. (1968), 'Generation of abnormal harmonics in high voltage AC-DC power systems', *IEEE Trans. on Power Apparatus and Systems*, Vol. PAS-87, No. 3, Pp. 873–882.

REEVE, J. and KRISHNAYYA, P.C.S. (1968), 'Unusual current harmonics arising from high-voltage dc transmission.', *IEEE Trans. on Power Apparatus and Systems*, Vol. PAS-87, No. 3, Pp. 883–893.

REEVE, J., BARON, J.A. and KRISHNAYYA, P.C.S. (1971), 'A general approach to harmonic current generation by hvdc convertors.', *IEEE Trans. on Power Apparatus and Systems*, Vol. PAS-90, No. 6, Pp. 2785–2791.

RICHTER, S.L. and DECARLO, R.A. (1983), 'Continuation methods : theory and applications', *IEEE Trans. on Automatic Control*, Vol. AC-28, No. 6, June, Pp. 660–665.

RISSIK, H. (1939), *Fundamental Theory of Arc Convertors*, Chapman & Hall Ltd.

ROBINSON, G.H. (1966), 'Harmonic phenomena associated with the Benmore-Haywards HVDC transmission scheme', *New Zealand Engineering*, January, Pp. 16–29.

SEMLYEN, A., ACHA, E. and ARRILLAGA, J. (1987), 'Newton-type algorithms for the harmonic phasor analysis of non linear power circuits in periodical steady state with special reference to magnetic non-linearities.', *IEEE Winter Power Meeting*, Vol. WM 170, No. 4, February.

SIMMONS, R.H. (1983), *Harmonic Filters at Tiwai*, Technical Report, New Zealand Aluminium Smelters.

SINGLETON, R.C. (1969), 'An algorithm for computing the mixed radix fast Fourier transform', *IEEE Trans. on Audio & Electroacoustics*, Vol. AU-17, No. 2, June, Pp. 93–103.

TAMBY, J.F. and JOHNS, V.I. (1988), 'Q'HARM, a new harmonic powerflow algorithm for small power systems.', *IEEE Trans. on Power Systems*, Vol. 3, No. 3, August, Pp. 949–955.

TRAUB, J.F. (1964), *Iterative Methods for the Solution of Equations*, Prentice Hall.

TSCHAPPU, F. (1981), 'Problems in the exact measurement of electrical energy in networks having harmonic content in the current.', *Landis & Gyr Review*, Vol. 28-2, Pp. 8–15.

WATSON, N.R. (1987), *Frequency-Dependent A.C. System Equivalents for Harmonic Studies and Transient Convertor Simulation*, PhD thesis, University of Canterbury, New Zealand.

WATSON, N.R., ARRILLAGA, J. and JOOSTEN, A.P.B. (1985), 'AC system equivalents for the dynamic simulation of HVDC convertors.', In 4^{th} *International Conference on AC and DC Power Transmission*, IEE Conf. Publ. 255, London, Pp. 349–399.

WOODFORD, D.A., GOLE, A.M. and MENZIES, R.W. (1983), 'Digital simulation of DC links and AC machines.', *IEEE Trans. on Power Apparatus and Systems*, Vol. PAS-102, No. 6, June, Pp. 1616–1623.

XIA, D. and HEYDT, G.F. (1982), 'Harmonic power flow studies part 1 - formulation and solution', *IEEE Trans. on Power Apparatus and Systems*, Vol. PAS-101, No. 6, June, Pp. 1252–1265.

YACAMINI, R. (1986), 'How hvdc schemes can excite torsional oscillations in turbo-alternator shafts', *IEE Proceedings*, Vol. 133, Part C, No. 6, September, Pp. 301–307.

YACAMINI, R. and de Oliveira, J.C. (1980), 'Harmonics in multiple convertor systems : a generalised approach', *IEE Proceedings*, Vol. 127, Part B, No. 2, March, Pp. 96–104.

YACAMINI, R. and de Oliveira, J.C. (1986), 'Comprehensive calculation of convertor harmonics with system impedances and control representation', *IEE Proceedings*, Vol. 133, Part B, No. 2, March, Pp. 95–102.